

# Long Noncoding RNA MANTIS Facilitates Endothelial Angiogenic Function

Editorial, see p 80

**BACKGROUND:** The angiogenic function of endothelial cells is regulated by numerous mechanisms, but the impact of long noncoding RNAs (lncRNAs) has hardly been studied. We set out to identify novel and functionally important endothelial lncRNAs.

**METHODS:** Epigenetically controlled lncRNAs in human umbilical vein endothelial cells were searched by exon-array analysis after knockdown of the histone demethylase JARID1B. Molecular mechanisms were investigated by RNA pulldown and immunoprecipitation, mass spectrometry, microarray, several knockdown approaches, CRISPR-Cas9, assay for transposase-accessible chromatin sequencing, and chromatin immunoprecipitation in human umbilical vein endothelial cells. Patient samples from lung and tumors were studied for MANTIS expression.

**RESULTS:** A search for epigenetically controlled endothelial lncRNAs yielded lncRNA n342419, here termed MANTIS, as the most strongly regulated lncRNA. Controlled by the histone demethylase JARID1B, MANTIS was downregulated in patients with idiopathic pulmonary arterial hypertension and in rats treated with monocrotaline, whereas it was upregulated in carotid arteries of *Macaca fascicularis* subjected to atherosclerosis regression diet, and in endothelial cells isolated from human glioblastoma patients. CRISPR/Cas9-mediated deletion or silencing of MANTIS with small interfering RNAs or GapmeRs inhibited angiogenic sprouting and alignment of endothelial cells in response to shear stress. Mechanistically, the nuclear-localized MANTIS lncRNA interacted with BRG1, the catalytic subunit of the switch/sucrose nonfermentable chromatin-remodeling complex. This interaction was required for nucleosome remodeling by keeping the ATPase function of BRG1 active. Thereby, the transcription of key endothelial genes such as *SOX18*, *SMAD6*, and *COUP-TFII* was regulated by ensuring efficient RNA polymerase II machinery binding.

**CONCLUSION:** MANTIS is a differentially regulated novel lncRNA facilitating endothelial angiogenic function.

Matthias S. Leisegang, PhD  
Christian Fork, PhD  
Ivana Josipovic, MSc  
Florian Martin Richter, PhD  
Jens Preussner, MSc  
Jiong Hu, PhD  
Matthew J. Miller, MSc  
Jeremy Epah  
Patrick Hofmann, MSc  
Stefan Günther, PhD  
Franziska Moll, MSc  
Chanil Valasarajan, MSc  
Juliana Heidler, PhD  
Yuliya Ponomareva, MSc  
Thomas M. Freiman, MD  
Lars Maegdefessel, MD, PhD  
Karl H. Plate, MD  
Michel Mittelbronn, MD  
Shizuka Uchida, PhD  
Carsten Künne, PhD  
Konstantinos Stellos, MD  
Ralph T. Schermuly, PhD  
Norbert Weissmann, PhD  
Kavi Devraj, PhD  
Ilka Wittig, PhD  
Reinier A. Boon, PhD  
Stefanie Dimmeler, PhD  
Soni Savai Pullamsetti, PhD  
Mario Looso, PhD  
Francis J. Miller, Jr., MD  
Ralf P. Brandes, MD

**Correspondence to:** Ralf P. Brandes, MD, Institut für Kardiovaskuläre Physiologie, Fachbereich Medizin der Goethe-Universität, Theodor-Stern-Kai 7, 60590 Frankfurt am Main, Germany. E-mail brandes@vrc.uni-frankfurt.de

Sources of Funding, see page 78

**Key Words:** epigenomics ■ glioblastoma ■ hypertension, pulmonary ■ neovascularization, physiologic ■ RNA, long noncoding

© 2017 The Authors. *Circulation* is published on behalf of the American Heart Association, Inc., by Wolters Kluwer Health, Inc. This is an open access article under the terms of the Creative Commons Attribution Non-Commercial-NoDerivs License, which permits use, distribution, and reproduction in any medium, provided that the original work is properly cited, the use is noncommercial, and no modifications or adaptations are made.

## Clinical Perspective

### What Is New?

- MANTIS is a long noncoding RNA strongly regulated by histone demethylase JARID1B.
- MANTIS maintains endothelial cell function.
- It interacts with the nucleosome-remodeling protein BRG1.
- It maintains ATPase activity of BRG1 by stabilizing the switch/sucrose nonfermentable complex.
- MANTIS promotes transcription of SOX18, SMAD6, and COUP-TFII by enabling RNA polymerase II binding to the transcriptional start sites.
- MANTIS is downregulated during pulmonary arterial hypertension but induced in tumor endothelium.

### What Are the Clinical Implications?

- MANTIS is a novel long noncoding RNA that positively affects endothelial angiogenic function.
- Altering MANTIS expression could be exploited to control the angiogenic process in situations of excessive or insufficient angiogenesis.

The endothelium forms the central vascular barrier to maintain vessel function and integrity. Healthy endothelium prevents thrombus formation, leukocyte adhesion, and smooth muscle cell proliferation, whereas activated endothelium has opposing properties.<sup>1</sup> Understanding how endothelial cells maintain or change their phenotype is key to preventing vascular disease development. Important aspects in this regulation are epigenetic mechanisms, but our understanding of vascular epigenetics is still in its beginning.

Epigenetic mechanisms regulating gene expression involve chromatin modifications without associated DNA sequence alterations. For example, trimethylation at histone 3 lysine 4 (H3K4) in promoter regions is generally associated with gene expression.<sup>2,3</sup> The H3K4 lysine-specific demethylase 5B (JARID1B) has been shown to maintain normal endothelial gene expression by limiting expression of gene repressors.<sup>4</sup> Several chromatin-modifying complexes have been found to be important for endothelial gene expression. In human umbilical vein endothelial cells (HUVECs), for example, polycomb repressor complex-2 (PRC2) regulates gene expression of *Ten-eleven translocation-1*.<sup>5</sup> Moreover, the catalytic subunit of the switch/sucrose nonfermentable (SWI/SNF) complex, Brahma related gene-1 (BRG1), is recruited to the endothelial nitric oxide synthase promoter under hypoxic conditions,<sup>6</sup> and to the *Selectin E* promoter under resting conditions.<sup>7</sup> Knockout of BRG1 or loss of PRC2 function results in mouse embryonic lethality,<sup>8,9</sup> highlighting the importance of epigenetic modifiers for vascular development. Moreover, BRG1 has been identified

as a central regulator of gene expression, eg, of *Chicken Ovalbumin Upstream Promoter Transcription-Factor-2* (COUP-TFII) in vascular cells.<sup>10</sup>

Epigenetic functions are also mediated by RNAs. Only a small portion of the human genome carries protein-coding potential; the majority is differentially and dynamically transcribed to produce noncoding RNAs, of which the majority are long noncoding RNAs (lncRNAs).<sup>11</sup> lncRNA is the most diverse, plastic, and poorly understood class of noncoding RNA. It is broadly defined as transcribed, but not translated, RNA molecules >200 nucleotides in length.<sup>12</sup> Many lncRNAs are associated with epigenetic factors, where they recruit chromatin-modifying complexes, such as PRC2, to target sites. Through this and other mechanisms, lncRNAs influence transcriptional activation or repression, depending on the interaction partner.<sup>11</sup> So far, only a few lncRNAs have been shown to contribute to vascular disease and endothelial cell integrity.<sup>13</sup> This contrasts with the important role of the endothelium in vascular biology. In the present study, we set out to identify epigenetically controlled endothelial lncRNAs possessing relevant and novel functions. Among them, we focused on the unreported lncRNA n342419, which we named MANTIS, and establish this as a disease-relevant element controlling vascular transcription factor expression through BRG1.

## METHODS

All methods are described in detail in the [online-only Data Supplement](#).

### Primers

The primers for quantitative real-time polymerase chain reaction are listed in [online-only Data Supplement Table I](#). The primers for chromatin immunoprecipitation are listed in [online-only Data Supplement Table II](#).

### Statistics

Unless otherwise indicated, data are given as means±standard error of mean. Calculations were performed with Prism 5.0 or BiAS.10.12. The latter was also used to test for normal distribution and similarity of variance. In case of multiple testing, Bonferroni correction was applied. For multiple group comparisons, analysis of variance followed by post hoc testing was performed. Individual statistics of dependent samples were performed by paired *t* test, of unpaired samples by unpaired *t* test, and, if not normally distributed, by Mann-Whitney test. *P* values of <0.05 were considered as significant. Unless otherwise indicated, *n* indicates the number of individual experiments.

### Study Approval

The study protocol for tissue donation from patients who have human idiopathic pulmonary hypertension was approved by the ethics committee (Ethik Kommission am Fachbereich

Humanmedizin der Justus Liebig Universität Giessen) of the University Hospital Giessen (Giessen, Germany) in accordance with national law and with Good Clinical Practice/International Conference on Harmonisation guidelines. Written informed consent was obtained from each individual patient or the patient's next of kin (AZ 31/93, 10/06, 58/15).<sup>14</sup>

Studies for human glioblastoma were covered by an ethics statement according to the guidelines of the University of Frankfurt, whose approval number for autopsy material is GS-249/11 and for resection material, GS-04/09.

Animal experiments regarding severe combined immunodeficiency mice were performed in accordance with the National Institutes of Health Guidelines on the Use of Laboratory Animals. The University Animal Care Committee and the Federal Authorities for Animal Research (Darmstadt, Germany) approved the study protocol.

Animal studies regarding rats were performed according to the guidelines of the University of Giessen and were approved by the local authorities (GI 20/10 Nr.44/2013).

Experiments on adult male cynomolgus monkeys were approved by the Institutional Care and Use Committee of the University of Iowa as approved experiments in this study.<sup>15</sup>

## RESULTS

### MANTIS Is a JARID1B-Suppressed lncRNA Downregulated in Human Idiopathic Pulmonary Arterial Hypertension

To identify epigenetically controlled lncRNAs, the impact of the knockdown of the histone demethylase JARID1B on endothelial RNA expression was determined by Exon arrays. JARID1B is one of the highest expressed histone demethylases in HUVECs.<sup>4</sup> The expression of several lncRNAs was altered by depletion of JARID1B with small interfering RNAs (siRNAs) (Figure 1A, [online-only Data Supplement Table III](#), [online-only Data Supplement Figure 1A](#)), of which n342419 and n406914 were most consistently regulated ([online-only Data Supplement Figure 1B](#)). Expression of n342419 was much higher than that of n406914 in HUVECs ([online-only Data Supplement Figure 1C](#)), and the RNA was also most strongly induced by JARID1B knockdown ([online-only Data Supplement Figure 1B](#)) and dependent on histone modification changes rather than direct transcriptional repression ([online-only Data Supplement Figure 1D](#)).

On the basis of these features, we decided to further focus on this uncharacterized lncRNA, which is genomically located as intronic antisense to *Annexin A4* (*ANXA4*) ([online-only Data Supplement Figure 1E](#)). Given the multiple cryptic names of n342419, ie, *ANXA4-AS*, *uc002sft.1*, and *AK125871*, we decided to name this lncRNA MANTIS based on its secondary structure. No indication of peptide-coding potential was found with open reading frame (ORF) determination by the RiboTaper<sup>16</sup> method and by the coding potential assessment tool<sup>17</sup> ([online-only Data Supplement](#)

[Figure 1F and 1G](#)). In contrast to the positive control DYR, artificial in vitro translation suggested that MANTIS does not encode a protein with a molecular weight >10 000 Dalton ([online-only Data Supplement Figure 1H](#)). None of the in silico predicted ORFs within the MANTIS sequence were identified in searches of a HEK Proteome with the PRIDE database (PXD000705, [online-only Data Supplement Tables IV and V](#)). A search for micropeptides after overexpression of MANTIS in HUVECs with subsequent liquid chromatography-tandem mass spectrometry without trypsination showed that none of the micropeptides found had any similarity to potential MANTIS ORFs, whereas the positive control yielded micropeptides encoded from GFP plasmid ([online-only Data Supplement Tables VI and VII](#)). A second experiment using MANTIS overexpressing HUVECs, this time with trypsination before liquid chromatography-tandem mass spectrometry, revealed no micropeptides with similarity to potential MANTIS ORFs, suggesting that MANTIS is noncoding ([online-only Data Supplement Tables VIII and IX](#)), thereby also minimizing the lack of detection by mass spectrometry, which does not exclude the presence of micropeptides. The expression of MANTIS was not restricted to HUVECs and even not to endothelial cells; MANTIS could also be detected in aortic, lymphatic, and pulmonary artery endothelial cells, in human smooth muscle cells isolated from different arteries, fibroblasts, MCF-7 cells, and THP-1 monocytes ([online-only Data Supplement Figure 1I](#)).

It is important to note that the expression of MANTIS was also altered in the disease context. In lungs from patients with end-stage idiopathic pulmonary arterial hypertension (IPAH), an isolated small-vessel disease accompanied by endothelial dysfunction, endothelial apoptosis, and proliferation,<sup>18</sup> MANTIS was downregulated, whereas JARID1B was upregulated (Figure 1B). A similar regulation pattern was also found in pulmonary artery endothelial cells ([online-only Data Supplement Figure 1IA](#)). Conversely, during vascular regeneration, JARID1B was downregulated and MANTIS was induced, as observed in the atherosclerosis regression phase in samples obtained from a *M. fascicularis* high-fat feeding study<sup>15</sup> (Figure 1C). In endothelial cells isolated from glioblastoma or adjacent healthy brain tissue, MANTIS was increased, whereas JARID1B was decreased (Figure 1D), which was also shown for MANTIS by RNA in situ hybridization using RNAscope (Figure 1E). Similarly, laminar flow induced MANTIS, whereas it decreased JARID1B expression (Figure 1F). To identify a functional role of MANTIS, loss-of-function approaches were used in the cell culture system with HUVECs. Because full-length MANTIS is only partially conserved beyond primates, studying its physiological importance by genetic knockout in mice is difficult. Therefore, we determined the capac-



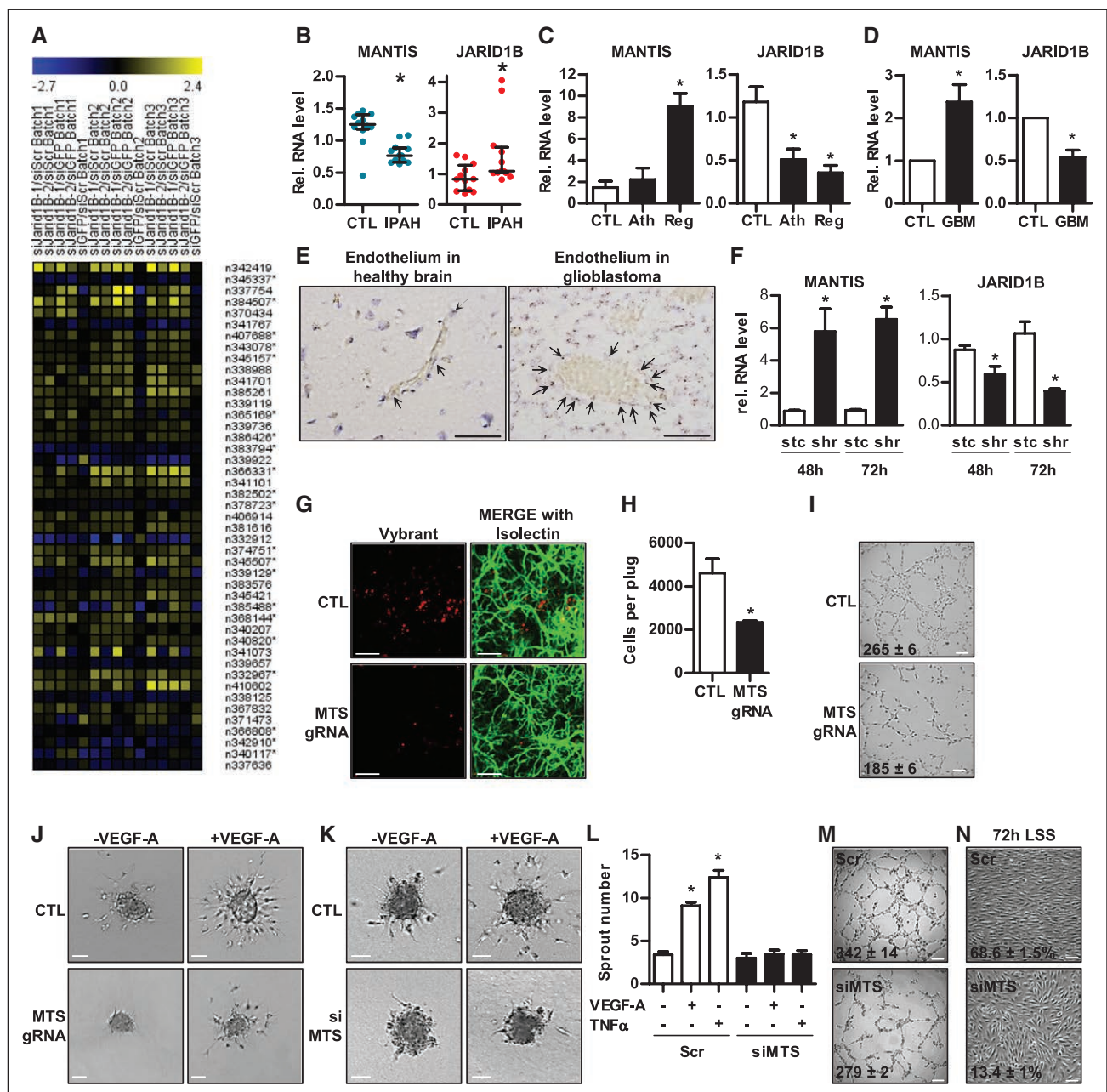


**Figure 1. Endothelial angiogenic capacity is dependent on lncRNA MANTIS.**

**A**, Affymetrix Exon-array heatmap comparing siJARID1B-1/siScr, siJARID1B-2/siScr, siJARID1B-1/siGFP, siJARID1B-2/siGFP, and siScr/siGFP levels of HUVEC batches 1 to 3. Scale bar shows color code from -2.7 (blue) to 2.4 (yellow) log<sub>2</sub> fold change. lncRNAs marked by an asterisk revealed >1 noncode accession numbers. See [online-only Data Supplement Table III](#) and [online-only Data Supplement Figure 1A](#) for all lncRNA names. **B**, qRT-PCR of MANTIS and JARID1B in lungs from control donors (CTL) or patients with IPAH. n=12. Median with interquartile range is shown, and Mann-Whitney test was used. **C**, qRT-PCR of MANTIS and JARID1B in monkey vessels treated either with a normal diet (CTL), a high-fat diet (Ath), or a high-fat diet and a subsequent recovery phase (Reg). n=3. One-way ANOVA, Bonferroni. **D**, qRT-PCR of MANTIS and JARID1B from endothelial cells isolated from glioblastoma (GBM) or adjacent healthy control (CTL) tissue. n=5. Paired t test. **E**, RNA in situ hybridization of endothelium of healthy brain or glioblastoma with RNAscope. Scale bar indicates 50  $\mu$ m. Arrows point to dots indicating MANTIS RNA. **F**, qRT-PCR measurements relative to  $\beta$ -Actin of MANTIS and JARID1B after laminar flow exposure (shr, 20 dyn/cm<sup>2</sup>) for 48 hours or 72 hours in HUVECs as indicated. Static (stc) samples served as control. n=4. Unpaired t test. **G**, CRISPR/Cas9 MANTIS guide RNAs (MTS gRNA) and control cells (CTL) after in vivo matrigel angiogenesis assay in mice. HUVECs were embedded in matrigel, stained with Vybrant dil (red), and injected. Isolectin GS-IB4 Alexa 647 conjugated stained vessels (green). Images were taken by light sheet microscopy 26 days after injection. Representative pictures are shown. Scale bar indicates 200  $\mu$ m. **H**, Quantification of cells per plug as shown in **G** 26 days after injection. n=3. Unpaired t test. **I**, Tube formation assay performed with MTS gRNA and CTL. Numbers indicate number of tubes  $\pm$  SEM. n=3. Scale bar indicates 200  $\mu$ m. **J**, Spheroid outgrowth assay with MANTIS (Continued)

ity of HUVECs with or without CRISPR/Cas9-mediated deletion of *MANTIS* to integrate into the vascular network of matrigels injected in severe combined immunodeficiency mice. Importantly, deletion of *MAN-TIS* resulted in a >50% reduction of the capacity of HUVEC to be retained in this model (Figure 1G and 1H, [online-only Data Supplement Figure IIB and IIC](#)). In addition, CRISPR/Cas9-mediated knockout of *MAN-TIS* in HUVECs greatly attenuated tube formation and sprouting (Figure 1I and 1J).

Because genetic deletion of *MANTIS* greatly reduced cellular health, siRNAs were used as a less drastic knockdown strategy. Of the 3 different siRNAs used, all reduced *MANTIS* expression, albeit siRNA-1 being most effective ([online-only Data Supplement Figure IID](#)). Therefore, siRNA-1 was used for the subsequent experiments. *MANTIS* siRNA-mediated depletion reduced endothelial sprouting (Figure 1K and 1L, [online-only Data Supplement Figure IIE and IIF](#)) and tube formation (Figure 1M), also in pulmonary artery endothelial cells ([online-only Data Supplement Figure IIG](#)). Moreover, it attenuated migration of HUVECs in Boyden-Chamber assays ([online-only Data Supplement Figure IIH](#)). In a competition-like spheroid outgrowth assay, si*MANTIS*-transfected cells were underrepresented in the tip cell position ([online-only Data Supplement Figure III and IIJ](#)). Also, the ability of HUVECs to properly orientate toward the direction of flow was lost after the knockdown of the lncRNA (Figure 1N).

The regulation of *MANTIS* by JARID1B was further studied by chromatin immunoprecipitation experiments. JARID1B bound H3K4me3-rich regions near the transcriptional start site (TSS) of *MANTIS* ([online-only Data Supplement Figure IIK](#)). Knockdown of JARID1B increased H3K4me3 close to the TSS of *MANTIS* ([online-only Data Supplement Figure IIL](#)), whereas other family members such as JARID1A and JARID1C did not regulate *MANTIS* ([online-only Data Supplement Figure IIM](#)).

Together, these data suggest that the lncRNA *MANTIS* could be of importance during IPAH and glioblastoma and that its control by Jarid1B is essential to preserve multiple aspects of normal endothelial cell functions in culture and in a mouse in vivo model.

## MANTIS Interacts With the SWI/SNF Chromatin-Remodeling Complex Subunit BRG1

To get insights into the molecular mechanism by which *MANTIS* controls endothelial cell functions, we first evaluated the intracellular localization of *MANTIS* in HUVECs. RNA-fluorescence in situ hybridization demonstrated that the endogenous *MANTIS* RNA is localized in the nucleus, whereas the negative control *ACTINB* mRNA was predominantly localized in the cytosol. Also, after overexpression, *MANTIS* was retained in the nucleus (Figure 2A).

To identify candidates as interaction partners of *MANTIS*, RNA-pulldown experiments with 3'-biotinylated *MANTIS* lncRNA or 3'-biotinylated pcDNA3.1+ negative control RNA with nuclear extracts from HUVECs were performed (Figure 2B). As expected, *MANTIS* was strongly enriched in the 3'-biotinylated *MANTIS* pulldowns in comparison with the controls (Figure 2C). Electrospray ionization mass spectrometry of the samples identified several coprecipitating proteins as candidates for interaction (Figure 2D and 2E, [online-only Data Supplement Table X](#)), with BRG1 having the highest score. The ATPase BRG1 is a known regulator of endothelial cell functions and has been shown to be increased in humans with thoracic aortic aneurysms and to impact on proliferation, apoptosis, and myocardin-specific gene regulation in vascular smooth muscle cells.<sup>19,20</sup> Importantly, reverse RNA immunoprecipitation and RNA chromatin immunoprecipitation all confirmed *MANTIS* as an interaction partner of BRG1. The interaction of *MANTIS* with BRG1 was specific: *MANTIS* was not pulled down by SMARCA5, the catalytic subunit of the ISWI chromatin-remodeling complex,<sup>21</sup> or IgG (Figure 2F and 2G). BRG1 also did not coprecipitate with MEG3 lncRNA or U12 snRNA. These data show that *MANTIS* and the SWI/SNF catalytic subunit BRG1 are interacting. Potentially, this interaction mediates the physiological effects of *MANTIS*.

## MANTIS Is Required for the Gene Expression of SOX18, SMAD6, and COUP-TFII

A key function of lncRNAs associated with chromatin-remodeling complexes is the regulation of transcriptional

**Figure 1 Continued.** gRNA and CTL. Cells treated with or without VEGF-A are shown. Scale bar indicates 50  $\mu$ m. **K**, Spheroid outgrowth assay after siMTS. Scr served as negative control. Cells treated  $\pm$  VEGF-A are shown. Scale bar indicates 50  $\mu$ m. **L**, Quantification of sprout numbers from the spheroid outgrowth assays seen in **K** or [online-only Data Supplement Figure IIE](#).  $n=10$ . One-way ANOVA, Bonferroni. **M**, Tube formation assay after siMTS. Scr served as negative control. Numbers indicate number of tubes  $\pm$  SEM.  $n=3$ . Scale bar indicates 200  $\mu$ m. **N**, Images of cells treated with scrambled or siMTS after 72 h of laminar flow (LSS, 20 dyn/cm<sup>2</sup>). Numbers indicate number of cells orientated in direction of the flow  $\pm$  SEM.  $n=4$ . Scale bar indicates 100  $\mu$ m. All qRT-PCR data are relative to  $\beta$ -actin. Error bars are defined as mean  $\pm$  SEM. \* $P<0.05$ . ANOVA indicates analysis of variance; HUVEC, human umbilical vein endothelial cell; IPAH, idiopathic pulmonary arterial hypertension; lncRNA, long noncoding RNA; qRT-PCR, quantitative real-time polymerase chain reaction; Scr, scrambled; SEM, standard error of the mean; siMTS, *MANTIS* siRNA; and VEGF-A, vascular endothelial growth factor A.

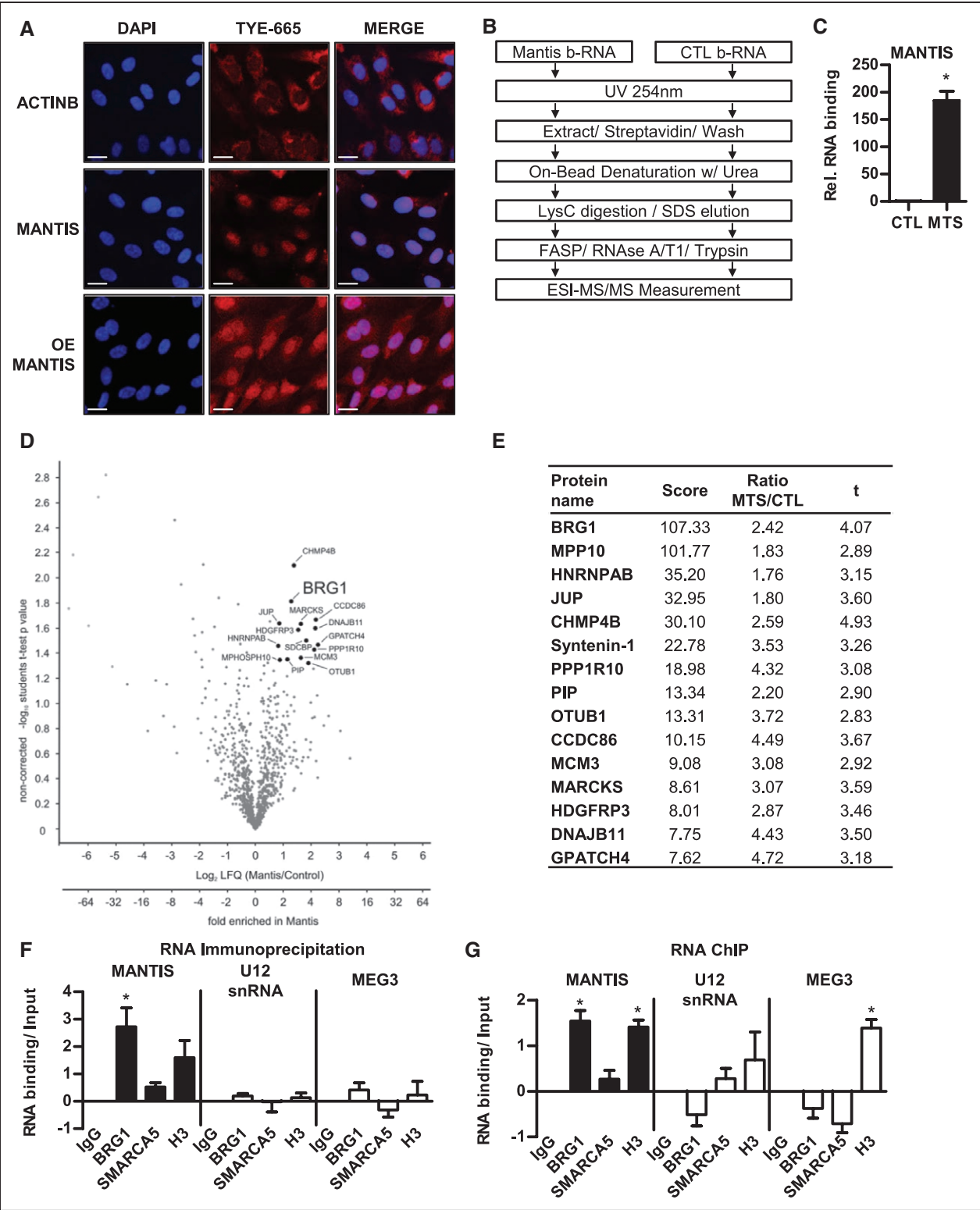


**Figure 2. The nuclear localized MANTIS lncRNA interacts with the SWI/SNF complex member BRG1.** **A**, RNA fluorescence in situ hybridization (FISH) of HUVECs with TYE-665–modified probes against ACTINB and MANTIS. DAPI was used to stain nuclei. MANTIS overexpression (OE) samples were treated with an additional overexpression of pcDNA3.1+MANTIS for 48 hours before FISH. Scale bar indicates 20  $\mu$ m. **B**, Scheme of RNA pulldown assay with subsequent preparation for mass spectrometric measurements. b-RNA indicates biotinylated RNA. **C**, qRT-PCR after RNA pulldown assay by measuring the amount of MANTIS RNA (MTS) in the eluates relative to the negative control RNA (CTL). n=4. Paired *t* test. **D**, Volcano plot of log<sub>2</sub> ratio of MANTIS versus control interaction partner proteins after RNA pulldown assay and ESI-MS/MS measurements. n=3. Noncorrected  $-\log_{10}$  Student *t* test. LFQ indicates label-free quantification. **E**, Proteins (Continued)



events.<sup>22</sup> Thus, microarrays were used to identify the impact of MANTIS knockdown on endothelial gene expression. Depletion of MANTIS with LNA-GapmeRs led to downregulation of a high number of angiogenesis-related mRNAs, among them SRY (Sex Determining Region Y)-Box 18 (SOX18), Mothers against decapentaplegic homologue 6 (SMAD6), and COUP-TFII, and on upregulation of stress-induced genes like interleukin 6 and superoxide dismutase 2 (Figure 3A, [online-only Data Supplement Table XI](#)); however, genes neighboring the MANTIS locus in the genome (ANXA4, AAK1, GCML1, snRNP27) were not affected, excluding a *cis*-regulatory activity of MANTIS in HUVEC (Figure 3B). To confirm these results, quantitative real-time polymerase chain reaction after depletion of MANTIS with either LNA-GapmeRs, siRNAs, or CRISPR/Cas9 deletion mutants was performed. All silencing approaches confirmed the data obtained with the microarrays (Figure 3C and 3D, [online-only Data Supplement Figure IIIA through IIIF](#)). Gene ontology (GO) analyses for genes downregulated in response to MANTIS knockdown yielded angiogenesis as the most significantly affected GO term (Figure 3E, [online-only Data Supplement Tables XII and XIII](#)). Indeed, it has been reported previously that *SOX18*, *SMAD6*, and *COUP-TFII* are key endothelial genes important for angiogenesis and other endothelial features mentioned in reference 23.

On this basis, mRNA data were validated on the protein level. Western blot analyses revealed that both, LNA-GapmeRs and siRNAs, as well, not only reduced MANTIS mRNA, but also *SOX18*, *SMAD6*, and *COUP-TFII* protein levels in HUVECs (Figure 3F through 3I). Given the potential function of *SOX18* for lymphatic and of *COUP-TFII* for venous specification, additional cell types were studied. Downregulating MANTIS, however, yielded similar responses in human dermal lymphatic endothelial cells, aortic arterial and pulmonary artery endothelial cells, and even vascular smooth muscle cells ([online-only Data Supplement Figure IIIG through IIIL](#)).

The fact that *SOX18*, *SMAD6*, and *COUP-TFII* were also downregulated in the samples of patients with IPAH in which also MANTIS was downregulated, might suggest that this interaction also occurs in the disease context (Figure 3J through 3L), because, in endothelial cells isolated from glioblastoma, *SOX18*, *SMAD6*, and *COUP-TFII* were increased ([online-only Data Supplement Figure IIIM through IIIO](#)).

To establish a link between these MANTIS target genes and endothelial angiogenic capacity, siRNA-based knockdown was performed (Figure 4A). Downregulation of either of *SMAD6*, *COUP-TFII* or *SOX18* all attenuated endothelial sprouting in the spheroid outgrowth assay (Figure 4B through 4D). However, overexpression of *SMAD6*, *COUP-TFII*, or *SOX18* after MANTIS knockdown ([online-only Data Supplement Figure IVA and IVB](#)) failed to normalize endothelial sprouting capacity ([online-only Data Supplement Figure IVC and IVD](#)). This might suggest that several factors acting in concert are affected by MANTIS or that technical difficulties arising from multiple transfections and from the great size of the MANTIS plasmid render these studies infeasible. To address the second aspect, we searched for a fragment of MANTIS with RegRNA2.0,<sup>24</sup> which might be sufficient to rescue endothelial function after MANTIS knockdown. A small part of ≈450 nt of MANTIS Exon 3 contains an Alu element, which could be of functional importance ([online-only Data Supplement Figure IE](#)). Overexpression of this element (MANTIS-mut) indeed partially rescued the sprouting in response to vascular endothelial growth factor A (Figure 4E through 4H). Thus, MANTIS maintains endothelial angiogenic capacity through an induction of *SMAD6*, *COUP-TFII*, and *SOX18*, and this effect is potentially mediated by the Alu element in Exon 3. Interestingly, a corresponding SINE B1 (short interspersed nucleotide element) was also found in mice and rats at a similar position within the Intron of *ANXA4*. In CD31+ positive cells isolated from rats exposed to monocrotaline, a model system frequently used to study pulmonary arterial hypertension,<sup>25</sup> expression of this putative homologue MANTIS fragment was downregulated, tentatively together with *SOX18*, *SMAD6*, and *COUP-TFII* (Figure 4I). This might suggest that this lncRNA is conserved from humans to rats and that the Alu element is important in regulating IPAH.

## MANTIS and BRG1 Facilitate RNA Polymerase II Binding by Reducing Heterochromatin

BRG1 functions as an ATP-dependent helicase in the SWI/SNF chromatin-remodeling complex.<sup>26</sup> Interestingly, it has been shown that BRG1 promotes *COUP-TFII* gene expression in vascular endothelium during mu-

**Figure 2 Continued.** enriched after RNA pulldown assay, their score, ratio MANTIS/CONTROL (MTS/CTL), and *t* value. **F**, MANTIS lncRNA (**Left**), U12 snRNA (**Middle**), and MEG3 lncRNA (**Right**) binding to complexes RNA immunoprecipitated with IgG, anti-BRG1, anti-SMARCA5, and anti-H3 were measured with qRT-PCR. The binding was analyzed relative to the input. Log2 values are shown. n=6. One-way ANOVA, Bonferroni. **G**, MANTIS lncRNA (**Left**), U12 snRNA (**Middle**), and MEG3 lncRNA (**Right**) binding to complexes RNA-chromatin immunoprecipitated with IgG, anti-BRG1, anti-SMARCA5, and anti-H3 were measured with qRT-PCR. The binding was analyzed relative to the input. Log10 values are shown. n=6. One-way ANOVA, Bonferroni. Error bars are defined as mean ± SEM. \**P*<0.05. ANOVA indicates analysis of variance; DAPI, 4',6-diamidino-2-phenylindole; ESI-MS/MS, electrospray ionization-tandem mass spectrometry; HUVEC, human umbilical vein endothelial cell; lncRNA, long noncoding RNA; qRT-PCR, quantitative real-time polymerase chain reaction; SEM, standard error of the mean; and SWI/SNF, switch/sucrose nonfermentable.

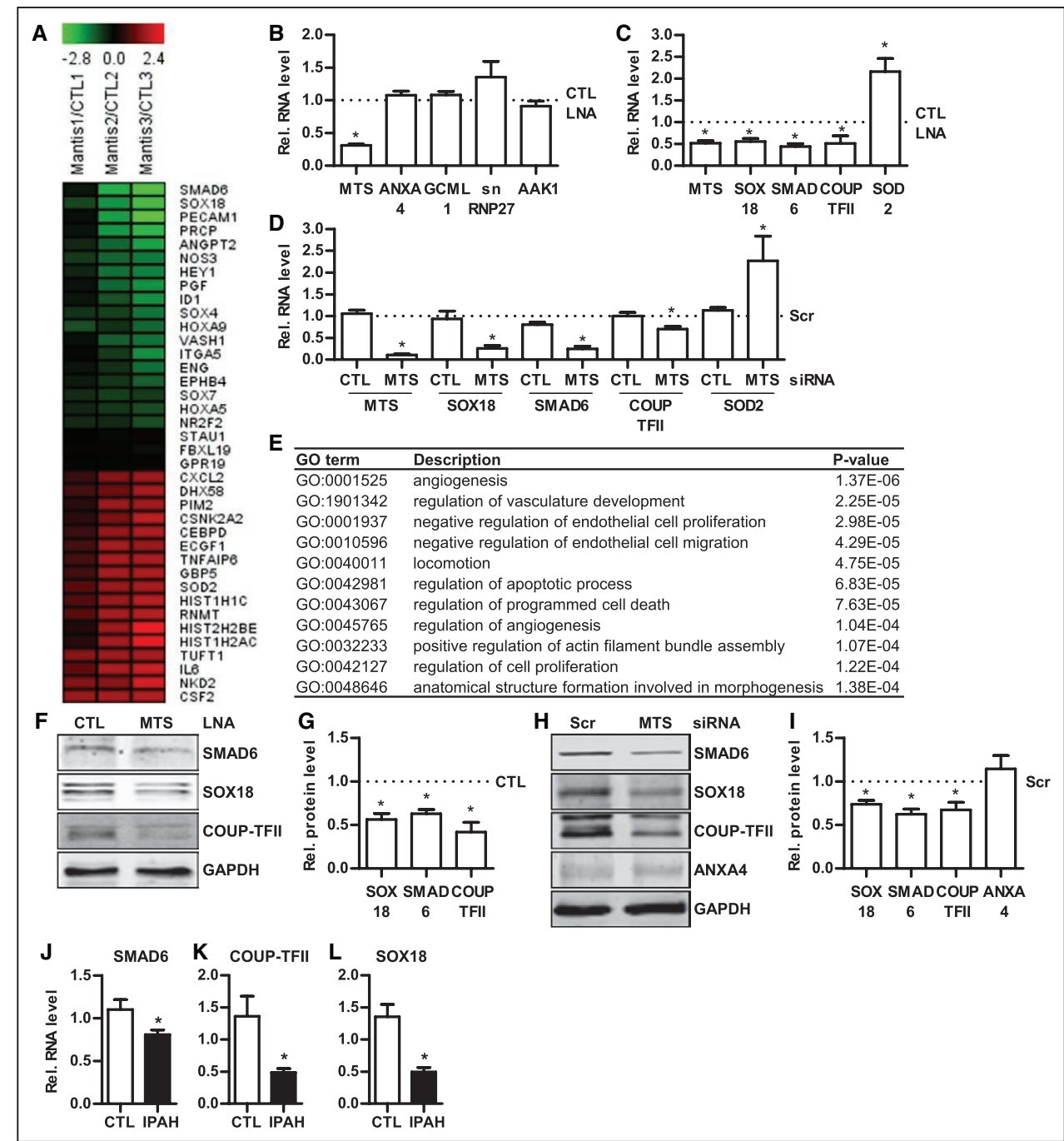


**Figure 3. LncRNA MANTIS is required for SMAD6, COUP-TFII, and SOX18 expression.**  
**A**, Illumina Bead-Chip Array heat map comparing gene expression after MANTIS LNA-GapmeR versus Control LNA-GapmeR treatments for 48 hours. Scale bar shows color code from -2.8 (green) to 2.4 (red) log2 fold change. Only representative genes were shown. **B**, qRT-PCR after LNA-GapmeR knockdown of MANTIS lncRNA. Expression levels of MANTIS, ANXA4, GCML1, snRNP27, and AAK1 are shown. CTL LNA served as negative control and was set to 1. n=4, Paired *t* test. **C**, qRT-PCR after LNA-GapmeR based knockdown of MANTIS lncRNA. CTL served as negative control and was set to 1. Expression levels of MANTIS, SOX18, SMAD6, COUP-TFII, and SOD2 are shown. n=6. Paired *t* test. **D**, qRT-PCR after knockdown of MANTIS lncRNA with siRNA-1. Scrambled siRNA (Scr) and MANTIS siRNA-specific control siRNA (CTL) served as negative controls. Expression levels of MANTIS, SOX18, SMAD6, COUP-TFII, and SOD2 are shown. Scr was set to 1. n=7. One-way ANOVA, Bonferroni. **E**, Gene ontology (GO) analyses made with Gorilla using all significantly downregulated genes after MANTIS knockdown found in the array. **F**, Representative Western blot of HUVECs treated either with control or MANTIS LNA-GapmeRs. SMAD6, SOX18, and COUP-TFII antibodies were used. GAPDH served as control. **G**, Quantification of blots shown in **F**. CTL was set to 1. n=3, Paired *t* test. **H**, Representative Western blot of HUVECs treated either with control or MANTIS siRNA-1. SMAD6, SOX18, COUP-TFII, and ANXA4 antibodies were used. GAPDH served as control. **I**, Quantification of blots shown (*Continued*)



rine embryonic development by customizing its promoter for the transcriptional machinery.<sup>10</sup> To address the question whether MANTIS contributes to BRG1 nucleosome-remodeling activity, an Assay for Transposase Accessible Chromatin with subsequent DNA Sequencing (ATAC-Seq) was performed. The protein level of BRG1 was not changed by MANTIS depletion (Figure 5A). ATAC-Seq analysis after MANTIS knockdown revealed less open chromatin at the transcriptional start sites (TSS) of *SMAD6*, *SOX18*, and *COUP-TFII*, whereas the *MANTIS* TSS served as control (Figure 5B, [online-only data Supplement Figure VA](#), [online-only data Supplement Table XIV](#)). The decrease in open chromatin at the TSS of *SMAD6*, *SOX18*, and *COUP-TFII* could be detected by Formaldehyde-Assisted Isolation of Regulatory Elements (FAIRE) (Figure 5C), which is an alternative to DNase I.<sup>27</sup> To characterize the nucleosome occupancy, micrococcal nuclease (MNase) digestion was performed. MNase cuts preferentially linker DNA, whereas the nucleosomal DNA is partially protected because it is insensitive for MNase digestion.<sup>27</sup> As expected, MNase digestion resulted in increased nucleosome formation at the TSS of *SMAD6*, *SOX18*, and *COUP-TFII* (Figure 5D). Because BRG1 is involved in nucleosome remodeling, MANTIS may impact the compaction of chromatin and thus provides access of RNA polymerase II to the DNA. To demonstrate this, chromatin immunoprecipitation experiments of H3K27me3, heterochromatin protein 1 $\alpha$  (HP1 $\alpha$ ), histone 3 (H3), and histone 4 (H4) were performed. On the *GAPDH* promoter no difference was observed, whereas on *SOX18* TSS, *SMAD6* TSS, and *COUP-TFII* TSS, H3K27me3 binding was increased by depletion of MANTIS (Figure 5E). For *SOX18* and *SMAD6* TSS, an additional increase of H3, H4, and HP1 $\alpha$  binding was observed, which was only partially seen for *COUP-TFII* ([online-only data Supplement Figure VB through VD](#)). Consequently, *MANTIS* depletion decreased RNA polymerase II binding near the TSS of *SMAD6*, *SOX18*, and *COUP-TFII*, but not near the *GAPDH* TSS or further upstream of the promoters of *SMAD6*, *SOX18*, and *COUP-TFII* (Figure 5F). Importantly, and causative for the previous results, depletion of MANTIS resulted in a decreased binding of BRG1 near the TSS of *SMAD6*, *SOX18*, and *COUP-TFII* (Figure 5G), substantiating the concept that the nucleosome-remodeling activity of BRG1 on the *SMAD6*, *COUP-TFII*, and *SOX18* TSS is dependent on MANTIS, which may assist proper chromatin decompaction and thus may prepare the promoters for the recruitment of the RNA polymerase II transcriptional machinery.

## By Stabilizing the Interaction Between BRG1 and BAF155, MANTIS Is Required for the ATPase Function of SWI/SNF

It is thought that the remodeling activity of BRG1 is stimulated by BAF155.<sup>28</sup> To understand the functional role of MANTIS within the SWI/SNF complex, the interactions of BRG1 with its interaction partners BAF155 and BAF53A were studied by proximity ligation assays (Figure 6A). The binding of BRG1 to BAF155 was significantly reduced by depletion of MANTIS (Figure 6B), whereas the interaction for BAF53A was not changed and LIS1 served as negative control. Vice versa, overexpression of *MANTIS* or the *MANTIS* Alu element mutant, but not C- or N-terminal *MANTIS* deletion mutants, was sufficient to increase the interaction between BRG1 and BAF155 in the proximity ligation assay (Figure 6C and 6D). Importantly, the reduced interaction of BRG1 to BAF155 after knockdown of *MANTIS* was not a consequence of decreased BAF155 or BRG1 protein expression as determined by Western blot analysis (Figure 6E). Given that *MANTIS* depletion decreased the interaction of BRG1 with BAF155 and also decreased the ability of BRG1 to bind on its target gene promoters, we measured the ATPase activity of BRG1 after the protein was immunoprecipitated from cells with and without MANTIS depletion. Importantly, BRG1 ATPase activity was drastically decreased by MANTIS knockdown (Figure 6F). These findings indicate that MANTIS improves the ATPase activity of BRG1 by stabilizing its interaction with BAF155.

## DISCUSSION

In the present study, we identified the epigenetically regulated and previously unstudied lncRNA MANTIS (n342419) to be upregulated by knockdown of JARID1B and in vascular pathologies, whereas in IPAH MANTIS was repressed. Depletion of MANTIS reduced the endothelial angiogenic function *ex vivo* and *in vivo*. Mechanistically, MANTIS acts in *trans* through the SWI/SNF chromatin-remodeling factor BRG1 for which it facilitates the interaction with angiogenic genes and with the BRG1 stimulating factor BAF155. Thus, with the present work, we establish a putative link of a lncRNA acting through a novel mechanism of transacting lncRNAs in essential epigenetic regulatory mechanisms in endothelial cells, which is misregulated in patients with IPAH and glioblastoma (Figure 7). In contrast to *cis*-acting lncRNAs, which are often found to act on neigh-

**Figure 3 Continued.** in **H**. Scr was set to 1. n=4. Paired *t* test. **J** through **L**, qRT-PCR of *SMAD6* (**J**), *COUP-TFII* (**K**), and *SOX18* (**L**) in lungs from control donors (CTL) or patients with IPAH. n=12. Unpaired *t* test. All qRT-PCRs are relative to  $\beta$ -Actin. Error bars are defined as mean  $\pm$  SEM. \**P*<0.05. CTL indicates control; HUVEC, human umbilical vein endothelial cell; IPAH, idiopathic pulmonary arterial hypertension; lncRNA, long noncoding RNA; MTS, MANTIS; qRT-PCR, quantitative real-time polymerase chain reaction; Scr, scrambled; SEM, standard error of the mean; and SOD2, superoxide dismutase 2.

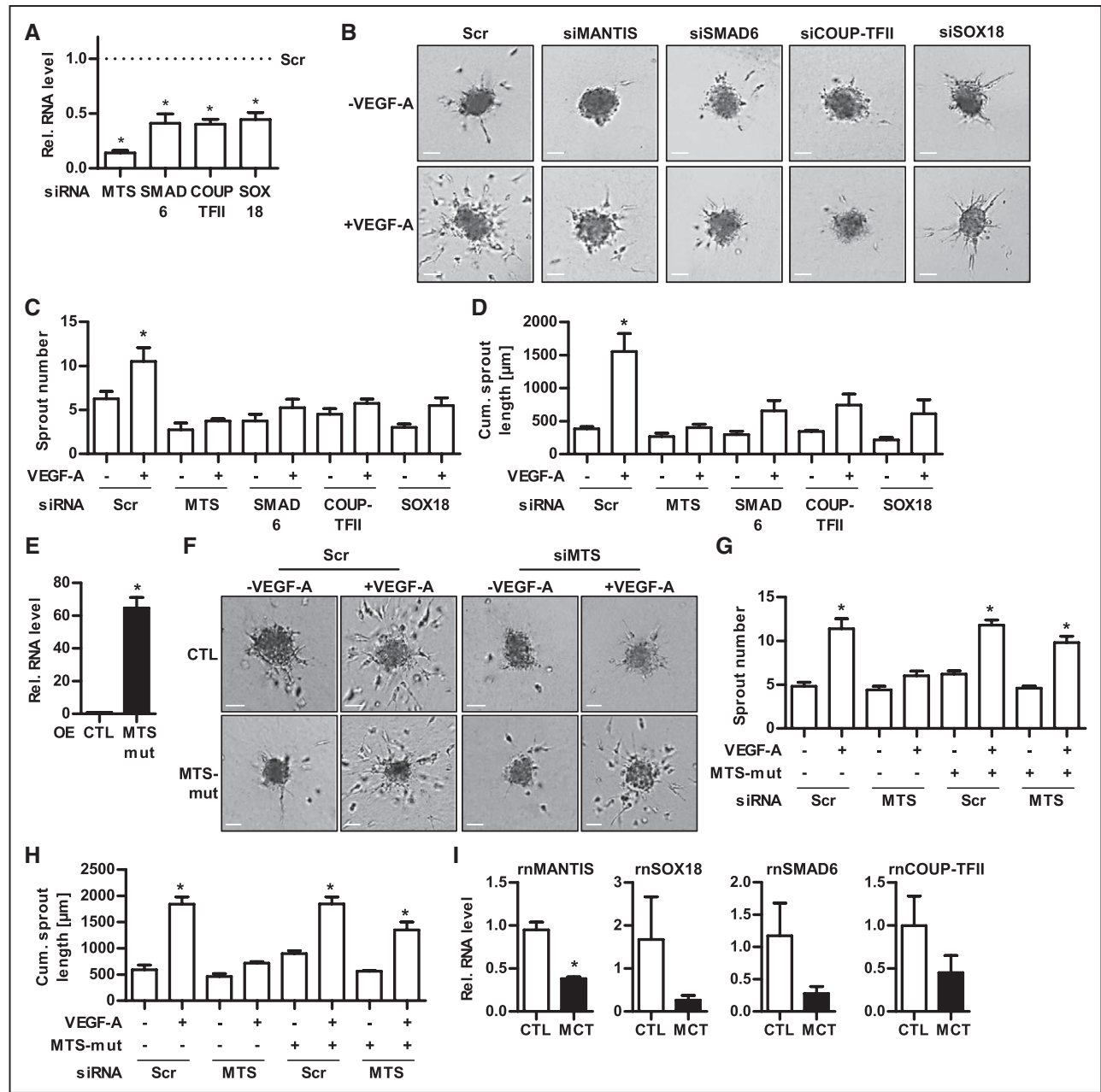


**Figure 4. SMAD6, SOX18, or COUP-TFII knockdown resemble MANTIS-deficient phenotype.**

**A**, qRT-PCR measurements after siRNA-based knockdown for 48 hours of MANTIS lncRNA (MTS), SMAD6, COUP-TFII, or SOX18. Scrambled siRNA (Scr) served as negative control and was set to 1. Expression levels of MANTIS (MTS), SMAD6, COUP-TFII, or SOX18 relative to  $\beta$ -ACTIN are shown.  $n=9$ . Paired  $t$  test. **B**, Spheroid outgrowth assay after MANTIS, SMAD6, COUP-TFII, or SOX18 siRNA-based knockdown for 48 hours. Scrambled siRNA (Scr) served as negative control. Cells treated with or without VEGF-A ( $\pm$ VEGF-A) are shown. Scale bar indicates 50  $\mu$ m. **C**, **D**, Quantifications of sprout numbers (**C**) and cumulative sprout length (**D**) from the spheroid outgrowth assays shown in **B**.  $n=4$ . One-way ANOVA, Bonferroni. **E**, qRT-PCR measurements of MANTIS-mutant (MTS-mut) after overexpression (OE) of HUVEC with CTL or MTS-mut.  $n=6$ . Paired  $t$  test. **F**, Spheroid outgrowth assay after Scrambled (Scr) or MANTIS siRNA knockdown (siMTS) with subsequent overexpression of either CTL or MTS-mut for 24 hours. Cells treated with or without VEGF-A ( $\pm$ VEGF-A) are shown. Scale bar indicates 50  $\mu$ m. **G**, **H**, Quantification of sprout numbers (**G**) and cumulative sprout length (**H**) from the spheroid outgrowth assays shown in **F**.  $n=5$ . One-way ANOVA, Bonferroni. **I**, qRT-PCR of MANTIS, SOX18, SMAD6, and COUP-TFII in PECAM-positive lung endothelial cells isolated from rats treated with saline (CTL) or monocrotaline (MCT).  $n=3$ . rn indicates *rattus norvegicus*. Unpaired  $t$  test. Error bars are defined as mean  $\pm$  SEM.  $*P<0.05$ . ANOVA indicates analysis of variance; HUVEC, human umbilical vein endothelial cell; PECAM, platelet endothelial cell adhesion molecule; qRT-PCR, quantitative real-time polymerase chain reaction; SEM, standard error of the mean; and VEGF-A, vascular endothelial growth factor A.

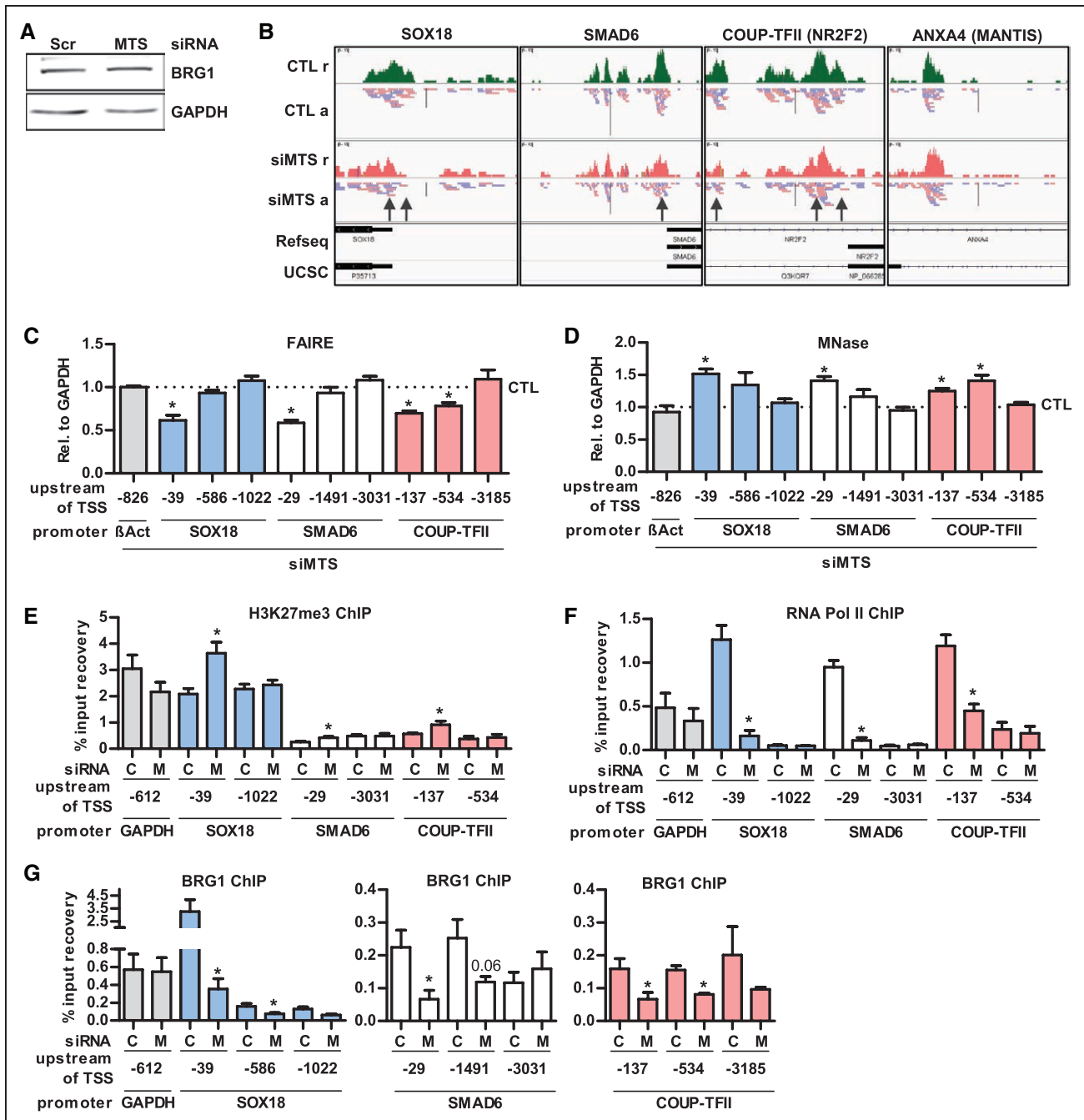


**Figure 5. MANTIS facilitates nucleosome remodeling by BRG1.**

**A**, Representative Western blot of HUVECs treated either with scrambled (Scr) or with MANTIS siRNA-1 (MTS) for 48 hours. GAPDH served as loading control. **B**, ATAC-Seq profiles of genomic loci of SOX18, SMAD6, COUP-TFII, and ANXA4 after transfection of HUVECs with scrambled (CTL) or MANTIS siRNA (siMTS) underlined with Refseq and University of California, Santa Cruz annotation. For all, number of reads ranges from 0 to 13. r indicates reads; and a, alignment. Arrows indicate regions of strong differences between CTL and siMTS. **C**, **D**, qPCR of indicated genomic loci relative to GAPDH after transfection of HUVEC with scrambled (CTL) or MANTIS siRNA (siMTS) with subsequent FAIRE (**C**) or Mnase (**D**). Numbers indicate nucleotide positions upstream of the TSS. CTL was set to 1.  $n=4$ , paired  $t$  test. **E** through **G**, ChIP of HUVECs transfected with scrambled (C) or MANTIS siRNA (M) with H3K27me3 (**E**,  $n=6$ ), RNA Pol II (**F**,  $n=3$ ), and BRG1 (**G**,  $n=4$ ) followed by qPCR for GAPDH promoter, Sox18 promoter regions at the transcription start site (TSS, -39 nt) or 586 nt and 1022 nt, SMAD6 promoter regions at the transcription start site (TSS, -29 nt) or 1491 nt and 3031 nt, and COUP-TFII promoter regions at the transcription start site (TSS, -137 nt) or 534 nt and 3185 nt. Numbers indicate nucleotide positions upstream of the TSS. Unpaired  $t$  test. Error bars are defined as mean  $\pm$  SEM.  $*P<0.05$ . ChIP indicates chromatin immunoprecipitation; FAIRE, Formaldehyde-Assisted Isolation of Regulatory Elements; HUVEC, human umbilical vein endothelial cell; MNase, micrococcal nuclease; nt, nucleotide; qPCR, quantitative polymerase chain reaction; RNA Pol II, RNA polymerase II; SEM, standard error of the mean; and TSS, transcriptional start site.



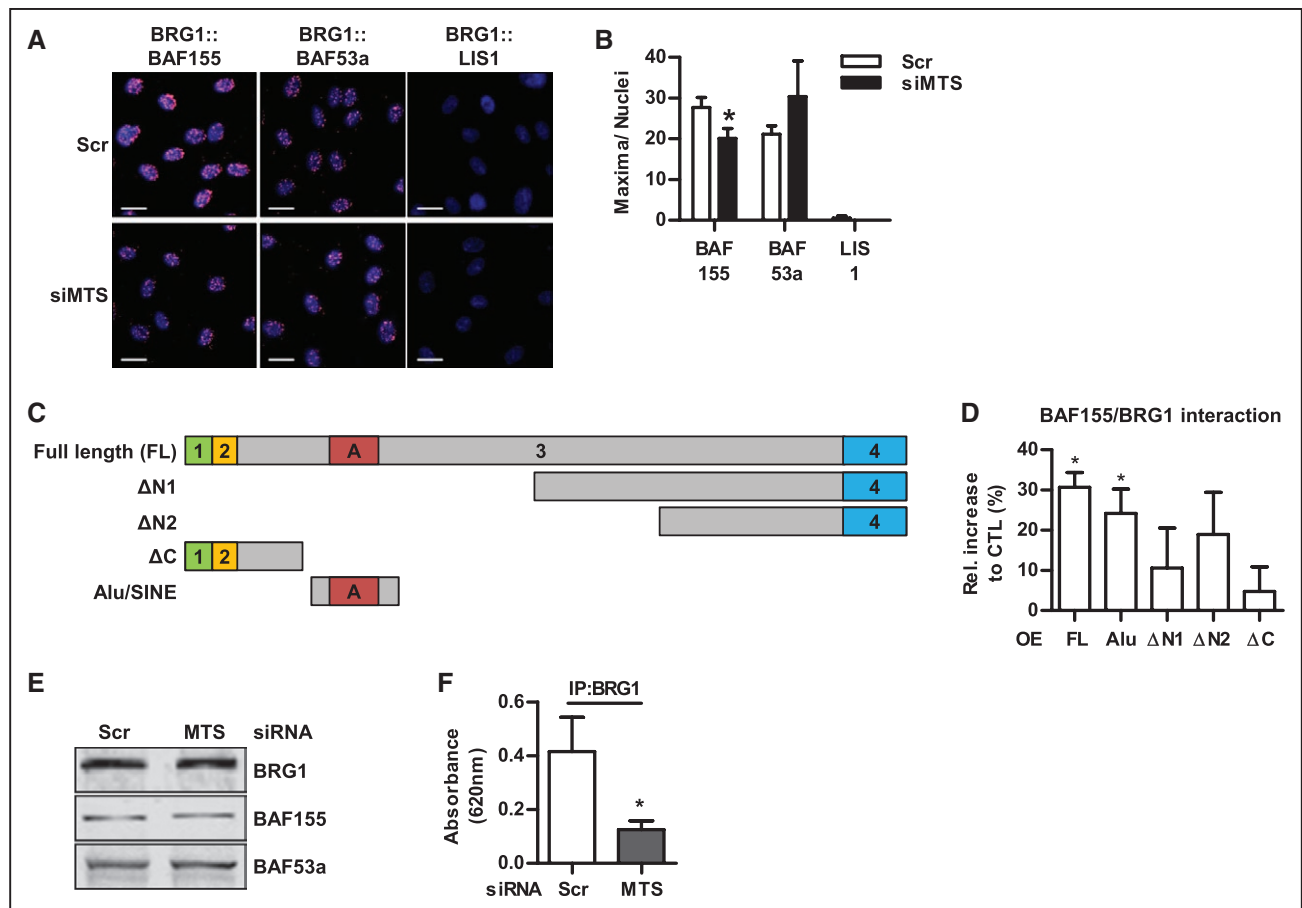


**Figure 6. MANTIS improves ATPase activity of BRG1 by stabilizing its interaction with BAF155.**

**A**, Proximity ligation assay (PLA) of HUVECs transfected with scrambled (Scr) or MANTIS siRNA-1 (siMTS) for BRG1 with BAF155, BAF53a, or LIS1. LIS1 served as negative control. Red dots indicate polymerase-amplified interaction signals. Scale bar indicates 20  $\mu$ m. **B**, Quantifications of PLA shown in **A**.  $n=3$ , Unpaired  $t$  test. Maxima indicate number of dots originating from polymerase-amplified interaction signal. **C**, Scheme of different MANTIS mutants used in **D**. Numbers indicate Exon number; A, Alu element. **D**, Relative increase of BRG1/BAF155 interaction from a PLA after overexpression of MANTIS mutants.  $n=6$ , Unpaired  $t$  test. **E**, Representative Western blot of HUVECs treated either with scrambled (Scr) or with MANTIS siRNA-1 (MTS) for 48 hours for BRG1, BAF155, and BAF53a. **F**, ATPase activity assay (absorbance at 620 nm) after BRG1 immunoprecipitation of HUVECs transfected with scrambled (Scr) or MANTIS siRNA-1 (MTS) for 48 hours.  $n=5$ , Paired  $t$  test. Error bars are defined as mean  $\pm$  SEM. \* $P<0.05$ . HUVEC indicates human umbilical vein endothelial cell.

boring gene expression by influencing RNA stability or local epigenetic processes, transacting lncRNAs typically function in miRNA sponging or regulating epigenetics in the form of scaffolding epigenetic complexes.<sup>11,29</sup> The involvement of the transacting lncRNA MANTIS in ATPase activity modulation therefore represents a novel and essential epigenetic regulatory mechanism in endothelial cells.

Expression of *Brg1* in *Tie2*<sup>+</sup> cells is critical for mouse embryonic development as yolk sac–derived blood cells from *Brg1*<sup>fl/fl</sup>:*Tie2*-Cre<sup>+/0</sup> embryos underwent apoptosis at embryonic day 9.5.<sup>30</sup> Moreover, after knockout, the yolk sac vessels exhibited failure to interconnect, which lead to dead-end vascular termini reflecting that sprouting or pruning progression failed. This supports the potential in vivo function of the proangiogenic lncRNA MANTIS. The endothelial BRG1 knockout vascu-

lar morphology could be rescued by LiCl treatment,<sup>31</sup> highlighting, on the one hand, the stabilization of the Wnt signaling molecule  $\beta$ -catenin, but, on the other hand, the importance of RNA.<sup>32</sup> Also the BAF155 homologue *Srg3*<sup>-/-</sup>*Tg*<sup>+</sup> mouse embryo yolk sacs showed poorly developed vasculatures accompanied by reduced expression of many angiogenesis-related genes.<sup>33</sup> This strengthens our hypothesis that the BRG1-BAF155 axis is required for angiogenesis-related gene expression. In this axis, our data suggest that MANTIS supports this interaction. We furthermore identified MANTIS lncRNA as dependent on the histone demethylase JARID1B. JARID1B, which is known to have a great overlap on target genes with polycomb proteins in embryonic stem cells, has been shown to function in the control of developmental processes like retina and eye development, neural differentiation, and respiratory failure.<sup>4,34</sup> Devel-

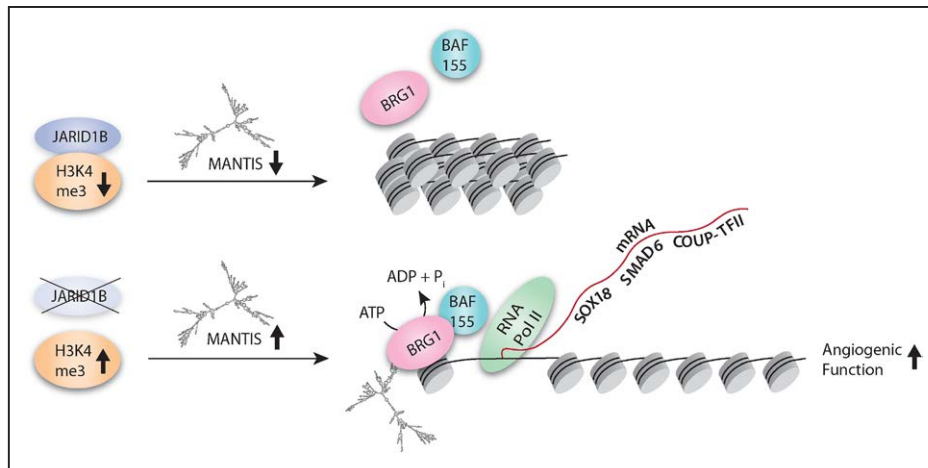


**Figure 7. Model of mechanism of action for the lncRNA MANTIS.**

**Upper,** MANTIS lncRNA expression is controlled by the histone demethylase JARID1B. Because of the limited expression of MANTIS, BRG1 and BAF155 assembly is decreased, leading to more heterochromatin formation at the TSS of *SOX18*, *SMAD6*, and *COUP-TFII*, limiting RNA Pol II binding and transcription of those genes. **Lower,** In case of JARID1B knockdown, H3K4me3 levels arise at the TSS of MANTIS, allowing more MANTIS expression. MANTIS interacts with BRG1, allowing increased binding of BAF155, which leads to a higher ATPase activity of BRG1 and euchromatin formation at the TSS of *SOX18*, *SMAD6*, and *COUP-TFII* allowing RNA Pol II binding and thereby transcription of *SOX18*, *SMAD6*, and *COUP-TFII*, which leads to increased angiogenic function. lncRNA indicates long noncoding RNA; RNA Pol II, RNA polymerase II; and TSS, transcriptional start site.

opmental importance was also shown for the knockout mice of the PRC2 components Suz12<sup>9</sup> and the endothelium-specific deletion of *Jarid2*, which led to cardiac defects.<sup>35</sup> MANTIS could serve here as a stimulus of BRG1 function to compensate the loss of JARID1B.

We identify the endothelial genes *SOX18*, *SMAD6*, and *COUP-TFII* as targets of MANTIS. These genes are known to be important in angiogenesis,<sup>23,36,37</sup> eg, (1) *SOX18* induced adipose-derived stromal cells with an endothelial phenotype involved in vascular patterning,<sup>36</sup> (2) *SMAD6* gene knockout led to cardiovascular defects,<sup>38</sup> and (3) deletion of *COUP-TFII* was embryonically lethal and caused impaired angiogenesis, abnormal heart development, and aberrant formations of the vasculature.<sup>39</sup> We explored how MANTIS collectively regulated these angiogenesis-related genes. BRG1 is known to be a critical regulator of *COUP-TFII* expression in the cardiovascular system.<sup>10,20</sup> Our data confirm this finding, but also demonstrate that BRG1 acts on *SOX18* and *SMAD6*. MANTIS directly interacts with BRG1, and increases its ATPase activity by promoting BAF155 interaction. Genome-wide effects could be identified by endothelial ATAC-Seq. Thus, MANTIS appears to keep the SWI/SNF complex intact and preserve the catalytic activity of BRG1. Indeed, loss of BRG1 binding on target gene promoters consistently correlated with a decrease of mRNA expression of these target genes after MANTIS knockdown. Even in the rat MCT model, where the putative homologous MANTIS in the form of its regulatory SINE B1 was reduced, the expression of these target genes tended to be reduced. Together with endothelial-specific deletion of BRG1 leading to

amelioration of pulmonary hypertension,<sup>40</sup> this finding suggests a critical role of the MANTIS-BRG1 axis in endothelial dysfunction, and offers a potential therapeutic option for pulmonary hypertension and glioblastoma. In case of pulmonary hypertension, several structural changes in the pulmonary arteries (loss of the distal pulmonary vasculature (vascular pruning), development of neointima and plexiform lesions, and remodeling of the distal pulmonary arteries contribute to the development and progression. Moreover, Masri et al<sup>41</sup> demonstrated that cells from the IPAH patients are impaired in their ability to form tube-like structures in culture, and this may be responsible for their inability to reconstitute the lost distal pulmonary vascular bed. This phenotype copies the results of MANTIS knockdown in endothelial cells. Quite the opposite situation is present in glioblastoma. In the endothelium of these tumors, expression of MANTIS is high, and a highly angiogenic situation is present in glioblastoma. Vessels show defective endothelium and abnormal morphology by, eg, dilatation, disorganization, and high permeability, which is a consequence of high levels of vascular endothelial growth factor A.<sup>42,43</sup> On this basis, it is attractive to speculate that MANTIS could be exploited to alter angiogenesis in patients.

Upregulation of MANTIS in Macaca aortae in the regression phase after atherosclerotic diet could imply an involvement of this lncRNA in vascular regeneration. Because MANTIS depletion affected several angiogenesis-relevant genes, it is unclear whether other target genes from the microarray experiment are directly dependent on MANTIS and the SWI/SNF complex.

The interaction between BRG1 and BAF155 has been demonstrated to increase ATPase activity of BRG1.<sup>28</sup> BAF155, however, was not identified as an interaction partner of MANTIS. Therefore, we speculate that MANTIS enhances the affinity of BRG1 to bind to BAF155 through binding to another so-far-unknown BAF155 recruiting factor. Such a protein could be GPATCH4, whose G-Patch domain is known to mediate RNA-protein interactions. Another possibility involves structural changes of BRG1 after MANTIS binding to enhance BAF155 binding affinity or to allow amino acid modifications. These could in turn enhance BRG1s affinity to bind to BAF155, possibly by the action of the MANTIS Alu element. In respect to BRG1 ATPase function, it has been reported that the lncRNA *EVF2* directly inhibits the ATPase and chromatin-remodeling activity of BRG1.<sup>44</sup> A similar inhibiting function on BRG1 could be found for the lncRNA *Myheart* (Mhrt). Mhrt was identified to inhibit myopathy and chromatin remodelers.<sup>45</sup> In ventricles of mouse hearts, Mhrt interacts with the helicase domain of BRG1, thereby repressing chromatin target recognition of BRG1. It is notable that BRG1 itself represses the expression of Mhrt. Although *EVF2* and Mhrt were predominantly studied in mice, and assuming that their function is conserved and that gene expression of them is given to a certain extent in the individual cells, they could represent counterparts to the BRG1 promoting lncRNA MANTIS. However, one can speculate that the SWI/SNF complex assembly is different from cell type to cell type. The current report of a facilitation of ATPase function is, however, novel. MANTIS appears to mediate this effect through a scaffolding function in SWI/SNF.

Taken together, these findings suggest that MANTIS lncRNA plays a significant and unique role for endothelial cell function by acting as a scaffolding lncRNA within a chromatin-remodeling complex, mediating and directing efficient key endothelial gene transcription.

## ACKNOWLEDGMENTS

The authors thank Chantal Sarah Hagège for helpful comments on the study and Cindy F. Höper for excellent technical assistance. The authors are grateful for Natascha Wilker, Tanja Lüneburg, Katalin Pálfi, Carmen Homberger, and Susanne Schütz for help with cell culture and animal experiments, Christoph Kruse for support with the laser scanning microscope, Claudia Koch for visualization of the summary figure, and Igor Ulitsky for help with evolutionary comparison studies. Dr Mittelbronn thanks the Luxembourg National Research Fond (FNR) for the support (FNR PEARL P16/BM/11192868 grant).

## SOURCES OF FUNDING

This work was supported by the German Research Foundation (DFG SFB 834 TP A1, TP B9, and SFB 1039 TP A1, SFB 815

TP Z1, EX147 "ECCPS"), the German Center of Cardiovascular Research (DZHK), and Goethe-University.

## DISCLOSURES

None.

## AFFILIATIONS

From Institute for Cardiovascular Physiology (M.S.L., C.F., I.J., M.J.M., J.E., F.M., R.P.B.), Functional Proteomics, SFB 815 Core Unit, Faculty of Medicine (F.M.R., J.H., I.W.), Institute of Vascular Signalling (J.H.), Institute of Cardiovascular Regeneration (P.H. Y.P., S.U., K.S., R.A.B., S.D.), Department of Neurosurgery (T.M.F.), Pharmazentrum Frankfurt, Institute of General Pharmacology and Toxicology (K.D.), Goethe University, Germany; ECCPS Bioinformatics and Sequencing Facility (J.P., S.G., C.K., M.L.) and Department of Lung Development and Remodeling (C.V., S.S.P.), Max-Planck-Institute for Heart and Lung Research, Bad Nauheim, Germany; Institute of Neurology (K.H.P., M.M., K.D.); Department of Vascular and Endovascular Surgery, Klinikum Rechts der Isar, Technical University Munich, Germany (L.M.); Luxembourg Centre of Neuropathology (M.M.); Laboratoire National de Santé, Dudelange, Luxembourg (M.M.); Luxembourg Centre for Systems Biomedicine, University of Luxembourg, Esch-sur-Alzette (M.M.); NORLUX Neuro-Oncology Laboratory, Department of Oncology, Luxembourg Institute of Health (M.M.); Cardiovascular Innovation Institute, University of Louisville, KY (S.U.); Department of Internal Medicine, Member of the German Center for Lung Research (DZL), Justus-Liebig University, Giessen, Germany (R.T.S., N.W., S.S.P.); Department of Medicine, Duke University and Durham VA Medical Center, NC (F.J.M.); and German Center of Cardiovascular Research (DZHK), Partner Site RheinMain, Frankfurt, Germany (M.S.L., C.F., I.J., J.H., J.E., P.H., F.M., Y.P., K.H.P., K.S., I.W., R.A.B., S.D., R.P.B.).

## FOOTNOTES

Received December 20, 2016; accepted March 17, 2017.

The online-only Data Supplement is available with this article at <http://circ.ahajournals.org/lookup/suppl/doi:10.1161/CIRCULATIONAHA.116.026991/-DC1>.

*Circulation* is available at <http://circ.ahajournals.org>.

## REFERENCES

1. Deanfield JE, Halcox JP, Rabelink TJ. Endothelial function and dysfunction: testing and clinical relevance. *Circulation*. 2007;115:1285–1295. doi: 10.1161/CIRCULATIONAHA.106.652859.
2. Kidder BL, Hu G, Zhao K. KDM5B focuses H3K4 methylation near promoters and enhancers during embryonic stem cell self-renewal and differentiation. *Genome Biol*. 2014;15:R32. doi: 10.1186/gb-2014-15-2-r32.
3. Benayoun BA, Pollina EA, Ucar D, Mahmoudi S, Karra K, Wong ED, Devarajan K, Daugherty AC, Kundaje AB, Mancini E, Hitz BC, Gupta R, Rando TA, Baker JC, Snyder MP, Cherry JM, Brunet A. H3K4me3 breadth is linked to cell identity and transcriptional consistency. *Cell*. 2014;158:673–688.
4. Fork C, Gu L, Hitzel J, Josipovic I, Hu J, SzeKa Wong M, Ponomareva Y, Albert M, Schmitz SU, Uchida S, Fleming I, Helin K, Steinhilber D, Leisegang MS, Brandes RP. Epigenetic regulation of angiogenesis by



- JARID1B-induced repression of HOXA5. *Arterioscler Thromb Vasc Biol.* 2015;35:1645–1652. doi: 10.1161/ATVBAHA.115.305561.
5. Neri F, Incarnato D, Krepelova A, Dettori D, Rapelli S, Maldotti M, Parlato C, Anselmi F, Galvagni F, Oliviero S. TET1 is controlled by pluripotency-associated factors in ESCs and downmodulated by PRC2 in differentiated cells and tissues. *Nucleic Acids Res.* 2015;43:6814–6826. doi: 10.1093/nar/gkv392.
  6. Fish JE, Yan MS, Matouk CC, St Bernard R, Ho JJ, Ho JJ Jr, Gavryushova A, Srivastava D, Marsden PA. Hypoxic repression of endothelial nitric-oxide synthase transcription is coupled with eviction of promoter histones. *J Biol Chem.* 2010;285:810–826. doi: 10.1074/jbc.M109.067868.
  7. Edelstein LC, Pan A, Collins T. Chromatin modification and the endothelial-specific activation of the E-selectin gene. *J Biol Chem.* 2005;280:11192–11202. doi: 10.1074/jbc.M412997200.
  8. Bultman S, Gebuhr T, Yee D, La Mantia C, Nicholson J, Gilliam A, Randazzo F, Metzger D, Chambon P, Crabtree G, Magnuson T. A Brg1 null mutation in the mouse reveals functional differences among mammalian SWI/SNF complexes. *Mol Cell.* 2000;6:1287–1295.
  9. Pasini D, Bracken AP, Hansen JB, Capillo M, Helin K. The polycomb group protein Suz12 is required for embryonic stem cell differentiation. *Mol Cell Biol.* 2007;27:3769–3779. doi: 10.1128/MCB.01432-06.
  10. Davis RB, Curtis CD, Griffin CT. BRG1 promotes COUP-TFII expression and venous specification during embryonic vascular development. *Development.* 2013;140:1272–1281. doi: 10.1242/dev.087379.
  11. Lee JT. Epigenetic regulation by long noncoding RNAs. *Science.* 2012;338:1435–1439. doi: 10.1126/science.1231776.
  12. Mattick JS, Rinn JL. Discovery and annotation of long noncoding RNAs. *Nat Struct Mol Biol.* 2015;22:5–7. doi: 10.1038/nsmb.2942.
  13. Uchida S, Dimmeler S. Long noncoding RNAs in cardiovascular diseases. *Circ Res.* 2015;116:737–750. doi: 10.1161/CIRCRESAHA.116.302521.
  14. Savai R, Al-Tamari HM, Sedding D, Kojonazarov B, Muecke C, Teske R, Capechchi MR, Weissmann N, Grimminger F, Seeger W, Schermuly RT, Pullamsetti SS. Pro-proliferative and inflammatory signaling converge on FoxO1 transcription factor in pulmonary hypertension. *Nat Med.* 2014;20:1289–1300. doi: 10.1038/nm.3695.
  15. Hathaway CA, Heistad DD, Piegors DJ, Miller FJ Jr. Regression of atherosclerosis in monkeys reduces vascular superoxide levels. *Circ Res.* 2002;90:277–283.
  16. Calviello L, Mukherjee N, Wyler E, Zauber H, Hirsekorn A, Selbach M, Landthaler M, Obermayer B, Ohler U. Detecting actively translated open reading frames in ribosome profiling data. *Nat Methods.* 2016;13:165–170. doi: 10.1038/nmeth.3688.
  17. Wang L, Park HJ, Dasari S, Wang S, Kocher JP, Li W. CPAT: coding-potential assessment tool using an alignment-free logistic regression model. *Nucleic Acids Res.* 2013;41:e74. doi: 10.1093/nar/gkt006.
  18. Rabinovitch M. Molecular pathogenesis of pulmonary arterial hypertension. *J Clin Invest.* 2012;122:4306–4313. doi: 10.1172/JCI60658.
  19. Zhou J, Zhang M, Fang H, El-Mounayri O, Rodenberg JM, Imbalzano AN, Herring BP. The SWI/SNF chromatin remodeling complex regulates myocardin-induced smooth muscle-specific gene expression. *Arterioscler Thromb Vasc Biol.* 2009;29:921–928. doi: 10.1161/ATVBAHA.109.187229.
  20. Wang S, Zhang X, Yuan Y, Tan M, Zhang L, Xue X, Yan Y, Han L, Xu Z. BRG1 expression is increased in thoracic aortic aneurysms and regulates proliferation and apoptosis of vascular smooth muscle cells through the long non-coding RNA HIF1A-AS1 *in vitro*. *Eur J Cardiothorac Surg.* 2015;47:439–446. doi: 10.1093/ejcts/ezu215.
  21. Varga-Weisz PD. Chromatin remodeling: a collaborative effort. *Nat Struct Mol Biol.* 2014;21:14–16. doi: 10.1038/nsmb.2748.
  22. Nakagawa S, Kageyama Y. Nuclear lncRNAs as epigenetic regulators-beyond skepticism. *Biochim Biophys Acta.* 2014;1839:215–222. doi: 10.1016/j.bbagr.2013.10.009.
  23. Park C, Kim TM, Malik AB. Transcriptional regulation of endothelial cell and vascular development. *Circ Res.* 2013;112:1380–1400. doi: 10.1161/CIRCRESAHA.113.301078.
  24. Chang TH, Huang HY, Hsu JB, Weng SL, Horng JT, Huang HD. An enhanced computational platform for investigating the roles of regulatory RNA and for identifying functional RNA motifs. *BMC Bioinformatics.* 2013;14(suppl 2):S4. doi: 10.1186/1471-2105-14-S2-S4.
  25. Gomez-Arroyo JG, Farkas L, Alhussaini AA, Farkas D, Kraskauskas D, Voelkel NF, Bogaard HJ. The monocrotaline model of pulmonary hypertension in perspective. *Am J Physiol Lung Cell Mol Physiol.* 2012;302:L363–L369. doi: 10.1152/ajplung.00212.2011.
  26. Fan HY, Trotter KW, Archer TK, Kingston RE. Swapping function of two chromatin remodeling complexes. *Mol Cell.* 2005;17:805–815. doi: 10.1016/j.molcel.2005.02.024.
  27. Meyer CA, Liu XS. Identifying and mitigating bias in next-generation sequencing methods for chromatin biology. *Nat Rev Genet.* 2014;15:709–721. doi: 10.1038/nrg3788.
  28. Phelan ML, Sif S, Narlikar GJ, Kingston RE. Reconstitution of a core chromatin remodeling complex from SWI/SNF subunits. *Mol Cell.* 1999;3:247–253.
  29. Mercer TR, Mattick JS. Structure and function of long noncoding RNAs in epigenetic regulation. *Nat Struct Mol Biol.* 2013;20:300–307. doi: 10.1038/nsmb.2480.
  30. Griffin CT, Brennan J, Magnuson T. The chromatin-remodeling enzyme BRG1 plays an essential role in primitive erythropoiesis and vascular development. *Development.* 2008;135:493–500. doi: 10.1242/dev.010090.
  31. Curtis CD, Griffin CT. The chromatin-remodeling enzymes BRG1 and CHD4 antagonistically regulate vascular Wnt signaling. *Mol Cell Biol.* 2012;32:1312–1320. doi: 10.1128/MCB.06222-11.
  32. Nilsen TW. Selective precipitation of large RNAs. *Cold Spring Harb Protoc.* 2012;12:1302–1303. doi: 10.1101/pdb.prot072322.
  33. Han D, Jeon S, Sohn DH, Lee C, Ahn S, Kim WK, Chung H, Seong RH. SRG3, a core component of mouse SWI/SNF complex, is essential for extra-embryonic vascular development. *Dev Biol.* 2008;315:136–146. doi: 10.1016/j.ydbio.2007.12.024.
  34. Albert M, Schmitz SU, Kooistra SM, Malatesta M, Morales Torres C, Reikling JC, Johansen JV, Abarrategui I, Helin K. The histone demethylase Jarid1b ensures faithful mouse development by protecting developmental genes from aberrant H3K4me3. *PLoS Genet.* 2013;9:e1003461. doi: 10.1371/journal.pgen.1003461.
  35. Mysliwiec MR, Bresnick EH, Lee Y. Endothelial Jarid2/Jumonji is required for normal cardiac development and proper Notch1 expression. *J Biol Chem.* 2011;286:17193–17204. doi: 10.1074/jbc.M110.205146.
  36. Fontijn RD, Favre J, Naaijken BA, Meinster E, Pauw NJ, Ragghoe SL, Nauta TD, van den Broek MA, Weijers EM, Niessen HW, Koolwijk P, Horrevorts AJ. Adipose tissue-derived stromal cells acquire endothelial-like features upon reprogramming with SOX18. *Stem Cell Res.* 2014;13(3 pt A):367–378. doi: 10.1016/j.scr.2014.09.004.
  37. Topper JN, Cai J, Qiu Y, Anderson KR, Xu YY, Deeds JD, Feeley R, Gimeno CJ, Woolf EA, Tayber O, Mays GG, Sampson BA, Schoen FJ, Gimbrone MA Jr, Falb D. Vascular MADs: two novel MAD-related genes selectively inducible by flow in human vascular endothelium. *Proc Natl Acad Sci USA.* 1997;94:9314–9319.
  38. Galvin KM, Donovan MJ, Lynch CA, Meyer RI, Paul RJ, Lorenz JN, Fairchild-Huntress V, Dixon KL, Dunmore JH, Gimbrone MA Jr, Falb D, Huszar D. A role for smad6 in development and homeostasis of the cardiovascular system. *Nat Genet.* 2000;24:171–174. doi: 10.1038/72835.
  39. Pereira FA, Qiu Y, Zhou G, Tsai MJ, Tsai SY. The orphan nuclear receptor COUP-TFII is required for angiogenesis and heart development. *Genes Dev.* 1999;13:1037–1049.
  40. Chen D, Fang F, Yang Y, Chen J, Xu G, Xu Y, Gao Y. Brahma-related gene 1 (Brg1) epigenetically regulates CAM activation during hypoxic pulmonary hypertension. *Cardiovasc Res.* 2013;100:363–373. doi: 10.1093/cvr/cvt214.
  41. Masri FA, Xu W, Comhair SA, Asosingh K, Koo M, Vasanji A, Drazba J, Anand-Apte B, Erzurum SC. Hyperproliferative apoptosis-resistant endothelial cells in idiopathic pulmonary arterial hypertension. *Am J Physiol Lung Cell Mol Physiol.* 2007;293:L548–L554. doi: 10.1152/ajplung.00428.2006.
  42. Jain RK, di Tomaso E, Duda DG, Loeffler JS, Sorensen AG, Batchelor TT. Angiogenesis in brain tumours. *Nat Rev Neurosci.* 2007;8:610–622. doi: 10.1038/nrn2175.
  43. Plate KH, Breier G, Weich HA, Risau W. Vascular endothelial growth factor is a potential tumour angiogenesis factor in human gliomas in vivo. *Nature.* 1992;359:845–848. doi: 10.1038/359845a0.
  44. Cajigas I, Leib DE, Cochrane J, Luo H, Swyter KR, Chen S, Clark BS, Thompson J, Yates JR 3rd, Kingston RE, Kohtz JD. Ebf2 lncRNA/BRG1/DLX1 interactions reveal RNA-dependent inhibition of chromatin remodeling. *Development.* 2015;142:2641–2652. doi: 10.1242/dev.126318.
  45. Han P, Li W, Lin CH, Yang J, Shang C, Nurnberg ST, Jin KK, Xu W, Lin CJ, Lin CJ, Xiong Y, Chien HC, Zhou B, Ashley E, Bernstein D, Chen PS, Chen HS, Quertermous T, Chang CP. A long noncoding RNA protects the heart from pathological hypertrophy. *Nature.* 2014;514:102–106. doi: 10.1038/nature13596.

## Long Noncoding RNA MANTIS Facilitates Endothelial Angiogenic Function

Matthias S. Leisegang, Christian Fork, Ivana Josipovic, Florian Martin Richter, Jens Preussner, Jiong Hu, Matthew J. Miller, Jeremy Epah, Patrick Hofmann, Stefan Günther, Franziska Moll, Chanil Valasarajan, Juliana Heidler, Yuliya Ponomareva, Thomas M. Freiman, Lars Maegdefessel, Karl H. Plate, Michel Mittelbronn, Shizuka Uchida, Carsten Küne, Konstantinos Stellos, Ralph T. Schermuly, Norbert Weissmann, Kavi Devraj, Ilka Wittig, Reinier A. Boon, Stefanie Dimmeler, Soni Savai Pullamsetti, Mario Looso, Francis J. Miller, Jr. and Ralf P. Brandes

*Circulation*. 2017;136:65-79; originally published online March 28, 2017;  
doi: 10.1161/CIRCULATIONAHA.116.026991

*Circulation* is published by the American Heart Association, 7272 Greenville Avenue, Dallas, TX 75231  
Copyright © 2017 American Heart Association, Inc. All rights reserved.  
Print ISSN: 0009-7322. Online ISSN: 1524-4539

The online version of this article, along with updated information and services, is located on the  
World Wide Web at:

<http://circ.ahajournals.org/content/136/1/65>

Free via Open Access

Data Supplement (unedited) at:

<http://circ.ahajournals.org/content/suppl/2017/03/28/CIRCULATIONAHA.116.026991.DC1>

**Permissions:** Requests for permissions to reproduce figures, tables, or portions of articles originally published in *Circulation* can be obtained via RightsLink, a service of the Copyright Clearance Center, not the Editorial Office. Once the online version of the published article for which permission is being requested is located, click Request Permissions in the middle column of the Web page under Services. Further information about this process is available in the [Permissions and Rights Question and Answer](#) document.

**Reprints:** Information about reprints can be found online at:  
<http://www.lww.com/reprints>

**Subscriptions:** Information about subscribing to *Circulation* is online at:  
<http://circ.ahajournals.org/subscriptions/>

# Supplemental Material

## Long noncoding RNA MANTIS facilitates endothelial angiogenic function

Matthias S. Leisegang, PhD<sup>1,18</sup>, Christian Fork, PhD<sup>1,18</sup>, Ivana Josipovic, MSc<sup>1,18</sup>, Florian Martin Richter, PhD<sup>2</sup>, Jens Preussner, MSc<sup>3</sup>, Jiong Hu, PhD<sup>4,18</sup>, Matthew J. Miller, MSc<sup>1</sup>, Jeremy Epah<sup>1,18</sup>, Patrick Hofmann, MSc<sup>5,18</sup>, Stefan Günther, PhD<sup>3</sup>, Franziska Moll, MSc<sup>1,18</sup>, Chanil Valasarajan, MSc<sup>16</sup>, Juliana Heidler, PhD<sup>2</sup>, Yuliya Ponomareva, MSc<sup>5,18</sup>, Thomas M. Freiman, MD<sup>6</sup>, Lars Maegdefessel, MD, PhD<sup>7</sup>, Karl H. Plate, MD<sup>8,18</sup>, Michel Mittelbronn, MD<sup>8,9,10,11,12</sup>, Shizuka Uchida, PhD<sup>5,13</sup>, Carsten Künne, PhD<sup>3</sup>, Konstantinos Stellos, MD<sup>5,18</sup>, Ralph T. Schermuly, PhD<sup>14</sup>, Norbert Weissmann, PhD<sup>14</sup>, Kavi Devraj, PhD<sup>8,15</sup>, Ilka Wittig, PhD<sup>2,18</sup>, Reinier A. Boon, PhD<sup>5,18</sup>, Stefanie Dimmeler, PhD<sup>5,18</sup>, Soni Savai Pullamsetti, PhD<sup>14,16</sup>, Mario Looso, PhD<sup>3</sup>, Francis J. Miller Jr., MD<sup>17</sup>, Ralf P. Brandes, MD<sup>1,18\*</sup>

<sup>1</sup>Institute for Cardiovascular Physiology, Goethe-University, Frankfurt, Germany;

<sup>2</sup>Functional Proteomics, SFB 815 Core Unit, Faculty of Medicine, Goethe-University, Frankfurt, Germany;

<sup>3</sup>Max-Planck-Institute for Heart and Lung Research, ECCPS Bioinformatics and Sequencing Facility, Bad Nauheim, Germany;

<sup>4</sup>Institute of Vascular Signalling, Goethe-University, Frankfurt, Germany;

<sup>5</sup>Institute of Cardiovascular Regeneration, Goethe-University, Frankfurt, Germany;

<sup>6</sup>Department of Neurosurgery, Goethe-University, Frankfurt, Germany;

<sup>7</sup>Department of Vascular and Endovascular Surgery, Klinikum rechts der Isar, Technical University Munich, Munich, Germany;

<sup>8</sup>Institute of Neurology (Edinger-Institute), Goethe-University, Frankfurt, Germany;

<sup>9</sup>Luxembourg Centre of Neuropathology (LCNP), Luxembourg;

<sup>10</sup>Laboratoire National de Santé, Dudelange, Luxembourg;

<sup>11</sup>Luxembourg Centre for Systems Biomedicine (LCSB), University of Luxembourg, Esch-sur-Alzette, Luxembourg;

<sup>12</sup>NORLUX Neuro-Oncology Laboratory, Department of Oncology, Luxembourg Institute of Health (L.I.H.), Luxembourg;

<sup>13</sup>Cardiovascular Innovation Institute, University of Louisville, Louisville, KY, USA;

<sup>14</sup>Department of Internal Medicine, Member of the German Center for Lung Research (DZL), Justus-Liebig University, Giessen, Germany;

<sup>15</sup>Pharmazentrum Frankfurt, Institute of General Pharmacology and Toxicology, Goethe-University, Frankfurt, Germany;

<sup>16</sup>Max-Planck-Institute for Heart and Lung Research, Department of Lung Development and Remodeling, Member of the German Center for Lung Research (DZL), Bad Nauheim, Germany;

<sup>17</sup>Department of Medicine, Duke University and Durham VA Medical Center, Durham, NC, USA;

<sup>18</sup>German Center of Cardiovascular Research (DZHK), Partner site RheinMain, Frankfurt, Germany;

\* corresponding author

Ralf P. Brandes, MD

Institut für Kardiovaskuläre Physiologie

Fachbereich Medizin der Goethe-Universität

Theodor-Stern Kai 7

60590 Frankfurt am Main, Germany

Tel.: +49-69-6301-6995

Fax.: +49-69-6301-7668

Email: [brandes@vrc.uni-frankfurt.de](mailto:brandes@vrc.uni-frankfurt.de)



## Supplemental Methods

### Materials.

Human recombinant VEGF-A 165 was purchased from R&D (293-VE) and human recombinant TNF- $\alpha$  was from Peprotech (300-01A). The following antibodies were used: Anti-COUP-TFII (TA324540, Origene), Anti-GAPDH (PA1-16777, Thermo Fisher), Anti-BRG1 (A300-813A, Bethyl), Anti-BAF155 (A301-021A, Bethyl), Anti-JARID1B (A301-813A, Bethyl), Anti-BAF53a (A301-391A, Bethyl), Anti-BAF60a (A301-595A, Bethyl), Anti-LIS1 (A300-409A, Bethyl), Anti-H3K27me3 (pAb-069-050, Diagenode), Anti-HP1 $\alpha$  (A300-877A, Bethyl), Anti-ANXA4 (R2053-1, Abiocode), Anti-SMARCA5 (SNF2h/ISWI, Bethyl, A301-017A-T), Anti-SOX18 (H-140, Santa Cruz), Anti-SMAD6 (ab13727, Abcam), Anti-beta-ACTIN (4970, Cell Signaling), Anti-H3-pan (C15310135, Diagenode), Anti-H4-pan (C15410156, Diagenode), Anti-PolIII (C15100055, Diagenode).

### Human lung samples and patient characteristics.

Human explanted lung tissues from subjects with IPAH or control donors were obtained during lung transplantation. Samples of donor lung tissue were taken from the lung that was not transplanted. All lungs were reviewed for pathology and the IPAH lungs were classified as grade III or IV.

### Experimental mice and light sheet microscopy.

All experimental procedures were approved by the local governmental authorities and were performed in accordance with the local animal protection guidelines. CRISPR/Cas9 HUVEC and control HUVEC were stained with Vybrant Dil Cell-Labeling solution (V-22885, Thermo Fisher) and embedded as spheroids into matrigel and injected into SCID-Mice similar as described previously by others<sup>1</sup>. After 26 days, Isolectin GS-IB<sub>4</sub> from *Griffonia simplicifolia*, Alexa Fluor® 647 Conjugate (I32450, Thermo Fisher) was injected via the tail vein and was allowed to circulate for at least 10 min. Afterwards, animals were killed and perfused transcardially. The plugs were dissected and fixed in 4% Paraformaldehyde (PFA) overnight and subsequently cleared following the 3DISCO procedure<sup>2</sup>. Imaging was carried out with the Ultramicroscope II (UM-II, LaVision Biotec, Bielefeld) at 20x magnification (10 Zoom body + 2x Objective). Pictures were taken with Neo 5.5 (3-tap) sCOMs Camera (Andor, Mod.No.: DC-152q-C00-FI). The ImSpectorPro Version 5.0.110 was used. 3D Images and quantification were performed with Imaris (Bitplane Version 7.6). Auto fluorescence signals were deleted manually with the surface function. Background subtraction was done with the background subtraction algorithm (filter width = 2000 $\mu$ m). Cells were detected and counted with the Spots-Algorithm (Estimated Diameter = 10.0  $\mu$ m; Background Subtraction = true; Intensity Center Ch=3" above 720; Region Growing Type = Local Contrast). Lower threshold was chosen depending to the background signal.

### Experimental monkeys.

*Macacae fasciculari* vessels were kindly provided by one of the co-authors (FJM) and originated from <sup>3</sup>. Cynomolgus monkeys were fed either with a normal diet, an atherosclerotic diet for 47 $\pm$ 10 (mean  $\pm$  SE) months, or an atherosclerotic diet with an additional recovery/regression phase for 8 months. 500ng of RNA was reverse transcribed and expression levels of GAPDH, JARID1B and MANTIS were measured with qRT-PCR with *Macacae fascicularis* specific primers. Relative expression of target genes was normalized to GAPDH and analyzed by the delta-delta Ct method with the MxPro qPCR software (Stratagene).

#### Experimental rats, MCT treatment and isolation of lung vascular endothelial cells.

Rat studies were performed according to the guidelines of the University of Giessen and were approved by the local authorities (GI 20/10 Nr.44/2013). Adult male Sprague-Dawley rats (300-350 g body weight (BW)) were given a subcutaneous injection of saline (healthy control, n=3) or monocrotaline (MCT; 60 mg/kg BW, n=3) as described<sup>4</sup>. The BW changes and survival were monitored from 1 to 35 days for all groups.

After euthanasia by removing blood, rat lung vascular endothelial cells were isolated after explantation of the lung. The lung tissue was separated from heart, trachea and oesophagus, cut into small slices (1mm) and washed in Hank's balanced salt solution (HBSS, without CaCl<sub>2</sub>, MgCl<sub>2</sub>) to remove remaining blood. Minced tissues were transferred in sterile tubes containing 40ml HBSS (with CaCl<sub>2</sub> and MgCl<sub>2</sub>), 5U/ml Dispase and 20mg Dnase. Tissue was digested for 90min in a water bath with gentle shaking at 37°C. By using continuous pipetting, cells were released from the lung tissue and the residual tissue was removed by filtering the suspension through 70µm mesh filter into a tube with Medium 199 (Gibco) containing 10% FCS. The cell suspension was centrifuged at 290g for 5min at room temperature (RT). After centrifugation the cell pellet was washed with 5ml HBSS containing 0.5% BSA. The cells were resuspended in 800µl HBSS containing 0.5% BSA. For binding the mouse anti-rat CD31 (550300, BD Pharmingen) antibody to the Dynabeads M-450 Tosylactivated (14013, Invitrogen), 40µl Dynabeads were coated with 8µl of the antibody. Then the cell suspension was incubated with the antibody coupled beads in an end-over-end shaker at RT for 90min. The unbound cells were removed by washing 3 to 5 times with HBSS containing 0.5% BSA using a magnetic device (Dyna MPC-1, Invitrogen).

#### Brain microvessel isolation from glioblastoma (GBM) patients.

Fresh brain specimens were obtained from GBM patients within 3h post surgery. For patients, where the normal appearing healthy tissue was not available, healthy material was obtained from epilepsy or dementia patients or autopsy material within a day postmortem. An ethics statement covered all studies on these subjects. The ethics approval number for autopsy material is GS-249/11 and for resection material GS-04/09. Human brain microvessels (HBMV) were isolated as described previously with a few modifications<sup>5</sup>. Briefly, the specimen obtained in ice-cold microvessel buffer (MVB, 15mM HEPES, 147mM NaCl, 4mM KCl, 3mM CaCl<sub>2</sub>, 1.2mM MgCl<sub>2</sub>, 5mM glucose and 0.5% BSA, pH 7.4) was cleared of blood and any meningeal tissue using forceps. The tissue was homogenized in 3-fold ice-cold MVB buffer by 15 up and down strokes in a tight-fitting douncer (0.25 mm clearance, 10ml Wheaton) attached to an electrical overhead stirrer (2000 rpm, VOS 14, VWR). After centrifugation of the homogenate (400xg, 10 min, 4°C), the pellet was resuspended in 4-fold 25% BSA (in PBS) followed by centrifugation (2000xg, 30 min, 4°C). Myelin fat appearing in the top buoyant layer after the centrifugation was aspirated. The pellet was resuspended in 3ml ice-cold MVB (per gram) of the starting material. The resuspended microvessels were filtered through 100-micron sterile nylon mesh cell strainer (BD) to remove large vessels and tissue aggregates. The filtrate was further applied to 40-micron sterile nylon mesh (BD) to trap the microvessels and to remove platelets, cell debris and nuclei as filtrate. After washing the mesh once with ice-cold MVB, microvessels were lysed directly on the mesh with ice-cold RLT-Plus RNA lysis buffer (Qiagen). The samples were vortexed for 1 min and stored at -80°C until use.

### Cell culture.

Pooled human umbilical vein endothelial cells (HUVECs) were purchased from Lonza (CC-2519, Lot No. 371074, 369146, 314457, 192485, 186864, 171772, Walkersville, MD, USA) and PELOBiotech (PB-CH-190-813, Lot No. QC-18P13F11, Planegg, Germany). Human aortic endothelial cells (HAoEC) were purchased from PeloBiotech (304K-05a). Human pulmonary artery endothelial cells (PAEC) were obtained from Promocell (C-12241, Heidelberg, Germany). HUVECs, HAoECs and PAECs were cultivated in a humidified atmosphere of 5% CO<sub>2</sub> at 37°C. To culture the cells, Fibronectin-coated (356009, Corning Incorporated, USA) dishes were used. Endothelial growth medium (EGM), consisting of endothelial basal medium (EBM) supplemented with human recombinant epidermal growth factor (EGF), EndoCGS-Heparin (PeloBiotech, Germany), 8% fetal calf serum (FCS) (S0113, Biochrom, Germany), penicillin (50 U/ml) and streptomycin (50 µg/ml) (15140-122, Gibco/Lifetechnologies, USA) was used. For HAoEC, 16% FCS was used instead of 8%. For each experiment, at least three different batches of HUVEC from passage 3 were used.

Human aortic smooth muscle cells (HAoSMC, 354-05a), human coronary artery smooth muscle cells (CASM, 350-05a) and human carotid artery smooth muscle cells (CTASM, 3514-05a) were purchased from PeloBiotech (Planegg, Germany) and cultured in a humidified atmosphere of 5% CO<sub>2</sub> at 37°C in smooth muscle cell medium (PB-MH-200-2190) supplemented with 8% FCS, penicillin (50 U/ml), streptomycin (50 µg/ml), EGF, fibroblast growth factor, glutamine, and insulin from singlequots (PeloBiotech, Planegg, Germany).

Human dermal lymphatic endothelial cells (HDLEC, #3111203.4, #394Z027.3, #4092401.3) were purchased from Promocell (Heidelberg, Germany) and cultured in a humidified atmosphere of 5% CO<sub>2</sub> at 37°C in endothelial cell growth medium MV2 (Promocell, Heidelberg, Germany).

Human foreskin fibroblasts, obtained from Gibco (Lifetechnologies, Carlsbad, CA, USA), were cultured in DMEM/F12 (#11039-021) supplemented with 10% FCS, penicillin (50 U/ml), and streptomycin (50 µg/ml) in a humidified atmosphere of 5% CO<sub>2</sub> at 37°C.

The human monocytic cell line THP-1 and cancer cell line MCF-7, obtained from ATCC (LGC Promochem, Wesel, Germany), were cultured in RPMI medium containing stable glutamine, 8% FCS and 1% penicillin/streptomycin (PAA Laboratories, Cölbe, Germany) in a humidified atmosphere of 5% CO<sub>2</sub> at 37°C.

### Knockdown and overexpression procedures.

For small interfering RNA (siRNA) treatments, endothelial cells (80–90% confluent) were transfected with GeneTrans II according to the instructions provided by MoBiTec (Göttingen, Germany). All siRNAs (Stealth RNAi) were from Invitrogen. MANTIS and MANTIS-Control (C) siRNAs were designed with the BLOCK-iT RNAi designer (Invitrogen). The siRNAs had the following sequences: MANTIS-1: 5'-AAA UGA AGC AGC CUU GUU GUC UGG G, MANTIS-1-C: AAA UCU GAA GCG ACG UUC UGU UGG G, MANTIS-2: AAC AGA AGA AGA UCC AGC AGU UAU A, MANTIS-3: UUU GAU GGA ACC UUG UUC CAU GAG G. As negative control, scrambled Stealth RNAi™ Med GC (Life technologies) was used. Other siRNAs used targeted JARID1B (stealth siRNA, HSS173871, Invitrogen), SMAD6 (stealth siRNA, HSS106261, Invitrogen), COUP-TFII (stealth siRNA, HSS110656, Invitrogen) and SOX18 (Silencer select, s195242, #4392420, Invitrogen). The siRNA knockdown started for rescue experiments 24h prior to overexpression and did not exceed 48h in total. For shear stress experiments, 24h prior to

the application of the laminar flow the transfection was performed. All other siRNA experiments were performed for 48h. Small hairpin RNA (shRNA) treatments were performed exactly as described in<sup>6</sup>. For Locked nucleic acid (LNA)-GapmeR (Exiqon) treatment, the transfection was performed with the Lipofectamine RNAiMAX (Invitrogen) transfection reagent according to manufacturer's protocol. All LNA-GapmeR transfections were performed for 48h. The LNA-GapmeRs were designed with the Exiqon LNA probe designer and contained the following sequences: For MANTIS 5'-ACA TAG ATG GAC TCT T-3' and as negative Control 5'-AAC ACG TCT ATA CGC-3'.

Plasmid overexpression in HUVECs was performed with the Neon electroporation system (Invitrogen) with the following plasmids: pCMV-SOX18 (SC113502, Origene), pCMV-SMAD6 (SC320357, Origene), pCMV-COUP-TFII (SC108069, Origene) and pcDNA3.1+MANTIS-mutant (MTS-mut). PcDNA3.1+MANTIS was obtained from Biomatik (Canada). PcDNA3.1+MANTISΔC, pcDNA3.1+MANTISΔN1 and pcDNA3.1MANTISΔN2 were generated as described. As a negative control, empty pcDNA3.1+ was used. Plasmid transfection for Spheroid sprouting assay was performed for 48h.

### RNAscope

RNA in situ hybridization was performed with the RNAscope 2.5 HD Detection reagent (322310, Advanced Cell Diagnostics (ACD), Newark, CA, USA) as a single-plex chromogenic brown assay according to manufacturer's instructions with minor changes. Briefly, formalin fixed paraffin-embedded sections were deparaffinized and treated with hydrogen peroxide for 10min. Afterwards, target retrieval was carried out using the Braun steamer. The sections were incubated in boiling 1 x Retrieval solution for 20min. Then they were incubated with protease Plus for 30min at 40°C using the HybEZ System. The probe (MANTIS (Hs-AK12587) (ACD #483551)) and amplification steps were carried out according to instructions except that Amp5 was incubated for 60min. To detect the signal, sections were incubated with DAB for 20min at RT. Finally sections were counterstained with 10% Gill's Hematoxylin No. 1 for 20sec and blued in tap water. After dehydration sections were mounted using EcoMount and analyzed by light microscopy.

### Affymetrix Exon-Array and Illumina BeadChip Array.

For Exon-Array experiments, HUVECs were transfected with control (Scrambled Stealth RNAi™ Med GC, 12935-300, Invitrogen) or JARID1B stealth siRNAs (HSS173871, Invitrogen). 48h after transfection, RNA was isolated with the miRNeasy Mini Kit (Qiagen) and a GeneChip Human Exon 1.0 ST array (Affymetrix) was used. Data was analyzed by using the noncoder web interface<sup>7</sup> and the Robust Multichip Average normalization method.

For Illumina Array experiments, HUVECs were transfected with control or MANTIS LNA-GapmeRs (Exiqon) for 48h and RNA was isolated subsequently with the miRNeasy Mini Kit (Qiagen). Afterwards, the Illumina HumanHT12-v4 Expression BeadChip Array was performed (ServiceXS). Raw data was used to generate a data intensity table by extracting all average microarray signals per gene symbol and sample. Next, a log2 data transformation was used to variance-stabilize the signals and the robust spline normalization<sup>8</sup> implemented in the *lumi* package<sup>9</sup> was used to normalize variance-stabilized data. For detection of differentially expressed genes, *limma*<sup>10</sup> was used to fit a linear model for each gene and a series of normalized array data. We next calculated moderated t-statistics, F-statistics and log-odds of differential expression by empirical Bayes moderation of the standard



errors towards a common value<sup>10</sup> and calculated the adjusted p-value according to Benjamini-Hochberg.

Gene Ontology terms were searched by using the web-interface of Gorilla with standard parameters (<http://cbl-gorilla.cs.technion.ac.il/>)<sup>11</sup>, where the p-value is the enrichment p-value computed according to the mHG (minimal hypergeometric) or HG model.

#### RNA isolation, Reverse transcription and quantitative real-time PCR (qRT-PCR).

Total RNA Isolation was performed with the RNA Mini Kit (Bio&Sell). Reverse transcription was done with SuperScript III Reverse Transcriptase (Thermo Fisher) and oligo(dT)<sub>23</sub> together with random hexamer primers (Sigma). CopyDNA amplification was measured with qRT-PCR using Eva Green Master Mix and ROX as reference dye (Bio&Sell) in a Mx3000P cycler (Stratagene). Relative expression of target genes was normalized to  $\beta$ -Actin or 18S ribosomal RNA and analyzed by the delta-delta Ct method with the MxPro qPCR software (Stratagene).

#### Protein Isolation and Western Analyses.

Cells were washed 2 times in Hanks solution (Applichem) and lysed with Triton X-100 lysis buffer (20 mM Tris/Cl pH 7.5, 150 mM NaCl, 10 mM NaPP<sub>i</sub>, 20 mM NaF, 1% Triton, 2 mM Orthovanadat (OV), 10 nM Okadaic Acid, protein-inhibitor mix (PIM), 40  $\mu$ g/ml Phenylmethylsulfonylfluorid (PMSF)). Afterwards, cells were centrifuged for 10 min at 16,000 g. Protein concentration was determined with the Bradford assay. Afterwards, cell extract was boiled in Laemmli buffer, equal amounts of protein were separated with SDS-PAGE and gels were blotted onto a nitrocellulose membrane. After blocking in Rotiblock (Carl Roth, Germany), first antibody was applied. Infrared-fluorescent-dye-conjugated secondary antibodies were purchased from Licor (Bad Homburg, Germany). Signals were detected with an infrared-based laser scanning detection system (Odyssey Classic, Licor, Bad Homburg, Germany).

#### CRISPR/Cas9.

Guide RNA (gRNA) development was based on the web-interfaces of CRISPR design (<http://crispr.mit.edu/>) or CHOPCHOP (<https://chopchop.rc.fas.harvard.edu/>). The pSpCas9(BB)-2A-Puro (PX459) V2.0 was a gift from Feng Zhang (Addgene plasmid # 62988) and used as cloning backbone. The CRISPR/Cas9 procedure in HUVEC was carried out after<sup>12</sup>. Briefly, two PX459 V2.0 plasmids containing gRNA sequences for targeting the *MANTIS* gene at the 5' site and at the 3' site were used in combination for transfection. The following oligonucleotides were used for annealing: For pSpCas9(BB)-2A-Puro-5'Exon1-MANTIS 5'-CAC CGC TTC ATT TTG AGG GCT CGT C-3' and 5'-AAA CGA CGA GCC CTC AAA ATG AAG C-3' and for pSpCas9(BB)-2A-Puro-3'Exon4-MANTIS 5'-CAC CGC TAC CAC TTG GCA ACC CGC T-3' and 5'-AAA CAG CGG GTT GCC AAG TGG TAG C-3'. After cloning, plasmids were purified and sequenced. The transfection of a GFP control plasmid (pcDNA3.1-GFP) or the pSpCas9(BB)-2A-Puro-5'Exon1-MANTIS and pSpCas9(BB)-2A-Puro-3'Exon4-MANTIS constructs into HUVEC was achieved using the NEON electroporation system (Invitrogen), afterwards puromycin (1  $\mu$ g/mL) was used as selection reagent for 5 days.

#### Shear stress exposure.

Untreated or 24h siRNA-treated  $2 \times 10^5$  HUVECs were plated overnight on fibronectin coated  $\mu$ -slides I<sup>0.4</sup> Luer (Ibidi) and cultured in a humidified atmosphere of 5% CO<sub>2</sub> at 37°C in EGM. The next day, medium was replaced by new EGM and the cells were exposed to laminar flow (20 dynes/cm<sup>2</sup>) under

the control of the Ibidi perfusion system for 72h to mimic shear stress. In parallel, the static control samples were treated identically except that these were not exposed to shear stress. Afterwards, images were taken with an Axiovert135 (Zeiss) microscope. HUVECs under static conditions without laminar flow served as negative control.

#### Matrigel assay (Tube formation).

Matrigel Growth Factor Reduced (BD) was prepared and incubated with  $1 \times 10^5$  HUVECs in EBM and 1%FCS for 4h similar to <sup>13</sup>. After stopping with 4% PFA, tube formation images were acquired on an Axiovert135 microscope (Zeiss). Tube number quantification was analyzed with the help of AxioVision software (Zeiss).

#### Spheroid outgrowth assay.

HUVEC spheroids were generated as described in <sup>14</sup>. Images were acquired with an Axiovert135 microscope (Zeiss). For quantification of the cumulative sprout number, ten spheroids per condition were analyzed with the help of the AxioVision software (Zeiss). Treatments with VEGF-A 165 were performed for 16h with a concentration of 10ng/mL.

For the competition-like spheroid outgrowth assay, spheroids of HUVEC were made from two differently treated groups. For this, HUVEC were transduced with lentivirus to express Yellow Fluorescent Protein (YFP) and Cyan Fluorescent Protein (CFP), respectively. The cell population expressing CFP was used as control cells transfected with scrambled siRNA, whereas the other expressing YFP was transfected with MANTIS siRNA. Both cell populations were mixed (1:1) and the spheroid assay was performed as described above. Images were taken with the laser scanning microscope LSM 510 META (Zeiss) and processed with ZEN 2011 software (Zeiss).

#### Boyden-chamber assay.

Boyden-chamber assays were performed similar to <sup>15</sup>. For the boyden-chamber assay, 200,000 HUVEC were plated on membrane inserts (FluoroBlok, 3µm pore size, BD Bioscience, Heidelberg, Germany) in the presence of EBM, whereas the lower chamber contained EBM supplemented with 4% FCS. HUVEC on the upper surface of the filter were removed mechanically after 20h. Then, HUVEC in the lower chamber were fixed (4% paraformaldehyde in PBS), stained with DAPI and counted.

#### In vitro transcription and RNA 3'end biotinylation.

Prior to in vitro transcription, pcDNA3.1+MANTIS or control pcDNA3.1+ were linearized with SmaI (Thermo Fisher). After precipitation and purification of linearized DNA, DNA was in vitro transcribed according to the manufacturers protocol with T7 Phage RNA Polymerase (NEB), and DNA was digested with RQ DNase I (Promega). The remaining RNA was purified with the RNeasy Mini Kit (Qiagen) and biotinylated at the 3'end with the Pierce RNA 3'end biotinylation kit (Thermo Fisher).

#### RNA pulldown assay and peptide purification for mass spectrometry.

The RNA pulldown assay was performed similar to <sup>16</sup>. For proper RNA secondary structure formation, 150ng of 3'end biotinylated MANTIS RNA or control RNA was heated for 2 min at 90°C in RNA folding buffer (10 mM Tris pH 7.0, 0.1 M KCl, 10 mM MgCl<sub>2</sub>), and then put on RT for 20 min.  $1 \times 10^7$  HUVECs were used per sample. Isolation of nuclei was performed with the truCHIP™ Chromatin Shearing Kit (Covaris, USA) according to the manufacturers protocol without shearing the samples. Formaldehyde samples were crosslinked prior to cell harvest and quenched. Folded Bait RNA was incubated in

nuclear cell extracts for 3h at 4°C. After incubation, UV samples were UV crosslinked according to <sup>17</sup>. Afterwards, Streptavidin M-270 Dynabeads (80 µL Slurry, Thermo Fisher) were incubated with cell complexes for 2h at 4°C. After 4 washing steps with the lysis buffer of the truCHIP chromatin Shearing Kit (Covaris, USA), beads were put into a new Eppendorf tube. For western analysis, beads were boiled in Laemmli buffer and proteins were separated by SDS-PAGE, followed by immunoblotting. For RNA analysis, RNA was extracted with TRIzol (Thermo Fisher). Afterwards, RNA purification was performed with the RNeasy Mini Kit (Qiagen). After reverse transcription, qRT-PCR was performed. For mass spectrometric measurements in order to reduce complexity, samples were eluted stepwise from the beads. First elution was performed with 5 M Urea, 2 mM DTT, 50 mM Tris pH 7.5, for 15 min. Thiols were alkylated with 57 mM chloroacetamide for 20 min at RT in the dark. Beads were sedimented and supernatant was transferred to Microcon YM-30 (Millipore) spin filters (30 kDa cut-off) and centrifuged for 10 min. Proteins from beads and filters were digested overnight with 1 µg LysC (Wako) in 100 µL 2 M Urea, 50 mM Tris pH 7.5 and combined. Beads were washed with 100 µL ABC and supernatant was transferred to the digestion and the mixture was digested with 1 µg Trypsin (Promega) overnight at RT. Remaining proteins on beads were eluted for 10 min at 95°C in 4% SDS, 50 mM HEPES pH 7.6, 100 mM NaCl, 10 mM DTT. Subsequently the standard protocol of filter aided sample preparation (FASP) was performed<sup>18</sup> including RNase T1 (1000 U/µL, Thermo Scientific) and RNase A (4 µg/µL, Thermo Scientific) digestion using 1 µL each to elute crosslinked peptides. Peptides from both fractions were acidified by trifluoroacetic acid (TFA) to a final concentration of 0.1% and purified on multi-stop-and-go tips (StageTips) containing a stack of three C18-disks<sup>19</sup>. Peptides were resolved in 1% acetonitrile and 0.5% formic acid and further analyzed by Liquid chromatography/mass spectrometry (LC/MS).

#### Plasmid overexpression and peptide purification for mass spectrometry.

Plasmid overexpression in HUVECs for searching small peptides was performed with the Neon electroporation system (Invitrogen) with the following plasmids: pcDNA3.1+MANTIS, pcDNA3.1+ (empty vector) and pcDNA3.1-GFP. Pellets of transfected HUVECs were resuspended in 50 µL 6M Guanidine hydrochloride (GdmCl), 50 mM Tris/HCl, pH 8.5, 10 mM Tris(2-carboxyethyl)phosphine hydrochloride (TCEP) and incubated at 95°C for 5 min. Reduced thiols were alkylated with 40 mM chloroacetamide and samples were diluted with 25 mM Tris/HCl, pH 8.5, 10% acetonitrile to obtain a final GdmCl concentration of 0.6 M. Protein lysate was added to a 30 kDa cut-off filter unit and centrifuged. Flow-through was acidified with TFA to obtain a final concentration of 0.5%. In a parallel experiment, including the empty vector pcDNA3.1+, pcDNA3.1+MANTIS, but without pcDNA3.1GFP, the flow through was digested with 1 µg trypsin (Promega, sequencing grade) overnight at 37 °C. Digestion was stopped by adding TFA to a final concentration of 0.5 %. Acidified peptides were loaded on multi-stop-and-go tip (StageTip) containing six C18-disks. Purification and elution of peptides was performed as described<sup>19</sup>. Peptides were eluted in wells of microtiter plates, dried and resolved in 1% acetonitrile, 0.1 % formic acid and analyzed by LC/MS.

#### Mass spectrometry.

LC/MS was performed on Thermo Scientific™ Q Exactive Plus coupled to an ultra-high performance liquid chromatography unit (Thermo Scientific Dionex Ultimate 3000) via a Nanospray Flex Ion-Source (Thermo Scientific). Peptides were loaded on a C18 reversed-phase precolumn (Zorbax 300SB-C18, Agilent Technologies) followed by separation on in-house packed 2.4 µm Reprosil C18 resin (Dr. Maisch GmbH) picotip emitter tip (internal diameter 100 µm, internal diameter of the tip 10 µm, 15

cm long, New Objectives) with a flow rate of 400 nL/min using a gradient from mobile phase A (4% acetonitrile, 0.1% formic acid) to 44% mobile phase B (80% acetonitrile, 0.1% formic acid) for lncRNA MANTIS binding protein analysis. For micropeptide identification, the peptides were eluted using gradient from 5% to 80% mobile phase B. Mass spectrometry (MS) data were recorded by data dependent Top10 acquisition (selecting the ten most abundant precursor ions in positive mode for high energy collision dissociation fragmentation (HCD)). The Full MS scan range was 300 to 2500 m/z with resolution of 70000 at m/z 200, and an automatic gain control (AGC) value of  $3 \times 10^6$  total ion counts with a maximal ion injection time of 250 ms. Only higher charged ions (2+) were selected for MS/MS scans with a resolution of 17500, an isolation window of 2 m/z and an automatic gain control value set to  $1 \times 10^5$  ions with a maximal ion injection time of 150 ms. First fixed mass was 110 m/z for the analysis of Mantis binding proteins. Full MS and MS/MS data were acquired in profile mode by Xcalibur software.

#### Mass spectrometry- Data analysis.

X calibur Raw files were analyzed by proteomics software Max Quant (1.5.2.8)<sup>20</sup>. For the analysis of peptides without digestion the enzyme specificity was set to unspecific. For experiments with tryptic digestion the enzyme specificity was set to trypsin; missed cleavages were limited to 2. Acetylation of N-terminus (+42.01), carbamidomethylation (+57.02) and oxidation of methionine (+15.99) were selected as modification. Human reference proteome set from Uniprot (68506 entries, Download 8th April 2015) was supplemented with in silico predicted MANTIS ORFs and green fluorescent protein (GFP) ORFs and used for identification of peptides and proteins smaller than 30kDa in empty vector, MANTIS or GFP overexpressing HUVECs (**Supplemental Table 6-9**). In addition, a public available proteome dataset of HEK cells from a long online 2D SCX-RP UHPLC-MS/MS run (PXD000705<sup>21</sup>) from the PRIDE Database<sup>22</sup> was analysed using the same supplemented database (**Supplemental Table 4&5**). False discovery rate (FDR) was set to 1%.

**Supplemental Table 10** summarizes the data of the analysis of lncRNA MANTIS binding proteins obtained by database search of the human reference proteome set (68506 entries, Download 8th April 2015) and label free quantification from at least one identified peptide. The protein group file was uploaded to Perseus 1.5.1.6 and the data set was cleaned from reverse identifications, only identified by site and common contaminants. For label free quantification all proteins were quality filtered according to a minimum of three valid values in one group. For proteins with missing values in the other group a background value of half of the lowest value was imputed. Ratios between MANTIS and control were calculated from the average and log2 of the ratio was plotted against – log10 p values. Protein with p<0.05 and at least 1.5 fold enriched in MANTIS fraction were considered as protein of interest.

The mass spectrometry proteomics data have been deposited to the ProteomeXchange Consortium via the PRIDE<sup>22</sup> partner repository with the dataset identifiers PXD005951 (HUVEC <30 kDa, **Supplemental Tables 6&7**, without trypsin) and PXD005957 (HUVEC <30 kDa, **Supplemental Tables 8&9**, with tryptic digestion).



### RNA immunoprecipitation and protein immunoprecipitation.

1x10<sup>7</sup> HUVECs were used per sample. Nuclei isolation was performed with the truCHIP™ Chromatin Shearing Kit (Covaris, USA) according to the manufacturers protocol without shearing the samples. After pre-clearing with 20 µL DiaMag Protein A and Protein G (Diagenode), 10% of the pre-cleared sample served as input and the lysed nuclei were incubated with BRG1, SMARCA5 or H3 antibodies or IgG alone for 12h at 4°C. The complexes were then incubated with 50 µL DiaMag Protein A and Protein G (Diagenode) beads for 3h at 4°C, followed by 4 washing steps in Lysis Buffer from the truCHIP™ Chromatin Shearing Kit (Covaris, USA). Prior to elution, beads were put into a new Eppendorf tube. For protein immunoprecipitation experiments, beads were boiled in Laemmli buffer and western analyses was performed. For RNA immunoprecipitation, RNA was extracted with TRIzol (Thermo Fisher) followed by RNA purification with the RNeasy Mini Kit (Qiagen), reverse transcription and qRT-PCR.

### RNA Fluorescence in-situ hybridization.

Cells grown on fibronectin-coated coverslips were fixed in 4% PFA (in PBS, pH 7.4, 7 min at RT) and washed 3 times with PBS. Cells were permeabilized in PBS containing 0.5% Triton X-100 and 5 mM vanadyl complex (VRC, NEB) on ice for 10 min and again washed 3 times with PBS. Prior to hybridization, cells were rinsed once in 2xSSC. Hybridization was performed over night at 37°C in hybridization buffer (10% dextran sulfate, 50% formamide, 2xSSC, 400 µg E.coli tRNA, 0.02% RNase-free bovine serum albumin, 2 mmol/L VRC) and 10 nmol/L 5'TYE-665 labelled locked nucleic acid (LNA) detection probe (Exiqon). Custom LNA detection probes were designed with the Exiqon LNA probe designer tool and had the following sequences: for MANTIS 5'-TGT AGA CAG ATA TGA GGC CAG T-3' and for β-Actin mRNA 5'-TCA TGA GGT AGT CAG TCA GGT-3'. The cells were then washed 4 times for 15 min in buffer containing 2xSSC and 50% formamide and mounted in Vectashield containing DAPI. Images were taken with the laser scanning microscope LSM 510 META (Zeiss) and processed with ZEN 2011 software (Zeiss).

### In vitro protein synthesis and Coomassie staining.

In vitro protein synthesis of DYR-DHFR, pcDNA3.1+MANTIS and pcDNA3.1+ (empty vector) was performed with the PURExpress kit (E6800, NEB) according to the manufacturer's protocol. Afterwards, the reaction mixtures were boiled in Laemmli buffer, the proteins were separated with SDS-PAGE, the acrylamide gel was stained with Coomassie brilliant blue and finally the gel was destained using 50% methanol, 10% acetic acid until single bands appear.

### Chromatin Immunoprecipitation and RNA ChIP.

Preparation of cell extracts, crosslinking and isolation of nuclei was performed with the truCHIP™ Chromatin Shearing Kit (Covaris, USA) according to the manufacturers protocol. The procedure was similar to <sup>23</sup>. After sonification of the lysates with the Bioruptor Plus (10 cycles, 30 sec on, 90 sec off, 4°C; Diagenode, Seraing, Belgium), cell debris was removed by centrifugation and the lysates were diluted 1:3 in dilution buffer (20 mmol/L Tris/HCl pH 7.4, 100 mmol/L NaCl, 2 mmol/L EDTA, 0.5% Triton X-100 and protease inhibitors). Pre-clearing was done with 20 µL DiaMag protein A and protein G coated magnetic beads slurry (Diagenode, Seraing, Belgium) for 45 min at 4°C. The samples were incubated as indicated over night at 4°C with the antibodies indicated. 5% of the samples served as input. The complexes were collected with 50 µL DiaMag protein A and protein G coated magnetic beads (Diagenode, Seraing, Belgium) for 3h at 4°C, subsequently washed twice for 5 min

with each of the wash buffers 1-3 (Wash Buffer 1: 20 mmol/L Tris/HCl pH 7.4, 150 mmol/L NaCl, 0.1% SDS, 2 mmol/L EDTA, 1% Triton X-100; Wash Buffer 2: 20 mmol/L Tris/HCl pH 7.4, 500 mmol/L NaCl, 2 mmol/L EDTA, 1% Triton X-100; Wash Buffer 3: 10 mmol/L Tris/HCl pH 7.4, 250 mmol/L lithium chloride, 1% Nonidet p-40, 1% sodium deoxycholate, 1 mmol/L EDTA) and finally washed with TE-buffer pH 8.0. Elution of the beads was done with elution buffer (0.1 M NaHCO<sub>3</sub>, 1% SDS) containing 1x Proteinase K (Diagenode, Seraing, Belgium) and shaking at 600 rpm for 1h at 55°C, 1h at 62°C and 10 min at 95°C. After removal of the beads, the eluate was purified with the QiaQuick PCR purification kit (Qiagen, Hilden, Germany) and subjected to qPCR analysis. As a negative control primer targeting the GAPDH promoter was used.

RNA-ChIP experiments were performed similar to the ChIP experiments, but with the following changes: Washing was performed in a modified washing buffer 3 without lithium chloride. After the proteinase K elution step, DNA was digested with DNase I during the purification procedure with the RNA Mini Kit (Qiagen, Hilden, Germany) and samples were reverse transcribed as indicated.

#### Formaldehyde Assisted Isolation of Regulatory Elements (FAIRE) and MNase treatment.

FAIRE was performed similarly as described in <sup>24</sup>. HUVECs were crosslinked with 1% formaldehyde for 5 min, quenched with 125 mM glycine for 5 min, scraped, washed with PBS and lysed in 2 mL FAIRE buffer 1 (50 mM HEPES-KOH [pH 7.5], 140 mM NaCl, 1 mM EDTA, 10% glycerol, 0.5% NP-40, 0.25% Triton X-100) at 4°C for 10 min followed by centrifugation (5 min, 16,000 xg, 4°C). Afterwards, cell pellets were resuspended and incubated in 2 ml FAIRE buffer 2 (10 mM Tris-HCl [pH 8.0], 200mM NaCl, 1 mM EDTA, 0.5 mM EGTA) for 10 min at 22°C followed by centrifugation (5 min, 16,000 xg, 4°C). Cell pellets were resuspended in 400 µl FAIRE buffer 3 (10 mM Tris-HCl, [pH 8.0], 100 mM NaCl, 1 mM EDTA, 0.5 mM EGTA, 0.1% sodium deoxycholate, 0.5% N-lauroylsarcosine). Subsequently, samples were sheared (30 sec On, 90 sec Off, 10 cycles, 4°C) with a Bioruptor Plus (Diagenode, Seraing, Belgium) to an average length of 200-400bp and cleared by centrifugation (5 min, 16,000 xg, 4°C). 10% of each sample was used as input. Samples were further extracted with phenol/chloroform/isoamylalcohol (Roti Phenol/C/I) and the aqueous phase was collected and precipitated with EtOH over night. After resuspension in TE-Buffer, input and extracted DNA were de-crosslinked at 65°C for 6 h and the DNA was purified with the QIAquick PCR purification kit (Qiagen, Hilden, Germany).

For MNase experiments, which were performed similar to <sup>25</sup>, but with several modifications, HUVECs were crosslinked identical to the FAIRE protocol, but lysed in 2mL MNase buffer 1 (50 mM HEPES-KOH [pH 7.5], 10 mM NaCl, 3 mM MgCl<sub>2</sub>, 10% glycerol, 0.5% NP-40, 0.25% Triton X-100) at 4°C for 10 min followed by centrifugation (5 min, 16,000 xg, 4°C). Next, cell pellets were resuspended and incubated in 2 ml MNase buffer 2 (10 mM Tris-HCl [pH 8.0], 15 mM NaCl, 60 mM KCl, 0.1% sodium deoxycholate, 0.5% N-lauroylsarcosine) for 10 min at 22°C followed by centrifugation (5 min, 16,000 xg, 4°C). After removal of the supernatant, cell pellets were washed in 2mL MNase buffer 3 (10 mM Tris-HCl [pH 8.0], 1mM CaCl<sub>2</sub>), centrifuged (2 min, 13,000 xg, 4°C), and the sedimented chromatin pellet was resuspended in 200 µl MNase buffer 3. 5% of each sample was used as input. Samples were digested with mononuclear Nuclease (Mnase, ThermoFisher) for 10min at 37°C and the reaction was stopped with stopping buffer (8.6% SDS, 7mM EDTA [pH 8.0]). After proteinase K treatment for 30min at RT, samples were de-crosslinked at 65°C for 6 h and the DNA was purified with the QIAquick PCR purification kit (Qiagen, Hilden, Germany).

### Cloning of MANTIS mutants.

To generate MTS-mut with the putative functional region of MANTIS into pcDNA3.1+, the region of MANTIS was PCR amplified with 5'-ATT TGG TAC CCA AAT GTC TTC AAG GTA TAA AAA TGT GGT CTA-3' and 5'- ATT TGG GCC CGT GCT GGA TGC AGA TAA TGT TTG ACT CCT-3' and both, pcDNA3.1+ and the PCR fragment, were digested with Acc65I/ApaI prior to ligation and *E.coli* transformation.

To generate the other mutants in a pcDNA3.1+ background, the full length pcDNA3.1+MANTIS was digested with either XbaI/Acc65I (for ΔN1), with BlnI/Acc65I (for ΔN2) or with Eco47III/ApaI (for ΔC), followed by Klenow Fill-In (for ΔN1 and ΔN2) or 3'-5' exonuclease (for ΔC) treatments. After re-circularization, all plasmids were verified by sequencing.

### Cloning of pGL3 MANTIS 1kb and Luciferase Reporter Assay.

To clone 1kb upstream of the MANTIS TSS into pGL3 luciferase reporter plasmid, genomic DNA was PCR amplified with 5'-CGG CAT GGT ACC CTA TGT CTG ACA CAT AGT AGA GCT TAA TAA AC-3' and 5'- ATT TGC TAG CTA GGC AAA AGA ACA GAA CAG CTC ACA GTC ACA GAG-3'. The resulting PCR product and pGL3 were digested with Acc65I/NheI, followed by ligation and DNA preparation. The final plasmid pGL3-MANTIS\_1kb was verified by sequencing. HUVECs overexpressing JARID1B or a catalytically dead-mutant of JARID1B (pCMV-J1B-Mut) were transiently transfected with pGL3 or 1kb promoter of MANTIS in pGL3 with Lipofectamine 3000 (Thermo Fisher) according to the manufacturers protocol. pCMV-J1B-Mut as well as pCMV-J1B were kindly provided by K. Helin (University of Copenhagen, Denmark). Luciferase activity was determined with the assay kit from Promega (Mannheim, Germany) in a TECAN infinite M2000Pro plate reader (Mannedorf, Switzerland) and normalized to the empty pGL3 control vector (Promega).

### Proximity Ligation Assay.

Proximity Ligation Assays (PLA) were performed as described in the manufacturer's protocol (Duolink II Fluorescence, OLink, Upsalla, Sweden). Briefly, after siRNA knockdown in HUVEC, cells were fixed in phosphate buffered formaldehyde solution (4%), permeabilized with Triton X-100 (0.2%), blocked with serum albumin solution (3%) in phosphate buffered saline and incubated overnight with the antibodies indicated. Samples were washed and incubated with the respective PLA-probes for 1h at 37°C. After washing, samples were ligated for 30 min (37°C). After an additional washing step, the amplification with polymerase was allowed for 100 min (37°C). The nuclei were stained using DAPI. Images were acquired by confocal microscope (LSM 510, Zeiss).

### BRG1 ATPase Assay.

The ATPase Assay after immunoprecipitation with BRG1 antibodies precipitates was performed directly on magnetic beads as described in <sup>26</sup> and in the manufacturer's protocol (Innova Biosciences, ATPase Assay Kit, Cambridge, UK).

### Assay for Transposase Accessibility (ATAC)-Sequencing.

HUVECs were treated with siRNAs against Scrambled or MANTIS siRNA for 48h. 100.000 cells were used for ATAC library preparation using Tn5 Transposase from Nextera DNA Sample Preparation Kit (Illumina). The cell pellet was resuspended in 50 µL PBS and mixed with 25 µL TD-Buffer, 2.5 µL Tn5, 0.5 µL 10% NP-40 and 22 µL H<sub>2</sub>O. The Cell/Tn5 mixture was incubated at 37°C for 30 min with occasional snap mixing. Transposase treatment was followed by 30 min incubation at 50°C together

with 500 mM EDTA pH8.0 for optimal recovery of digested DNA fragments. To neutralize EDTA, 100  $\mu$ L of 50 mM  $MgCl_2$  was added followed by purification of the DNA fragments by MinElute PCR Purification Kit (Qiagen). Amplification of library together with indexing was performed as described elsewhere<sup>27</sup>. Libraries were mixed in equimolar ratios and sequenced on NextSeq500 platform using V2 chemistry. The samples were sequenced on Illumina NextSeq hardware and assessed for quality. Trimmomatic version 0.33 was employed to trim reads after a quality drop below a mean of Q20 in a window of 5 nt<sup>28</sup>. Only reads above 30 nt were cleared for further analyses. In order to normalize all samples to the same sequencing depth, 27 million reads per sample were randomly selected for further analysis. These were mapped versus the hg19 version of the human genome with STAR 2.4.2a<sup>29</sup> using only unique alignments to exclude reads with uncertain arrangement. The reads were deduplicated to avoid PCR artefacts leading to multiple copies of the same original fragment. The MUSIC peak caller (version from Dec. 2015)<sup>30</sup> was employed in punctate mode to accommodate for the range of peak widths typically expected for ATAC-seq. The maximum qvalue was set to 0.2 and the p-value normalization window length was changed to 1500. Peaks overlapping ENCODE blacklisted regions (known misassemblies, satellite repeats) were excluded. Peaks were annotated with the promoter (TSS  $\pm$  5000 nt) of the gene most closely located to the centre of the peak based on reference data from GENCODE v19. In order to be able to compare peaks in different samples (scrambled and MANTIS siRNA), the resulting lists of significant peaks were overlapped and unified to represent identical regions. The counts per unified peak per sample were computed with BigWigAverageOverBed (UCSC Genome Browser Utilities, <http://hgdownload.cse.ucsc.edu/downloads.html>). Raw counts for unified peaks were submitted to DESeq2 for normalization<sup>31</sup>. Spearman correlations were produced to identify the degree of reproducibility between samples using R. To permit a normalized display of samples in IGV, the raw BAM files were normalized for sequencing depth (number of mapped deduplicated reads per sample) and noise level (number of reads inside peaks versus number of reads not inside peaks). Two factors were computed and applied to the original BAM files using bedtools genomecov resulting in normalized BigWig files for IGV. Raw data of ATAC-Seq is available at GEO datasets (GSE83427).



Supplemental Table 1: List of primers for qRT-PCR.

Name	Species	Forward Primer (5'-3')	Reverse Primer (5'-3')
$\beta$ -Actin	<i>Hs</i>	AAA GAC CTG TAC GCC AAC AC	GTC ATA CTC CTG CTT GCT GAT
MANTIS (n342419)	<i>Hs</i>	AAC TCC TGC TCC AAA CTC ACT C	CCA GAG ACT TTC CAT TCT GAT G
N337754	<i>Hs</i>	GCT GGG AAT GTG TCC CTA AC	GCT GGT AGC AAG CCA GTA AG
N345337	<i>Hs</i>	CAT TGT GGC CTC AGC AGA AG	CCG CGA TAC CGT TTC TGA TG
N332912	<i>Hs</i>	GCC ACT GGC TTA TTC CAT AG	CCT GTG TCT TCT CAC CAT TC
N339736	<i>Hs</i>	GCC TTG AAG CAG GTT AGA TG	CCC TGA AGC AAC TGA TTG TC
N406914	<i>Hs</i>	GAC TCG TGG GTA CGC ATA GG	TAC TGG TGG CGA GGT GAG AC
JARID1B	<i>Hs, Mf</i>	TGA GGA TGA AGA TGC CAT CTG CC	ACA GCG CAC ACA GAT GTA GTC TTC
U12 snRNA	<i>Hs</i>	GCC CGA ATC CTC ACT GCT AA	TCG CAA CTC CCA GGC ATC
MEG3	<i>Hs</i>	GAG TGT TTC CTT CCC CAA GG	GCG TGC CTT TGG TGA TTC AG
SOX18	<i>Hs</i>	CAT GGT GTG GGC AAA GGA C	GCC GGT ACT TGT AGT TGG G
SMAD6	<i>Hs</i>	CCT CTA TGC GGT GTA CGA C	GAT GCC GAA GCC GAT CTT G
SOD2	<i>Hs</i>	CCC TGG AAC CTC ACA TCA AC	GGC TGT AAC ATC TCC CTT GG
COUP-TFII	<i>Hs</i>	CGC CTT TAT GGA CCA CAT ACG	TCC ACA TGG GCT ACA TCA GAG
ANXA4	<i>Hs</i>	GCA GCA ATA TGG ACG GAG C	CAG GTC CTG GGC ATC CTG TC
GCML1	<i>Hs</i>	CAG AAC AGG ACA GTG AGG TG	CGA TTG GTG TAA GTT ACA AG
snRNP27	<i>Hs</i>	CTT CTC GAC TGA AAG AAA G	CTG CCT GTA CTT CCT CTT C
AAK1	<i>Hs</i>	CAG AAG GGT CTA CGT GGA ATC	CAG TTC CAG CAG AAA ATG AGG
PRCP	<i>Hs</i>	TTT GCC TGC TTG GCC TAT C	TAG CTC CAA CCC AGT GTT C
IL6	<i>Hs</i>	ACA GCC ACT CAC CTC TTC AGA ACG	CAG CTC TGG CTT GTT CCT CAC TAC
TUFT1	<i>Hs</i>	AGC AGA AAG AGG CAG AAG TC	CTT GGC AGT CAG CAT TGT TG
PECAM1	<i>Hs</i>	GCG GTA TTC AAA GAC AAC CC	ATC ACC TTC ACC CTC AGA AC
RNMT1	<i>Hs</i>	GGA CCT GGG ATG TGG TAA AG	CGC TGC TGA CAC TGT TTG AC
SOX7	<i>Hs</i>	CCA AGG ACG AGA GGA AAC G	GCC GGT ACT TGT AGT TGG G
HEY1	<i>Hs</i>	GCC AGC ATG AAG CGA GCT C	GGG TCA GAG GCA TCT AGT CC
18S rRNA	<i>Hs</i>	CTT TGG TCG CTC GCT CCT C	CTG ACC GGG TTG GTT TTG AT
GAPDH	<i>Hs</i>	TGC ACC ACC AAC TGC TTA GC	GGC ATG GAC TGT GGT CAT GAG
MANTIS-mut	<i>Hs</i>	ATC TCC TGA CCT CGT GAT CC	GGC TTG GTT GCT TCC GTA TG
MANTIS	<i>Mf</i>	AAC TCC TGC TCC AAA CTC ACT C	TGA AGC AGC CTT GTT GTC
GAPDH	<i>Mf</i>	TGC ACC ACC AAC TGC TTA GC	GGC GTG GAC TGT GGT CAT GAG
MANTIS	<i>Rn</i>	GGG TGG GTA CAC CTG GAA TC	ACA GGA GGC TGC TGT CTG AG
SOX18	<i>Rn</i>	CCT TCT TCC CAC CGC CTT TG	TGC CCA GGG TGC CAT AGT AG
SMAD6	<i>Rn</i>	GCA CGC AGT GGA GCT GAA AC	GGA GAC AGC CGA GAA TAG GG
COUP-TFII	<i>Rn</i>	ACA TCA TGG GCA TCG AGA AC	GTG CTG CAT TCA ACA CGA AC
$\beta$ -Actin	<i>Rn</i>	TGC CCA TCT ATG AGG GTT AC	TCT CTT GCT CGA AGT CTA GG

Hs, *Homo sapiens*; Mf, *Macaca fascicularis*; Rn, *Rattus norvegicus*

Supplemental Table 2: List of primers for ChIP.

Name	Forward Primer (5'-3')	Reverse Primer (5'-3')
βACTIN 826nt from TSS	TCT GTG GCA CAT GGA GTC TTG GTC	ACA CAG CCT GGG TCT GGG CCC AC
GAPDH 612nt from TSS	TGG TGT CAG GTT ATG CTG GGC CAG	GTG GGA TGG GAG GGT GCT GAA CAC
MANTIS 10-117nt after TSS	AAC TCC TGC TCC AAA CTC ACT C	TGA AGC AGC CTT GTT GTC
MANTIS 684-773nt from TSS	GCT AGG CCA GGT AGT TTG	GCT ACC CTC CAG TTA GC
MANTIS 352-471nt from TSS	GCT CAA GCA CAG AAG AAG	GTG CAC CTA AAG GGA AAG
SMAD6 29-93nt up TSS	TCT AGA CTG GCA TAT GAT GG	TTT GTT CTC CTC AAA CGC ACA CTG
SMAD6 1491-1586nt up TSS	GTG TCT CAG TCC GAT CTT TC	ACC CTT TGC TGA GCT TTA CC
SMAD6 3031-3104nt up TSS	TTT AAT CCG GCA TCG GCT AC	AAG ACA CTG AGG CAC AAA GG
SOX18 39-142nt up TSS	AAT CCC GCC CGG CCT GAG AAG AAA G	GAT ATA GCG GCT CAG GGC CAA TCG
SOX18 586-669 up TSS	TCT TTG TGG GCT CCG TCC AG	CCT CAC TCC CAA ACC AAC TC
SOX18 1022-1155nt up TSS	CAC AGG CTC AGG GTC ACA AG	CTC CAG GCA GGG TCA GAA TC
COUP-TFII 3185-3265nt up TSS	GAG CTC CAG TGT GGT GGA AG	CCG TCC TCC AGG ATT CAT TG
COUP-TFII 137-234nt up TSS	GCT AAG TTG CAG CAG TCG TG	GAG GGA ATG CGA TTT ATA GG
COUP-TFII -534-617nt up TSS	CCT CTC GCG GAG CCT TTA AGA GAC G	ACA TCC CGC ACC CGA GGT TTC

Supplemental Table 3: LncRNAs significantly altered in the Exon array after JARID1B knockdown

NONCODE_id	logFC siJarid1b-1/siScr	p-value* siJarid1b-1/siScr	logFC siJarid1b-2/siScr	p-value* siJarid1b-2/siScr	logFC siJarid1b-1/siGFP	p-value* siJarid1b-1/siGFP	logFC siJarid1b-2/siGFP	p-value* siJarid1b-2/siGFP	logFC siJarid1b-1/siJarid1b-2	p-value* siJarid1b-1/siJarid1b-2	logFC siScr/siGFP	p-value* siScr/siGFP	NONHSAT No.	Chr. Pos. Hg19
n342419	1.958	0	1.304	1.00E-05	1.856	0	1.202	2.00E-05	0.653	0.00248	-0.102	0.55311	NONHSAT071358, Mantis	chr2:70,016,684-70,026,080
n345337,n339305	-0.333	0.00941	-0.76	2.00E-05	-0.363	0.00567	-0.79	1.00E-05	0.427	0.00199	-0.03	0.77801	NONHSAT143945	chr16:81,417,177-81,423,143
n337754	0.539	0.04837	0.631	0.02474	1.625	4.00E-05	1.718	2.00E-05	-0.093	0.70975	1.086	0.00098	NONHSAT137492	chrX:71,370,734-71,373,135
n384507,n345653	1.798	0	0.842	0.00028	1.937	0	0.98	8.00E-05	0.957	0.0001	0.139	0.40283	NONHSAT098244	chr4:128,758,922-128,761,883
n370434	0.598	0.01685	0.667	0.00942	1.177	0.00018	1.247	0.00011	-0.07	0.74859	0.58	0.01964	NONHSAT125246	chr8:16325251-16353693
n341767	-0.557	0.00314	-1.045	2.00E-05	-0.332	0.04583	-0.82	0.00018	0.488	0.00708	0.225	0.15533	NONHSAT134432	chr9:118,954,208-118,954,799
n407688,n341993,n335521,n335610,n380837,n380732	0.369	0.03381	0.408	0.02174	0.637	0.00158	0.675	0.00105	-0.038	0.8069	0.268	0.10648	NONHSAT030138	chr12:98,906,751-98,910,200
n343078,n343081	0.55	0.00032	0.342	0.0083	0.652	8.00E-05	0.444	0.00159	0.208	0.07623	0.102	0.35628	NONHSAT024403	chr11:117,162,062-117,162,865
n345157,n341158	0.288	0.01255	0.28	0.01437	0.384	0.00221	0.377	0.00252	0.007	0.94039	0.096	0.33879	NONHSAT025148	chr11:130731861-130744709
n338988	0.757	0.00164	0.716	0.00239	0.722	0.00226	0.68	0.00333	0.041	0.82466	-0.035	0.85043	NONHSAT075123	chr2:160,626,484-160,629,028
n341701	0.734	0.00825	1.058	0.00074	0.507	0.04782	0.832	0.0039	-0.324	0.18203	-0.227	0.34053	NONHSAT131922	chr9:77,109,925-77,111,785
n385261	1.162	0.0002	0.833	0.00235	1.094	0.00032	0.765	0.00407	0.329	0.1474	-0.068	0.7541	NONHSAT122865	chr7:115,893,170-115,895,118
n339119	0.416	0.01748	0.521	0.00506	0.403	0.02051	0.507	0.00592	-0.105	0.49593	-0.013	0.92958	NONHSAT076663	chr2:210,887,131-210,889,246
n365169,n365168,n365170	0.421	0.04413	0.566	0.01111	0.485	0.02405	0.629	0.00605	-0.144	0.45097	0.064	0.73638	not found in noncode	
n339736	0.315	0.0152	0.291	0.02238	0.39	0.00459	0.366	0.00671	0.024	0.83099	0.075	0.5094	NONHSAT093906	chr3:187,868,994-187,871,876
n386426,n385076,n345961	0.339	0.01504	0.34	0.01476	0.39	0.00691	0.392	0.00678	-0.001	0.9918	0.052	0.66772	NONHSAT118940	chr7:5,862,791-5,887,232
n383794,n409113	-0.617	0.0008	-0.758	0.00016	-0.3	0.04684	-0.442	0.00721	0.142	0.31148	0.316	0.03782	NONHSAT076543	chr2:206980285-206982288
n339922	-0.765	0.0088	-0.544	0.04477	-0.999	0.00165	-0.778	0.00801	-0.221	0.37643	-0.234	0.35064	NONHSAT059854	chr18:71,589,174-71,589,866
n366331,n339642	1.226	0.00165	0.815	0.01853	0.949	0.00078	0.949	0.0083	0.411	0.19055	0.134	0.65835	NONHSAT092690	chr3:150,180,819-150,184,174
n341101	0.641	0.01952	0.816	0.00519	0.573	0.03251	0.749	0.00861	-0.176	0.46796	-0.067	0.77823	NONHSAT023724	chr11:94,276,131-94,277,949
n382502,n345800	0.343	0.00408	0.357	0.00314	0.284	0.01218	0.298	0.0093	-0.014	0.88125	-0.059	0.54524	NONHSAT041825	chr15:40,616,681-40,618,914
n342269,n378723,n384120,n378392,n377791	-0.232	0.02924	-0.268	0.01462	-0.253	0.01937	-0.289	0.00968	0.036	0.70259	-0.021	0.82005	NONHSAT084403	chr22:25,675,290-25,679,061
n406914	0.491	0.01442	0.582	0.00553	0.428	0.02776	0.52	0.01059	-0.092	0.5968	-0.062	0.71842	NONHSAT090901	chr3:101395274-101398057
n381616	0.524	0.00687	0.579	0.00371	0.426	0.02062	0.482	0.01101	-0.056	0.72983	-0.098	0.5465	NONHSAT018224	chr11:17,353,589-17,371,521
n332912	-1.492	0.00103	-0.862	0.02638	-1.634	0.00052	-1.003	0.01247	-0.631	0.08691	-0.142	0.68038	NONHSAT127418	chr8:81,454,721-81,455,338
n374751,n374961	0.508	0.00778	0.382	0.03244	0.579	0.00352	0.453	0.01448	0.126	0.43618	0.071	0.65712	NONHSAT041932	chr15:41,578,207-41,598,741
n345507,n365311	1.209	5.00E-05	0.723	0.00262	1.024	0.0002	0.538	0.0149	0.486	0.02426	-0.185	0.34012	NONHSAT076128	chr2:192,556,795-192,583,257
n339129,n365326,n345568,n383805	-0.417	0.01382	-0.435	0.01106	0.426	0.01241	0.408	0.01552	0.018	0.90199	0.843	0.00011	NONHSAT076795	chr2:217,081,612-217,084,915
n383576	0.27	0.02432	0.323	0.00985	0.233	0.04549	0.286	0.0185	-0.053	0.61968	-0.037	0.7284	NONHSAT068750	chr2:3664890-3665294
n345421	0.705	0.00282	0.647	0.00482	0.562	0.01098	0.505	0.01905	0.057	0.76123	-0.143	0.45161	NONHSAT008565	chr1:193,224,754-193,233,744
n385488,n385489,n377649	-0.554	0.01259	-0.85	0.00083	0.794	0.00136	0.499	0.02135	0.295	0.13983	1.349	2.00E-05	NONHSAT130385	chr9:21,454,267-21,559,697
n368145, n368144	0.764	0.00604	0.735	0.00759	0.625	0.01804	0.596	0.02271	0.029	0.89888	-0.139	0.54779	NONHSAT103689	chr5:130588746-130591276
n340207	0.492	0.01034	0.465	0.01405	0.433	0.01993	0.406	0.02707	0.028	0.86563	-0.059	0.71785	NONHSAT098131	chr4:121,843,097-121,844,760
n340820,n333701,n334084	0.568	0.00037	0.376	0.00642	0.477	0.00139	0.285	0.02738	0.192	0.11372	-0.092	0.42886	NONHSAT107192	chr6:3,751,345-3,754,105
n341073	1.623	1.00E-05	-0.569	0.01958	1.673	1.00E-05	-0.518	0.03012	2.191	0	0.051	0.81204	NONHSAT023193	chr11:76,512,704-76,515,138
n339657	-0.333	0.04722	-0.372	0.02975	-0.329	0.04924	-0.368	0.03104	0.039	0.79699	0.004	0.98117	NONHSAT079464	chr20:33,576,778-33,578,801
n332967,n332785	0.908	0.0013	0.819	0.00265	0.598	0.01647	0.508	0.03486	0.089	0.67963	-0.31	0.16963	NONHSAT106849	chr6:2,887,744-2,888,137
n410602	1.259	0.00286	0.846	0.02591	1.198	0.00393	0.786	0.03591	0.413	0.23483	-0.061	0.85642	NONHSAT106824	chr6:2,877,747-2,894,368
n338125	-0.576	0.00407	-0.595	0.00329	-0.356	0.0463	-0.376	0.03727	0.02	0.9035	0.219	0.1944	NONHSAT005108	chr1:110,856,618-110,857,022
n367832	0.556	0.0092	0.558	0.00904	0.411	0.03941	0.413	0.03873	-0.002	0.99224	-0.145	0.4277	NONHSAT105249	chr5:174,178,307-174,277,728
n371473	0.396	0.01918	0.509	0.0048	-0.45	0.00992	-0.336	0.03984	-0.113	0.44785	-0.845	0.00012	NONHSAT138671	chrX:134,169,666-134,174,761
n366808,n366809	-0.37	0.00723	-0.29	0.02588	-0.341	0.01157	-0.26	0.04141	-0.081	0.48547	0.03	0.79423	NONHSAT095597	chr4:14,166,079-14,244,437
n342910,n373367	-0.562	0.02968	-0.547	0.03348	-0.534	0.03686	-0.519	0.04156	-0.015	0.94663	0.028	0.9041	NONHSAT032007	chr12:131,780,414-131,783,039
n340117,n345640	-0.712	0.01843	-0.713	0.01825	0.589	0.04276	0.588	0.04318	0.001	0.99562	1.301	0.00039	NONHSAT096887	chr4:75,144,014-75,196,255
n337636	-0.554	0.00207	-0.464	0.00636	-0.401	0.01425	-0.311	0.04512	-0.09	0.52702	0.153	0.2905	NONHSAT000265	chr1:1,185,157-1,186,714

\* unadjusted p-values

Supplemental Table 11 Fold changes in MANTIS Illumina Array

SYMBOL	log2 FC LNA CTL/CTL	log2 FC LNA MANTIS/MANTIS	log2 FC LNA MANTIS/CTL	pValue LNA MANTIS/CTL
SMAD6	1.1561	1.01	-1.6174	0.049419463
SOX18	0.5095	0.3553	-1.6055	0.000911108
PECAM1	-0.1987	-0.9706	-1.5641	0.041417478
PRCP	-0.401	-0.8392	-1.3299	0.030139569
GIMAP4	-0.433	-0.9127	-1.2437	0.012065604
ANGPT2	-0.0936	-0.3604	-1.13	0.004270938
ALDH1A1	-0.5833	-0.3776	-1.0719	0.015591465
MALL	0.304	-0.0058	-1.0499	0.001073482
NOS3	-0.1867	-0.1007	-1.0472	0.002312621
HEY1	0.6987	0.845	-1.043	0.039092342
C5orf13	-0.2936	-0.4864	-1.0315	0.030618566
SNORA18	-0.0992	-0.1593	-1.0269	0.003728965
PAFAH1B3	-0.3748	-0.7998	-1.024	0.013534942
FAM69B	-0.0469	-0.1874	-1.0153	0.010340234
MARCH3	0.1515	-0.5221	-0.9947	0.033097747
LOC100134073	0.0459	-0.563	-0.9873	0.012528664
RGS5	0.1025	-0.0799	-0.983	0.049646578
PGF	0.4505	0.1948	-0.9803	0.033394811
FAM108C1	0.2162	0.0229	-0.9692	0.004681451
APLN	-0.3375	-0.7283	-0.9689	0.009693627
LOC100133609	0.2875	-0.5401	-0.9655	0.049060657
ESAM	-0.0022	-0.4335	-0.9554	0.003777405
MGC61598	0.4377	0.337	-0.9322	0.004973449
NOX4	-0.2557	-0.3635	-0.9194	0.007961236
HHIP	-0.1925	-0.771	-0.9101	0.046134658
HYAL2	-0.0776	-0.32	-0.9043	0.040167421
ID1	0.7816	0.4328	-0.8975	0.013789861
C1QTNF5	-0.1064	0.1579	-0.8906	0.01397281
NME4	-0.2175	-0.7779	-0.8885	0.048793714
PRKCDBP	0.2349	0.2029	-0.8833	0.002342542
SOX4	0.0749	0.1378	-0.8769	0.000226235
TMEM106C	-0.2548	-0.1714	-0.8701	0.036679531
HOXA9	0.3485	0.3322	-0.866	0.000346309
EMCN	-0.0377	-0.1015	-0.8585	0.038984772
C13orf15	0.4017	0.1091	-0.8515	0.001522545
RALA	-0.1846	-0.5095	-0.8433	0.028293307
PABPC1	0.0699	-0.5026	-0.8429	0.028995255
FLNB	0.2294	-0.0812	-0.834	0.039002148
TUBB3	-0.0573	-0.449	-0.8331	0.00260934
TM4SF18	0.0094	-0.062	-0.8317	0.006458019
MLLT11	0.1275	-0.2401	-0.8269	0.00349254
C8orf55	-0.2877	-0.4605	-0.8054	0.001121326
VASH1	0.0851	-0.088	-0.8043	0.049790294
LOC341315	0.1048	-0.0412	-0.8021	0.020795379
MORF4L2	0.0824	-0.6244	-0.8016	0.037717091
ITGA5	-0.2145	-0.7646	-0.7717	0.042025119
MAP3K1	0.0638	0.1137	-0.7712	0.018525703
PALMD	-0.1344	-0.2475	-0.7668	0.034643309
PECI	-0.0032	-0.213	-0.7635	0.000773168
GIMAP7	-0.2692	-0.2728	-0.7598	0.024315393
ATP6V0E2	-0.1007	-0.454	-0.7541	0.046214878
TNFAIP8L3	0.2564	0.1443	-0.7531	0.015559595
GIMAP8	-0.1526	-0.4279	-0.7515	0.002535429
NDUFS5	-0.1681	-0.6424	-0.7319	0.034357289
P15RS	-0.1277	-0.2796	-0.7281	0.016820365
LYPD1	-0.1104	-0.4828	-0.7188	0.006670455
SNORA8	-0.0652	0.0637	-0.7157	0.018332064
MIF	-0.1973	-0.543	-0.7135	0.00693651
FAM127A	0.067	-0.1606	-0.7127	0.005125124
KIAA0114	-0.0157	0.2323	-0.7104	0.000772081
LOC648470	-0.2769	-0.5216	-0.7008	0.039072032
MAGED1	-0.0784	-0.3123	-0.6988	0.00843239
HN1	0.0398	-0.0905	-0.6924	0.000236116
ENC1	0.134	0.1922	-0.6903	0.001293902
TRIP13	0.0087	-0.4836	-0.6831	0.026284928
LOC390466	-0.1016	-0.4783	-0.681	0.025051642
ARPC1A	0.021	-0.3566	-0.6804	0.04472876
CTXN1	-0.1453	-0.2775	-0.679	0.000792881
JAG2	-0.0271	-0.0368	-0.672	0.031718476
LOC100130561	0.0355	-0.2895	-0.6716	0.009281159
GIMAP6	-0.1459	-0.2426	-0.6709	0.003906397
LOC729217	-0.1392	-0.2599	-0.6689	0.000696312
RPS27L	-0.0398	-0.1021	-0.6631	0.000434648
FHOD1	0.1702	-0.1381	-0.6616	0.03656389
ENG	0.0612	-0.0271	-0.6597	0.009996997
MYO10	0.3259	0.1023	-0.658	0.011664167
EPHB4	-0.0874	-0.078	-0.652	0.00994254
TNFRSF21	-0.0121	-0.2101	-0.6511	0.00046991
DAAM1	0.2026	-0.0122	-0.6506	0.045490685
NPTX1	-0.0603	-0.09	-0.6475	0.006497759
LSM2	-0.055	-0.2901	-0.6464	0.003635162
PMP22	-0.0836	-0.4925	-0.6453	0.013199214
LOC646723	-0.1931	-0.2969	-0.645	0.001248048
LOC646576	0.1961	-0.2634	-0.6448	0.020273228
KCTD12	0.0504	0.0975	-0.6443	0.009775733
GNPDA1	-0.1918	-0.3487	-0.6439	0.001113003
FAM89B	0.1262	-0.0593	-0.6437	0.036632138
NGFRAP1	-0.2013	-0.3603	-0.6433	0.006294325
C14orf78	0.1282	-0.0628	-0.6402	0.025446357
LDHB	0.0252	-0.2561	-0.6399	0.007146078
MGST2	0.0775	0.0861	-0.6351	0.004137391
ST3GAL6	0.0246	-0.0384	-0.633	0.005872713
AK3	0.0135	0.0741	-0.6327	2.77516E-06
NUAK1	0.3483	0.1948	-0.6309	0.001145214
RCN2	0.1176	-0.0859	-0.6296	0.001923188
LOC100132863	0.3057	0.099	-0.6291	0.003127593
SOX7	0.0582	0.1077	-0.6287	0.000678402
HOXA5	0.0283	0.0862	-0.6282	0.002126835
FAM98A	0.0892	-0.2465	-0.6264	0.020132871
METTL3	-0.117	-0.2797	-0.6264	0.01091542
PDE4B	-0.0641	-0.1216	-0.6246	0.041477389
APEX1	-0.0504	-0.3464	-0.6226	0.016743204
HNRNPA0	0.0563	0.0291	-0.6209	0.000390443
NT5DC2	-0.0235	-0.0466	-0.619	0.024496967
PSME3	0.0968	-0.2002	-0.6187	0.020042719
EBPL	-0.2016	-0.3733	-0.6184	0.001808879
PEBP1	0.0231	-0.0976	-0.6094	0.00026006
CDK4	-0.2332	-0.1077	-0.6088	0.000905134
CALM3	0.0275	-0.2625	-0.6081	0.005162126
UCHL1	-0.3015	-0.3518	-0.6076	3.56872E-06
NR2F2	0.105	0.106	-0.6041	1.75662E-07
PLSCR3	-0.2617	-0.3901	-0.6035	0.004215018
CDK2AP1	-0.0832	-0.1879	-0.603	0.000162248
HEXB	0.2048	-0.2188	-0.6019	0.014063224
C20orf108	-0.0317	0.0377	-0.6007	2.44223E-05
PDCD1LG2	-0.0265	0.1537	0.6001	0.008550807
TYMP	0.0673	0.0459	0.6017	0.000155502
CCNYL1	0.0149	-0.1054	0.6031	0.016741524
SLCO4A1	0.0587	0.2324	0.6072	0.028420552
P2RX7	0.1846	0.1123	0.6078	0.02403089
TMUB2	0.0907	0.2581	0.6124	0.03772084
SUSD1	0.3268	0.3733	0.6128	0.000287069
SAP130	0.2728	0.2396	0.6135	0.000113231

Only genes in LNA MANTIS/CTL p<0.05 are shown



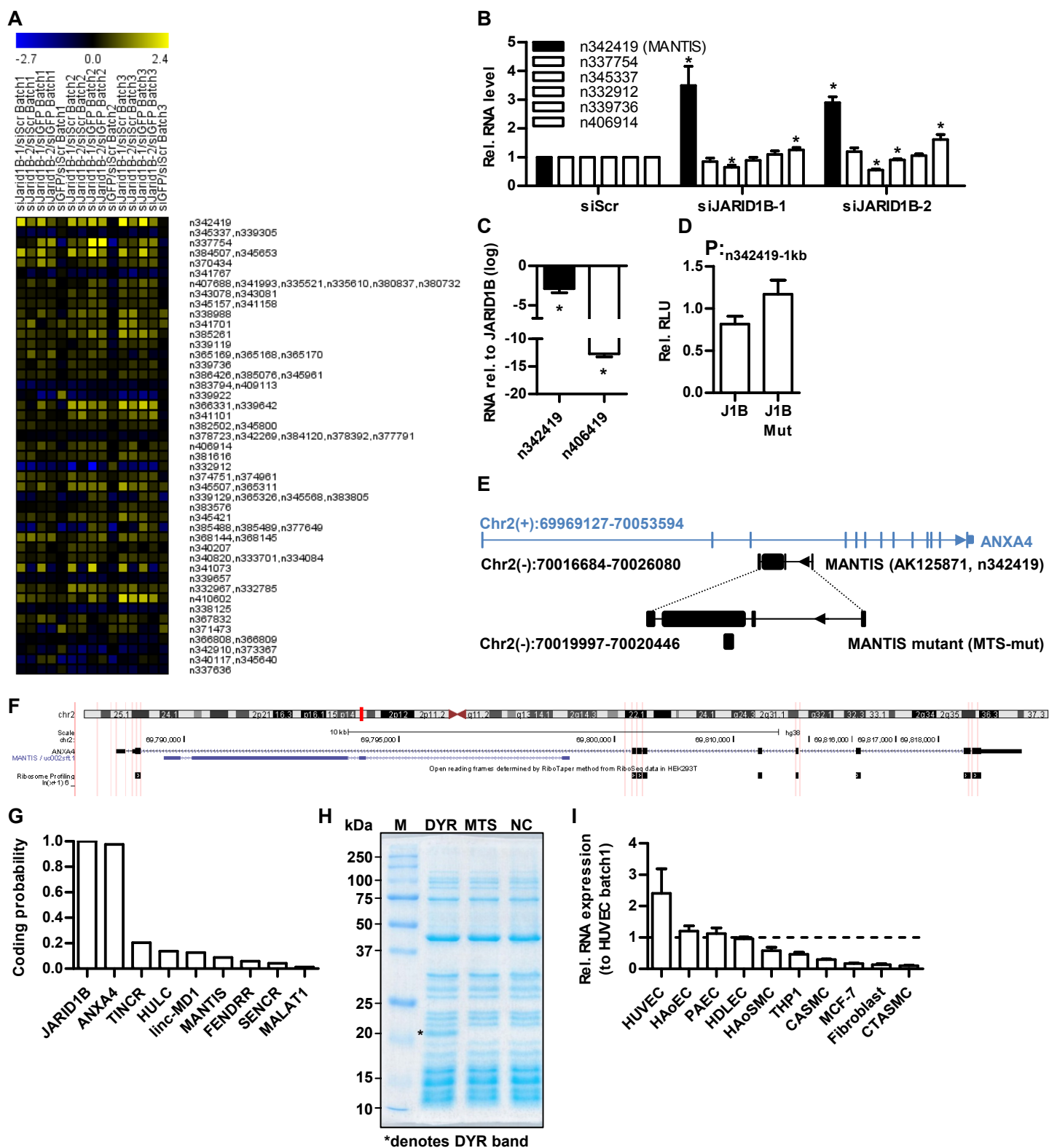
FAT1	0.0598	0.2767	0.6136	0.004755863
AFF3	0.2516	0.3837	0.6219	0.02197693
GLIPR1	0.0906	0.4081	0.623	0.018559113
HCG4	0.011	-0.2459	0.6236	0.019919708
ACSL1	0.4925	0.4181	0.6253	0.003860924
SFRS17A	0.2314	0.4223	0.6265	0.001961199
STX5	0.2998	0.2509	0.6287	0.021080203
LOC399491	0.3856	0.5981	0.6315	0.003697023
SESN2	0.0058	0.3035	0.6344	0.015513135
LY6E	-0.1839	-0.2809	0.638	0.034443777
FLNC	0.2753	0.3503	0.6401	0.001201444
NFE2L1	0.2439	0.2961	0.6416	0.000361724
KIF13B	0.2872	0.2397	0.6417	0.0379021
WDR51B	0.0651	0.2958	0.6439	0.044226404
TRIM26	0.0727	-0.0569	0.6484	0.001568771
LOC728734	0.1634	0.4133	0.6491	0.005298515
GMPR	-0.2244	-0.1709	0.6494	0.001520639
TAP2	-0.0847	-0.0923	0.6552	2.27853E-06
LOC100128274	-0.0531	0.0244	0.6555	0.012930846
UNC93B1	-0.0481	-0.1954	0.6556	0.020466199
NFIX	-0.0275	0.2217	0.6561	0.029167345
DDX58	-0.0036	-0.0723	0.6585	0.002466053
DDX60	-0.0279	0.0367	0.6589	0.005995079
RBCK1	0.2974	0.4213	0.6601	0.000782051
LAMC2	-0.1532	-0.4696	0.6668	0.022305654
APOBEC3G	0.0103	-0.034	0.6669	0.038914594
TNFAIP2	0.0946	-0.0954	0.67	0.002908611
BATF2	-0.3191	-0.3795	0.6722	0.018561273
HTATIP2	-0.0676	0.3626	0.6778	0.023654325
PSMB8	0.0517	-0.0243	0.6788	0.038225559
LOC440341	0.1636	0.5731	0.6897	0.021025068
TMEM123	0.07	0.1086	0.692	0.021370576
LOC440353	0.0964	0.3886	0.6949	0.014742289
MEG3	0.4335	0.5447	0.6951	0.005046136
LOC653496	0.4547	0.4001	0.6955	3.89793E-05
MX1	-0.0507	-0.0923	0.6993	6.29272E-05
LAMP3	0.0583	0.4338	0.6999	0.037939815
C1QTNF1	0.1648	0.0435	0.7019	0.000561974
LOC389386	0.0138	-0.1847	0.7025	0.004055299
OSBP15	0.1137	0.1226	0.7101	0.025446114
CXCL1	0.2959	0.1296	0.7153	0.001864448
GBP2	0.3699	0.389	0.724	0.000729145
LOC728888	0.237	0.3524	0.7261	0.00138053
EPB41L5	0.1127	0.5119	0.7273	0.01956718
LOC100132247	0.1085	0.2703	0.7282	0.000878813
VPS37D	0.2127	0.3642	0.7337	0.029037844
TNIP2	0.0804	0.2143	0.7353	0.037033299
OGFRL1	0.038	-0.1413	0.736	0.037225797
CENTA1	0.2314	0.3675	0.7404	0.000592525
CCNDBP1	0.1322	0.2845	0.7409	0.025333231
LOC399959	0.1803	0.4656	0.7426	0.00429703
GLS	0.155	0.1548	0.7426	0.010090964
PARP9	0.0245	-0.0237	0.7518	0.00346676
TAP1	-0.2265	-0.0981	0.7527	0.03537523
CCDC136	0.3257	0.2826	0.7528	0.000157284
SERPINB1	0.3839	0.5602	0.7564	0.041973012
C1orf24	0.4802	0.4792	0.7566	0.01335912
STAT2	-0.2058	-0.325	0.7647	0.002097844
LOC440348	0.1421	0.3993	0.7706	0.006697211
VEGFC	0.2048	0.0352	0.7718	0.000693801
ADORA2A	0.132	0.3198	0.7791	0.001033894
NRIP3	0.4877	0.6989	0.7817	0.045822164
WARS	-0.0247	0.0364	0.7893	0.012058284
DDX60L	0.107	-0.0047	0.7935	0.00182492
SLIT2	0.0789	-0.2097	0.7937	0.024408822
TNIP1	0.3377	0.1633	0.7967	0.01063807
ABCA1	0.4767	0.0618	0.7997	0.036489374
PLEKHA4	-0.0677	-0.0858	0.8096	0.000155041
USP36	0.2724	0.2401	0.815	0.000830131
DENND5A	0.3476	0.3593	0.8186	0.001919442
NPIP	0.196	0.5886	0.8269	0.011833527
MIR155HG	-0.1953	-0.3135	0.8297	0.010465328
PLEKHO2	0.0736	0.3121	0.8391	0.002055338
GCH1	-0.0096	0.0012	0.8561	0.001253082
TMEM62	-0.139	0.2348	0.8611	0.020331442
VIP	0.0585	0.5214	0.8624	0.019840837
TDRD7	0.1734	0.1877	0.8628	0.008723408
FAM129A	0.6501	0.5121	0.8642	0.008485159
GFPT2	0.2753	0.1248	0.865	0.037925761
IL20RB	-0.0584	0.4708	0.8715	0.036059779
TNFRSF9	0.2811	0.4349	0.8778	0.000767915
TMEFF2	0.2321	0.243	0.8807	2.42382E-05
LOC284023	0.1425	0.3188	0.885	0.001418701
IL1B	-0.0095	-0.5985	0.9069	0.044979038
H2AFJ	0.1555	0.4318	0.9082	0.030275281
LOC643384	0.0608	-0.2756	0.922	0.022908581
UBE2L6	0.1161	-0.0073	0.9301	0.000641423
VAV3	0.2048	0.6347	0.9317	0.022471945
ALCAM	0.2509	0.1504	0.9327	0.032288239
CSF3	-0.0695	-0.1114	0.9365	2.93058E-06
CRTAC1	0.0192	-0.1172	0.9372	0.001281841
CFB	-0.1566	-0.0755	0.9494	0.02899721
TAGLN	0.3533	0.3299	0.9724	0.015365603
NFKBIZ	-0.2813	-0.134	0.981	0.000286285
LITAF	0.1446	0.1092	1.0199	0.029107598
RUNX3	0.0557	0.0297	1.03	0.047029744
RIPK2	0.0263	-0.035	1.0372	0.002766834
IFI35	-0.038	-0.1412	1.0705	0.041496787
ACTA2	-0.0419	0.1377	1.0956	0.01666818
CXCL2	-0.7209	-0.743	1.126	0.027534636
DHX58	0.0927	0.0781	1.1365	0.004506941
PIM2	0.1314	0.4335	1.1509	0.040245254
CSNK2A2	0.3108	0.4882	1.1582	0.018757491
CEBPD	-0.0811	-0.2162	1.2433	0.047070744
ECGF1	0.0541	-0.0193	1.2479	0.041549722
TNFAIP6	0.3277	0.2127	1.309	0.045410978
GBP5	0.2085	0.2947	1.3121	0.025146063
SOD2	0.1372	0.2037	1.3218	0.004020659
HIST1H1C	0.5419	0.2275	1.3469	0.041908563
RNMT	0.5776	0.5214	1.3968	0.020987663
HIST2H2BE	0.0295	0.8312	1.4068	0.032585775
HIST1H2AC	0.2636	0.6215	1.41	0.041687472
TUFT1	0.2044	0.0576	1.4615	0.000746265
IL6	0.1239	0.0298	1.5319	0.019187988
NKD2	0.3482	0.2503	1.5339	6.17053E-05
CSF2	-0.329	-0.485	1.5825	0.000360621

**Supplemental Table 12: Full gene ontology (GO) analysis made with Gorilla with the genes upregulated after MANTIS depletion in the Illumina Bead-Chip array.**

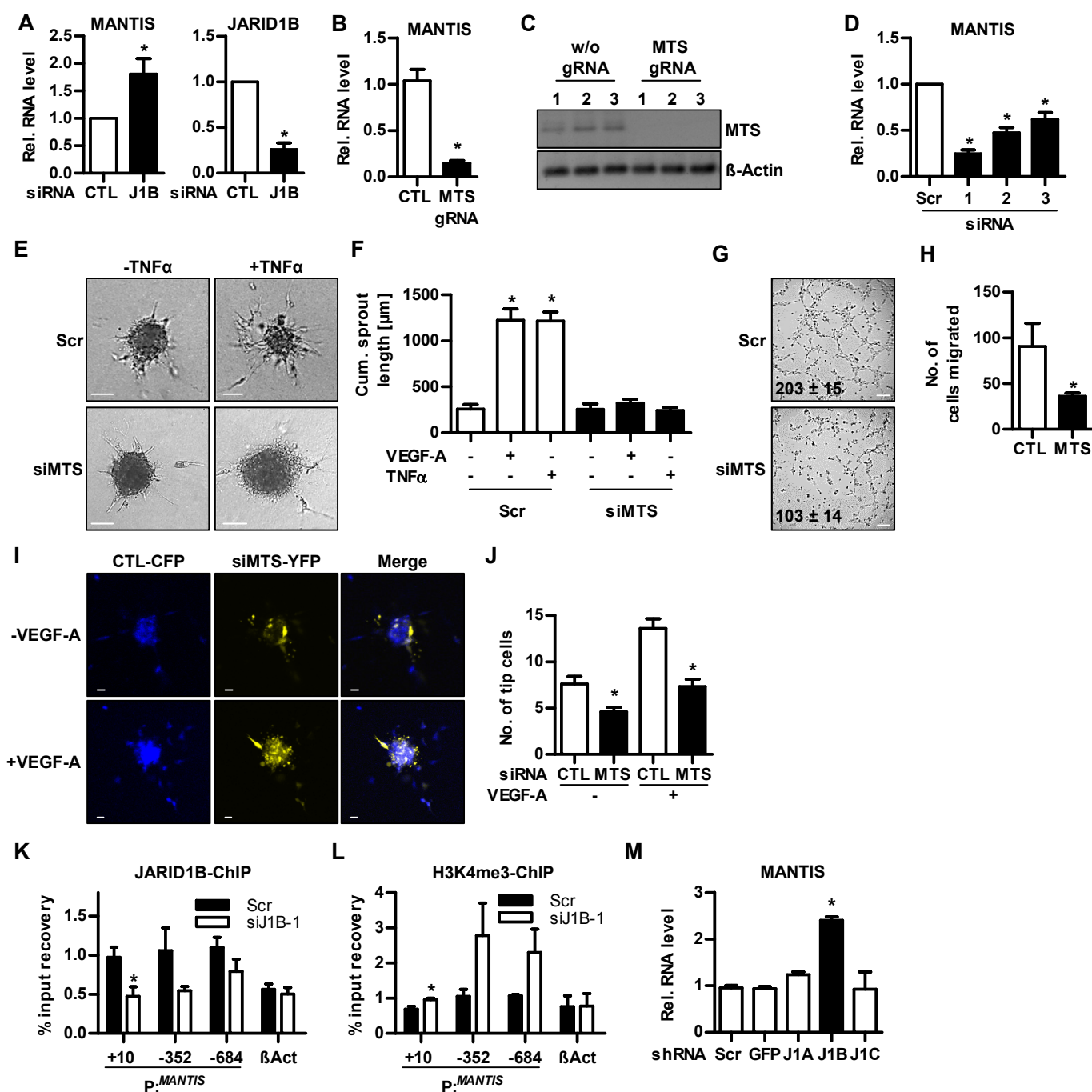
GO term	Description	P-value
GO:0043207	response to external biotic stimulus	3.45E-11
GO:0009607	response to biotic stimulus	7.63E-11
GO:0002376	immune system process	1.58E-10
GO:0006952	defense response	1.36E-09
GO:0009605	response to external stimulus	1.43E-08
GO:0019221	cytokine-mediated signaling pathway	1.50E-08
GO:0002684	positive regulation of immune system process	7.92E-08
GO:0002682	regulation of immune system process	8.16E-08
GO:0006955	immune response	1.09E-07
GO:0031347	regulation of defense response	2.59E-07
GO:0002237	response to molecule of bacterial origin	3.43E-07
GO:0051704	multi-organism process	3.91E-07
GO:0051707	response to other organism	6.53E-07
GO:0006954	inflammatory response	7.53E-07
GO:0009615	response to virus	1.09E-06
GO:0032103	positive regulation of response to external stimulus	1.43E-06
GO:0032496	response to lipopolysaccharide	1.72E-06
GO:0032101	regulation of response to external stimulus	2.17E-06
GO:0071219	cellular response to molecule of bacterial origin	3.45E-06
GO:0002697	regulation of immune effector process	3.94E-06
GO:0050921	positive regulation of chemotaxis	4.67E-06
GO:0050776	regulation of immune response	5.97E-06
GO:0098542	defense response to other organism	6.90E-06
GO:0071216	cellular response to biotic stimulus	8.63E-06
GO:0045088	regulation of innate immune response	9.99E-06
GO:0050896	response to stimulus	1.29E-05
GO:0048520	positive regulation of behavior	1.30E-05
GO:0002688	regulation of leukocyte chemotaxis	1.51E-05
GO:0008285	negative regulation of cell proliferation	1.92E-05

**Supplemental Table 13: Full gene ontology (GO) analysis made with Gorilla with the genes downregulated after MANTIS depletion in the Illumina Bead-Chip array.**

GO term	Description	P-value
GO:0001525	angiogenesis	1.37E-06
GO:1901342	regulation of vasculature development	2.25E-05
GO:0001937	negative regulation of endothelial cell proliferation	2.98E-05
GO:0010596	negative regulation of endothelial cell migration	4.29E-05
GO:0040011	locomotion	4.75E-05
GO:0042981	regulation of apoptotic process	6.83E-05
GO:0043067	regulation of programmed cell death	7.63E-05
GO:0045765	regulation of angiogenesis	1.04E-04
GO:0032233	positive regulation of actin filament bundle assembly	1.07E-04
GO:0042127	regulation of cell proliferation	1.22E-04
GO:0048646	anatomical structure formation involved in morphogenesis	1.38E-04
GO:0050678	regulation of epithelial cell proliferation	1.44E-04
GO:0010633	negative regulation of epithelial cell migration	1.51E-04
GO:0065008	regulation of biological quality	1.57E-04
GO:0010941	regulation of cell death	1.66E-04
GO:0001936	regulation of endothelial cell proliferation	1.77E-04
GO:0016477	cell migration	1.85E-04
GO:0043542	endothelial cell migration	1.91E-04
GO:0043488	regulation of mRNA stability	2.06E-04
GO:0043537	negative regulation of blood vessel endothelial cell migration	2.45E-04
GO:0043487	regulation of RNA stability	2.56E-04
GO:0007167	enzyme linked receptor protein signaling pathway	2.74E-04
GO:0043065	positive regulation of apoptotic process	2.82E-04
GO:0032268	regulation of cellular protein metabolic process	2.99E-04
GO:0043068	positive regulation of programmed cell death	3.04E-04
GO:0051495	positive regulation of cytoskeleton organization	3.14E-04
GO:0043534	blood vessel endothelial cell migration	3.61E-04
GO:0071156	regulation of cell cycle arrest	3.88E-04
GO:0050680	negative regulation of epithelial cell proliferation	4.39E-04
GO:0010604	positive regulation of macromolecule metabolic process	4.40E-04
GO:0048870	cell motility	4.54E-04

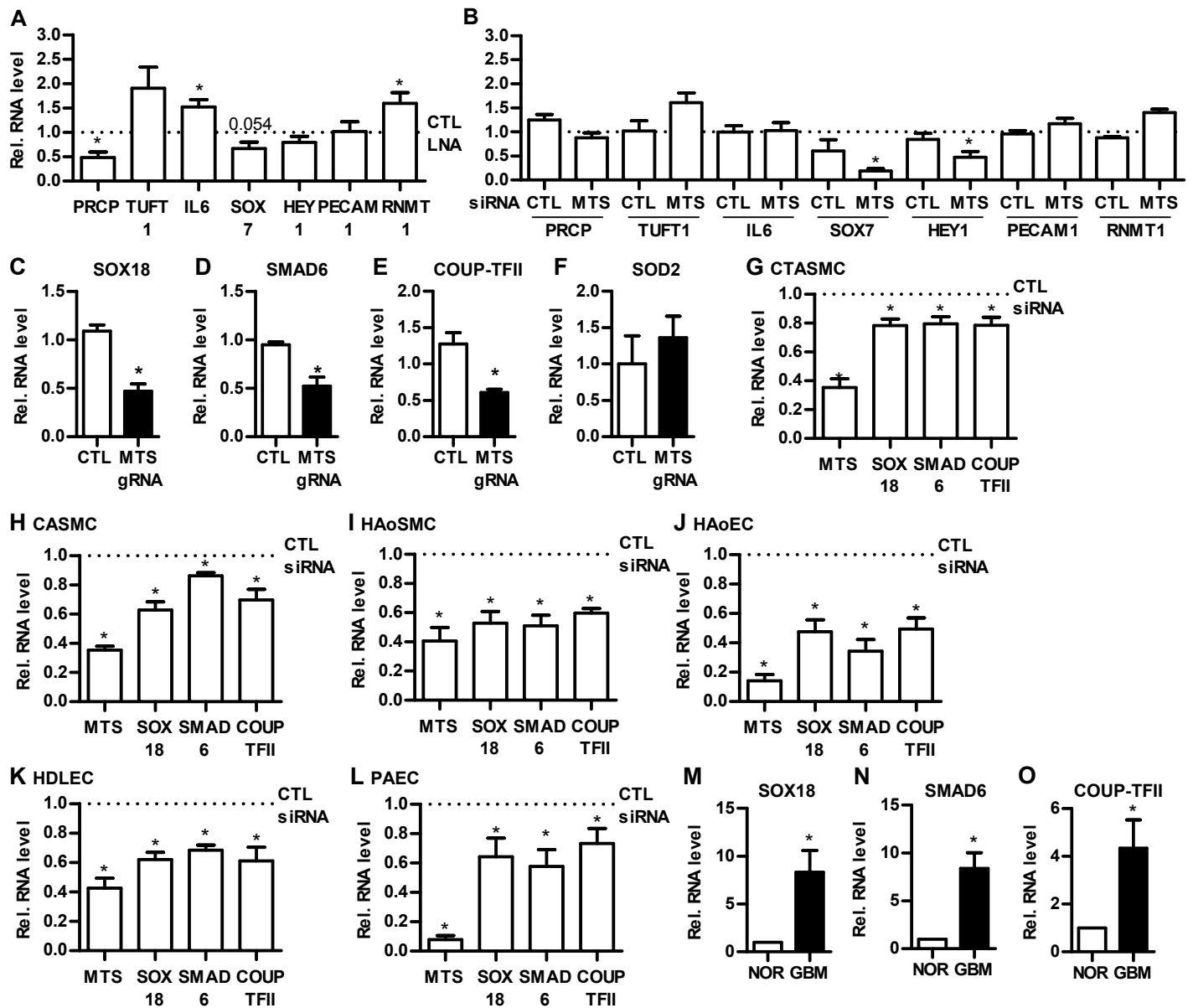


**Supplemental Figure 1:** (A) Full Affymetrix Exon-Array heat map comparing siJARID1B-1/siScr, siJARID1B-2/siScr, siJARID1B-1/siGFP, siJARID1B-2/siGFP, siJARID1B-1/siJARID1B-2 as well as siScr/siGFP levels of HUVEC batches 1-3. Scale bar shows colour code from -2.0 (blue) to 2.0 (yellow) log<sub>2</sub> fold change. Please see supplemental table 3 for more information about these lncRNAs. (B) siRNA knockdown with siScr, siJARID1B-1 and siJARID1B-2 in HUVEC and qRT-PCR of lncRNAs indicated. n=6, paired t-test. (C) QRT-PCR measurements of n342419 (MANTIS) and n406419 expression in HUVEC. Data is shown in log<sub>2</sub> scale relative to JARID1B RNA level. n=12. (D) Luciferase reporter assay of HUVECs transfected with an active JARID1B (J1B) or catalytically inactive JARID1B mutant (J1B Mut) plasmid and a n342419 1kb promoter plasmid. n=4, unpaired t-test. RLU, relative luminescence units. (E) Scheme of the genomic locus of MANTIS. Numbers indicate genomic position (GRCh37/hg19). (F) Open reading frames determined by the RiboTaper<sup>14</sup> (Ribosome profiling) method from RiboSeq data in HEK293T. The UCSC genome browser profile shows the genomic locus of MANTIS. (G) Prediction of the coding potential with CPAT<sup>15</sup>. (H) *In vitro* translation products performed with the PURExpress protein synthesis kit (NEB) from positive control (DYR), MANTIS (MTS) and negative control (NC) stained with Coomassie. M, protein ladder. (I) Expression level of MANTIS in different cell types. Data is normalized to HUVEC batch 1. n=6. Error bars are defined as mean  $\pm$  SEM. \*P<0.05.

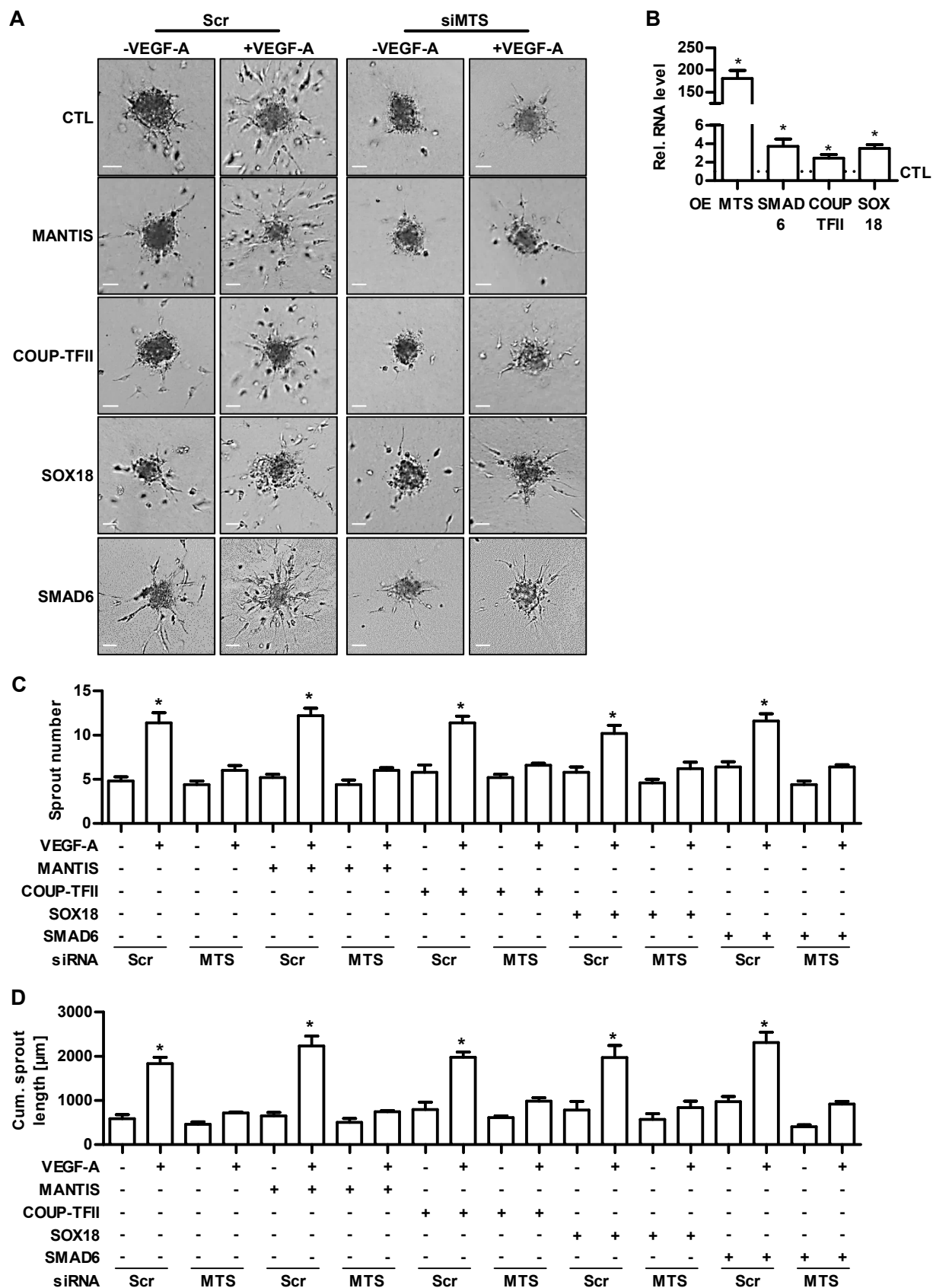


**Supplemental Figure 2:** (A) siRNA knockdown with siScr (CTL) and siJARID1B-1 in pulmonary artery endothelial cells (PAEC) and qRT-PCR of MANTIS and JARID1B. n=6, paired t-test. (B) MANTIS was measured after targeting with CRISPR/Cas9 gRNAs relative to control (CTL) with qRT-PCR. n=9, unpaired t-test. (C) Agarose gel after PCR of  $\beta$ -actin or MANTIS from RNA of HUVECs targeted either with MANTIS gRNAs or empty vector (w/o gRNAs). (D) MANTIS knockdown was performed with three different siRNAs for 48h and MANTIS expression was measured with qRT-PCR. Scr served as negative control. n=6. One-Way ANOVA, Bonferroni. (E) Spheroid outgrowth assay after MANTIS siRNA-based knockdown (siMTS). Scrambled siRNA (Scr) served as negative control. Cells treated with or without TNF $\alpha$  (+/- TNF $\alpha$ ) (10ng/mL; 16h) are shown. Scale bar indicates 50 $\mu$ m. (F) Quantification of the cumulative sprout length from the spheroid outgrowth assays seen in Figure 1K and Supplemental Figure 2E. n=10. One-Way ANOVA, Bonferroni. (G) Tube formation assay after scrambled (Scr) or MANTIS knockdown (siMTS) in pulmonary artery endothelial cells (PAEC). Scr served as negative control. Numbers indicate number of tubes  $\pm$  SEM. n=4. Scale bar indicates 200 $\mu$ m. (H) Boyden-Chamber assay of HUVECs transfected with siRNAs against scrambled (CTL) or MANTIS (MTS) and calculation of the number of cells migrated into the lower compartment. n=3, Unpaired t-test. (I) Competition-like spheroid outgrowth assay. HUVECs were transfected with lentivirus for CFP or YFP. CFP transfected cells were transfected with CTL siRNA, whereas YFP transfected cells were transfected with siRNAs against MANTIS (siMTS). Afterwards, cells were mixed and spheroid outgrowth assay was performed with or without VEGF-A treatment. Representative images were shown. Scale bar indicates 20 $\mu$ m. (J) Quantification of tip cells of the spheroid assay shown in Supplemental Figure 2I. n=15, unpaired t-test. (K, L) ChIP of HUVECs for JARID1B- (K) or H3K4me3-binding (L) treated with siRNAs against Scrambled (Scr) or JARID1B (siJ1B-1) followed by qPCR for different regions of the MANTIS (n342419) promoter. Numbers indicate nucleotide position relative the TSS (+10, -352, -684). The  $\beta$ ACTIN promoter served as negative control. n=3. Unpaired t-test. (M) HUVECs were treated with shRNAs against scrambled (Scr), GFP, JARID1A (J1A), JARID1B (J1B) or JARID1C (J1C) and MANTIS RNA levels were measured by qRT-PCR relative to  $\beta$ ACTIN. n=4, unpaired t-test. Error bars are defined as mean  $\pm$  SEM. \*P<0.05.

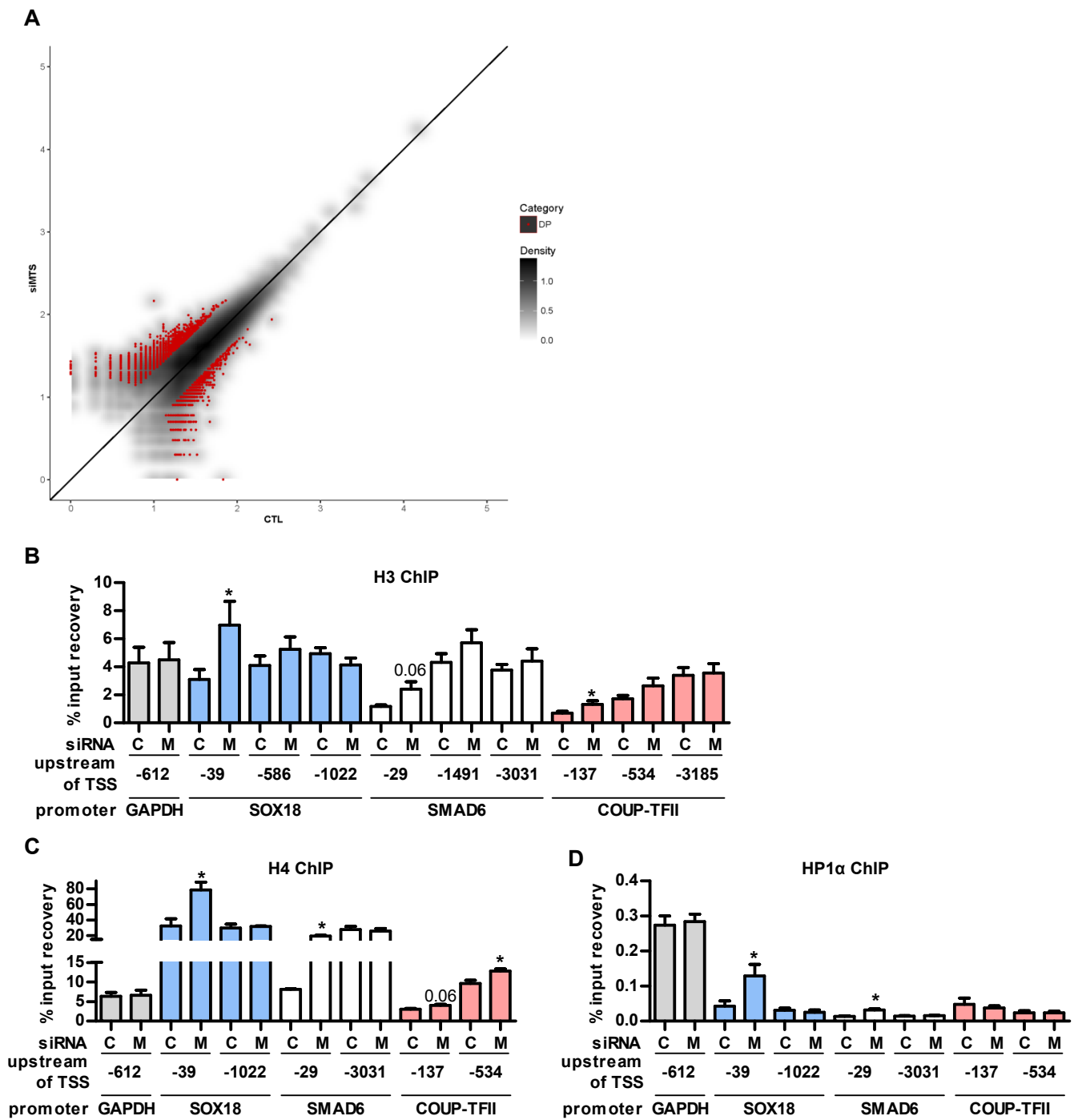




**Supplemental Figure 3:** (A) QRT-PCR measurements relative to  $\beta$ -Actin after LNA-GapmeR based knockdown for 48h of MANTIS IncRNA (MTS). CTL served as negative control and was set to 1. Expression levels of PRCP, TUFT1, IL6, SOX7, HEY1, PECAM1 and RNMT1 are shown. n=6. Paired t-test. (B) QRT-PCR measurements relative to  $\beta$ -Actin after knockdown for 48h of MANTIS IncRNA (MTS) with siRNA-1. Scrambled siRNA (Scr) and MANTIS siRNA-specific control siRNA (CTL) served as negative controls. Expression levels of PRCP, TUFT1, IL6, SOX7, HEY1, PECAM1 and RNMT1 are shown. Scr was set to 1 (dashed line). n=7, except TUFT1 and RNMT1 (n=6). One-way ANOVA, Bonferroni. (C-F) SOX18 (C), SMAD6 (D), COUP-TFII (E) and SOD2 (F) levels were measured after CRISPR/Cas9 mediated knockout of MANTIS (MTS gRNA) with qRT-PCR relative to  $\beta$ -ACTIN. n=9, unpaired t-test. (G-L) qRT-PCR relative to  $\beta$ -ACTIN for MANTIS, SOX18, SMAD6 and COUP-TFII after siRNA knockdown with scrambled (CTL siRNA) or MANTIS siRNA (siMTS) in carotid artery smooth muscle cells (G, CTASMC, n=7), coronary artery smooth muscle cells (H, CASMC, n=7), human aortic smooth muscle cells (I, HAoSMC, n=6), human aortic endothelial cells (J, HAoEC, n=7), human dermal lymphatic endothelial cells (K, HDLEC, n=7) and pulmonary artery endothelial cells (L, PAEC, n=6). CTL was set to 1 (dashed line). Paired t-test. (M-O) QRT-PCR of SOX18 (M), SMAD6 (N) and COUP-TFII (O) from endothelial cells isolated from glioblastoma (GBM) or adjacent healthy control (CTL) tissue. n=5. Paired t-test. Error bars are defined as mean  $\pm$  SEM. \* $P < 0.05$ .



**Supplemental Figure 4:** (A) Spheroid outgrowth assay of HUVECs transfected with scrambled (Scr) or MANTIS siRNA-1 (siMTS) for 48h and with overexpression of MANTIS, COUP-TFII, SOX18 or SMAD6 for 24h prior to stopping the assay. PcDNA3.1 (CTL) served as negative control. Cells treated with or without VEGF-A (+/- VEGF-A) are shown. Scale bar indicates 50μm. (B) HUVECs were transiently transfected with overexpression plasmids (OE) for 48h coding for MANTIS, SMAD6, COUP-TFII or SOX18 with subsequent qRT-PCR measurements. Expression levels of MANTIS (MTS), SMAD6, COUP-TFII and SOX18 relative to β-ACTIN are shown. PcDNA 3.1 (CTL) served as negative control and was set to 1. n=6. Paired t-test. (C, D) Quantification of sprout numbers (C) and cumulative sprout length (D) from the spheroid outgrowth assays seen in Supplemental Figure 4A. n=5. One-Way ANOVA, Bonferroni. Error bars are defined as mean +/- SEM. \*P<0.05.



**Supplemental Figure 5:** (A) Scatter plot of ATAC-Seq after knockdown with scrambled siRNA (CTL) or MANTIS siRNA (siMTS) in HUVEC showing log10 normalized peak counts separated into kernel density smoothing (black) and differential peaks (mean count > 10, log2 fold change > +1, red). (B-D) ChIP of HUVECs transfected with scrambled (C) or MANTIS siRNA (M) with H3 (B, n=5), H4 (C, n=3) and HP1α (D, n=6) followed by qPCR for GAPDH promoter, Sox18 promoter regions at the transcription start site (TSS, -39nt) or 586nt and 1022nt, SMAD6 promoter regions at the transcription start site (TSS, -29nt) or 1491nt and 3031nt, and COUP-TFII promoter regions at the transcription start site (TSS, -137nt) or 534nt and 3185nt. Numbers indicate nucleotide positions upstream of the TSS. Unpaired t-test. Error bars are defined as mean  $\pm$  SEM. \* $P$ <0.05.

## Supplemental References

1. Laib AM, Bartol A, Alajati A, Korff T, Weber H, Augustin HG. Spheroid-based human endothelial cell microvessel formation in vivo. *Nat Protoc.* 2009;4:1202-1215.
2. Erturk A, Becker K, Jahrling N, Mauch CP, Hojer CD, Egen JG, Hellal F, Bradke F, Sheng M, Dodt HU. Three-dimensional imaging of solvent-cleared organs using 3DISCO. *Nat Protoc.* 2012;7:1983-1995.
3. Hathaway CA, Heistad DD, Piegors DJ, Miller FJ, Jr. Regression of atherosclerosis in monkeys reduces vascular superoxide levels. *Circ Res.* 2002;90:277-283.
4. Pullamsetti SS, Berghausen EM, Dabral S, Tretyn A, Butrous E, Savai R, Butrous G, Dahal BK, Brandes RP, Ghofrani HA, Weissmann N, Grimminger F, Seeger W, Rosenkranz S, Schermuly RT. Role of Src tyrosine kinases in experimental pulmonary hypertension. *Arterioscler Thromb Vasc Biol.* 2012;32:1354-1365.
5. Gurnik S, Devraj K, Macas J, Yamaji M, Starke J, Scholz A, Sommer K, Di TM, Vutukuri R, Beck H, Mittelbronn M, Foerch C, Pfeilschifter W, Liebner S, Peters KG, Plate KH, Reiss Y. Angiopoietin-2-induced blood-brain barrier compromise and increased stroke size are rescued by VE-PTP-dependent restoration of Tie2 signaling. *Acta Neuropathol.* 2016;131:753-773.
6. Fork C, Gu L, Hitzel J, Josipovic I, Hu J, SzeKa WM, Ponomareva Y, Albert M, Schmitz SU, Uchida S, Fleming I, Helin K, Steinhilber D, Leisegang MS, Brandes RP. Epigenetic Regulation of Angiogenesis by JARID1B-Induced Repression of HOXA5. *Arterioscler Thromb Vasc Biol.* 2015;35:1645-1652.
7. Gellert P, Ponomareva Y, Braun T, Uchida S. Noncoder: a web interface for exon array-based detection of long non-coding RNAs. *Nucleic Acids Res.* 2013;41:e20.

8. Lin SM, Du P, Huber W, Kibbe WA. Model-based variance-stabilizing transformation for Illumina microarray data. *Nucleic Acids Res.* 2008;36:e11.
9. Du P, Kibbe WA, Lin SM. lumi: a pipeline for processing Illumina microarray. *Bioinformatics.* 2008;24:1547-1548.
10. Ritchie ME, Phipson B, Wu D, Hu Y, Law CW, Shi W, Smyth GK. limma powers differential expression analyses for RNA-sequencing and microarray studies. *Nucleic Acids Res.* 2015;43:e47.
11. Eden E, Navon R, Steinfeld I, Lipson D, Yakhini Z. GOrilla: a tool for discovery and visualization of enriched GO terms in ranked gene lists. *BMC Bioinformatics.* 2009;10:48.
12. Ran FA, Hsu PD, Wright J, Agarwala V, Scott DA, Zhang F. Genome engineering using the CRISPR-Cas9 system. *Nat Protoc.* 2013;8:2281-2308.
13. Josipovic I, Fork C, Preussner J, Prior KK, Iloska D, Vasconez AE, Labocha S, Angioni C, Thomas D, Ferreiros N, Looso M, Pullamsetti SS, Geisslinger G, Steinhilber D, Brandes RP, Leisegang MS. PAFAH1B1 and the lncRNA NONHSAT073641 maintain an angiogenic phenotype in human endothelial cells. *Acta Physiol (Oxf).* 2016; 218:13-27. doi: 10.1111/apha.12700.
14. Korff T, Augustin HG. Integration of endothelial cells in multicellular spheroids prevents apoptosis and induces differentiation. *J Cell Biol.* 1998;143:1341-1352.
15. Gu L, Hitzel J, Moll F, Kruse C, Malik RA, Preussner J, Looso M, Leisegang MS, Steinhilber D, Brandes RP, Fork C. The Histone Demethylase PHF8 Is Essential for Endothelial Cell Migration. *PLoS One.* 2016;11:e0146645.
16. Tsai MC, Manor O, Wan Y, Mosammaparast N, Wang JK, Lan F, Shi Y, Segal E, Chang HY. Long noncoding RNA as modular scaffold of histone modification complexes. *Science.* 2010;329:689-693.



17. Kramer K, Sachsenberg T, Beckmann BM, Qamar S, Boon KL, Hentze MW, Kohlbacher O, Urlaub H. Photo-cross-linking and high-resolution mass spectrometry for assignment of RNA-binding sites in RNA-binding proteins. *Nat Methods*. 2014;11:1064-1070.
18. Wisniewski JR, Zougman A, Nagaraj N, Mann M. Universal sample preparation method for proteome analysis. *Nat Methods*. 2009;6:359-362.
19. Rappsilber J, Mann M, Ishihama Y. Protocol for micro-purification, enrichment, pre-fractionation and storage of peptides for proteomics using StageTips. *Nat Protoc*. 2007;2:1896-1906.
20. Cox J, Mann M. MaxQuant enables high peptide identification rates, individualized p.p.b.-range mass accuracies and proteome-wide protein quantification. *Nat Biotechnol*. 2008;26:1367-1372.
21. Marino F, Cristobal A, Binai NA, Bache N, Heck AJ, Mohammed S. Characterization and usage of the EASY-spray technology as part of an online 2D SCX-RP ultra-high pressure system. *Analyst*. 2014;139:6520-6528.
22. Vizcaino JA, Csordas A, del-Toro N, Dianas JA, Griss J, Lavidas I, Mayer G, Perez-Riverol Y, Reisinger F, Ternent T, Xu QW, Wang R, Hermjakob H. 2016 update of the PRIDE database and its related tools. *Nucleic Acids Res*. 2016;44:D447-D456.
23. Wong MS, Leisegang MS, Kruse C, Vogel J, Schurmann C, Dehne N, Weigert A, Herrmann E, Brune B, Shah AM, Steinhilber D, Offermanns S, Carmeliet G, Badenhoop K, Schroder K, Brandes RP. Vitamin D promotes vascular regeneration. *Circulation*. 2014;130:976-986.
24. Simon JM, Giresi PG, Davis IJ, Lieb JD. Using formaldehyde-assisted isolation of regulatory elements (FAIRE) to isolate active regulatory DNA. *Nat Protoc*. 2012;7:256-267.

25. Chereji RV, Kan TW, Grudniewska MK, Romashchenko AV, Berezikov E, Zhimulev IF, Guryev V, Morozov AV, Moshkin YM. Genome-wide profiling of nucleosome sensitivity and chromatin accessibility in *Drosophila melanogaster*. *Nucleic Acids Res.* 2016;44:1036-1051.
26. Bultman SJ, Gebuhr TC, Magnuson T. A Brg1 mutation that uncouples ATPase activity from chromatin remodeling reveals an essential role for SWI/SNF-related complexes in beta-globin expression and erythroid development. *Genes Dev.* 2005;19:2849-2861.
27. Buenrostro JD, Giresi PG, Zaba LC, Chang HY, Greenleaf WJ. Transposition of native chromatin for fast and sensitive epigenomic profiling of open chromatin, DNA-binding proteins and nucleosome position. *Nat Methods.* 2013;10:1213-1218.
28. Bolger AM, Lohse M, Usadel B. Trimmomatic: a flexible trimmer for Illumina sequence data. *Bioinformatics.* 2014;30:2114-2120.
29. Dobin A, Davis CA, Schlesinger F, Drenkow J, Zaleski C, Jha S, Batut P, Chaisson M, Gingeras TR. STAR: ultrafast universal RNA-seq aligner. *Bioinformatics.* 2013;29:15-21.
30. Harmanci A, Rozowsky J, Gerstein M. MUSIC: identification of enriched regions in ChIP-Seq experiments using a mappability-corrected multiscale signal processing framework. *Genome Biol.* 2014;15:474.
31. Anders S, Huber W. Differential expression analysis for sequence count data. *Genome Biol.* 2010;11:R106.